# Removal of Organic Binder from Multilayer Ceramic Structures

Yuying Tang

B.S. Ceramics, Tsinghua University
1984

M.S. Ceramics, Tsinghua University
1987

Submitted to the Department of Materials Science and Engineering
in Partial Fulfillment of the Requirements of the Degree of
Doctor of Philosophy in Ceramics

at the

Massachusetts Institute of Technology

February 1994



Signature of Author _____
Department of Materials Science and Engineering
January 7, 1994

Certified by _____
Michael J. Cima
Norton Associate Professor of Ceramics
Thesis Supervisor

Accepted by _____
Carl V. Thompson II
Professor of Electronic Materials
Chairman, Department Committee on Graduate Students

**Removal of Organic Binder from Multilayer Ceramic Structures**

Yuying Tang

Submitted to the Department of Materials Science and Engineering
on January 7, 1994
in partial fulfillment of the requirements for the degree of
Doctor of Philosophy in Ceramics

## Abstract

Multilayer ceramic (MLC) capacitors and MLC packages are made up of ceramic films and metallic electrode layers. Knowledge of the structural homogeneity of ceramic green tapes and the compatibility between the ceramic tapes and electrode layers is essential to optimize processing conditions and to improve the quality of the final products. The structure of the ceramic green tapes determines the dimensional change of the tape during the binder removal and sintering processes. The mass transport from MLC greenware during binder removal and the compatibility between the ceramic tape and electrode layers determine delamination mechanisms during binder removal from MLC greenware. Such delaminations are the principal defects affecting the reliability of the MLCs.

The $BaTiO_3$ MLC capacitor was chosen as an example to study. Benzyl butyral phthalate (BBP) plasticized polyvinyl butyral (PVB), a thermoplastic system, was used as binder for the ceramic tape. The structure of the ceramic green tapes was examined. PVB chains were adsorbed on the surface of $BaTiO_3$ powder through hydrogen bonding, forming a 4.5 nm adsorption layer equivalent to 8.6% of the volume of $BaTiO_3$ powder. This adsorption layer has very low mobility, and behaves as part of the $BaTiO_3$ particles. The maximum packing density of the particles plus their adsorption layers was calculated to be 0.646, corresponding to a critical particle volume concentration (CPVC) of 0.598 for a green tape.

The dynamic mechanical analysis (DMA) of the green tapes was conducted over a wide temperature range (-80°C to 150°C). 50 vol% loading of ceramic particles in a green tape broadened the glass transition region of the binder matrix from the -70 to 20°C range to the -70 to 70°C range. The broad glass transition region was believed to have been caused by low mobility polymer layers near ceramic particle surfaces. Broadening of the glass transition region as well as shifting toward high temperatures occurred when the ceramic loading in the green tapes exceeded the CPVC of this system, due to the lack of free binder layer between ceramic particles. DMA indicates that the ceramic loading in a green tape should be below the CPVC in order for the tape to have enough flexibility to be processed.

The deformation of single layer ceramic tapes was measured *in situ* with a hot-stage/optical microscope during annealing and binder removal. Both the curvature and the

shrinkage of the green sheets were measured in the tape casting and transverse directions. The tapes bent toward the top surface due to a differential shrinkage across the tape thickness. The tape casting direction had higher curvature and shrinkage than the transverse direction. Annealing the tape at 70°C for 24 hours resulted in the same magnitude of curvature and the same amount of differential shrinkage in the casting and transverse directions. This leads to the conclusion that residual stresses in the polymer matrix from shearing and drying processes are the causes of this anisotropic deformation.

Three aspects of the delamination mechanism during binder removal from MLC greenware were evaluated: gas pressure within the electrode layer; stresses in the electrode and dielectric layers from differential shrinkage; and adhesive strength of the electrode and dielectric layers. Gas generation rates in both the ceramic tapes and electrode layers during binder removal were studied. A theoretical model was developed to calculate the gas pressure distribution in the electrode layers and to estimate the critical gas generation rate and the critical defect size above which delamination would propagate. The gas pressure was shown to increase with temperature and length of the electrode layer and to decrease with the porosity. The critical gas pressure to cause a delamination was shown to be inversely proportional to defect size in the electrode layers.

*In situ* observation of delamination in MLC capacitors during binder removal was conducted. Delamination during binder removal was shown to be a cohesive failure along the electrode layers. It nucleates within the electrode layer due to the stress from shrinkage mismatch between the electrode and dielectric layers. Propagation of delamination along the electrode layer occurs due to high gas pressure caused by a high gas generation rate. Delamination healed or partially healed after the binder in the electrode layer was removed, and this healing is controlled by the maximum strain level in the dielectric layers from delamination. A minor delamination can heal completely, while a major delamination caused either by a high gas pressure or by a thick electrode layer can only partially heal.

Thesis Supervisor: Prof. Michael J. Cima
Title: Norton Associate Professor of Ceramics

## TABLE OF CONTENTS

## List of Figures

**Chapter 4**

**Chapter 5**

## Chapter 6

## List of Tables

**Acknowledgments**

I am grateful to a lot of people for making my time at MIT enjoyable and productive. First of all, I thank my thesis advisor, Professor Cima, for his guidance and encouragement. I would also like to thank Professor Sadoway and Professor Eagar, my thesis committee members, for their time spent on my thesis and for their helpful suggestions. I thank the An Wang fellowship for providing me financial support during my first two years at MIT. I would like to thank the Ceramic Processing Research Consortium for providing funding for this research. My sincere thanks goes to Alan Devoe and the Presidio Company for kindly providing most of the samples used in this thesis.

I am grateful to Dr. Wendell Rhine for his guidance in chemistry. He is always there, willing to listen and ready to help. I am also grateful to Dr. Richard Pober for sharing his knowledge in ceramic processing. I thank Professor Armstrong, Professor Yannas, Professor Roylance, and Professor Kytomaa for helpful discussions.

Leonard Rigione and John Centorino have helped me with setting up equipment and keeping them going. I thank Eve Downing for her help with English writing. I thank Barbara Layne, Sally Gregg, and Barry Millsap for their help.

I owe a large part of my thesis work to my friends in the polymer program at MIT: Sam Gido, Robert Lescanec, Bruce Carvalho, Debbie Vezie, Stephanie Simmons, John Moali, Ramnath Subramaniam, Mary Chen, and Lars Genieser. I thank them for letting me use their facilities and for sharing their knowledge in polymer science with me. Sam Gido deserves special thanks for everything he has done – from editing my English writing to numerous helpful discussions.

I would like to thank my officemates for the warm atmosphere and for their friendship: Bertha Chang, Paul McIntyre, Hiroshi Sakai, Robert Hollock, David Linquist, Bill Rowe, Matthew Galla, and Barbara Kennedy. I thank the processing group for their help: Jennifer Lewis, Ann Hardy, Zhiping Jiang, Keigo Hirakata, Satbir Khanuja, Ming Liu and Kozo Sakamato. I would like to thank Dr. Neville Sonnenberg for his help with computers, and Jack Smith, Manfai Ng, and Chun Dong for their help.

I am grateful to several friends for being there: Xiaoquan Zhai, Mita Desai, Fan Zhang, Hua Ai, Guofeng You, Hua Shen, and Jessie Gido. Their friendship and encouragement made life a lot better.

Finally, I would like to thank my family for their love, support, and encouragement. My strong wish is that my farther, Jianyuan Tang, would have lived and witnessed this accomplishment.

# CHAPTER 1

# INTRODUCTION

The role of multilayer ceramic (MLC) technology in the electronic industry continues to expand. Two major MLC devices are multilayer ceramic packages and capacitors[1,2]. MLC packages are mechanically stable dielectric structures through which semiconductor chips are connected to one another or to the rest of the circuit. The MLC capacitors are helpful in reducing the size of electronic circuitry. Other kinds of multilayer ceramic devices include solid oxide fuel cells[3,4], multilayer filters[5], and laminated composites with reinforced mechanical properties[6-8].

Fabrication of multilayer ceramic devices is very complicated. It begins with the casting of thin sheets from a slurry in which ceramic powders are dispersed in a viscous liquid; the liquid contains dissolved organic binder and plasticizer, all diluted in a solvent system. Dried ceramic tapes are then cut to size, punched with via holes (packages), screened with metallic paste (packages, capacitors, and fuel cells), and laminated together to form multilayer greenware. This multilayer greenware is baked to remove the binders of both the ceramic tape and the metallurgy layer, and then fired to consolidate the entire structure.

The organic binder systems used in multilayer devices are critical to the final products, and they have to be completely removed prior to the sintering. The binder system of the ceramic tape has to provide the tape with high tensile and yield strength, sufficient flexibility for handling and machining, dimensional stability over time, and a uniform and reproducible shrinkage during binder removal and sintering. A binder system which satisfies these requirements should include a long chain polymer to provide strength to the film, a plasticizer to increase the flexibility, and a deflocculant to ensure a uniform

dispersion of the ceramic powder. This binder system usually occupies 40 to 50% of the total volume of the tape.

The binder system used for the metallization layer provides the viscosity to the paste required for screen printing, and it has to be compatible with the binder of the ceramic tape. This compatibility requires the following properties: (1) the solvent of the electrode binder should not dissolve the binder of the ceramic tape; (2) the electrode paste has to wet the ceramic tape to ensure a uniform electrode layer.

A major problem in all the multilayer ceramic technologies is delamination, which is defined as a separation along the interface of different materials, after the sintering. Other problems include difficulties for precise dimensional control, retention of carbon in fired products[9], and defects in either the dielectric or the electrode layers such as voids and cracks. Defects in fired MLC structures originate from many sources. One of the main sources is inhomogeneity of the laminated structure before firing. Multilayer ceramic devices are all composite systems. Thus a shrinkage mismatch between different materials, during binder removal and sintering, is inevitable. An example of this mismatch is that between the ceramic layer and the metallic layer in multilayer ceramic packages and capacitors. Structural inhomogeneity can also exist in tape cast ceramic sheets, such as a density gradient across the tape thickness[10,11]. The inhomogeneity in the green sheets tends to be amplified during the binder removal and the firing processes[12]. The resulting inhomogeneous shrinkage creates stresses which result in defect formation. Defects can also be introduced in the binder removal and the firing processes by such mechanisms as bubble formation, cracks, delamination, and carbon retention.

A scientific understanding of the physical and chemical processes in the fabrication of the multilayer ceramic devices is currently lacking, in spite of its importance in several

key electronic applications. The goal of this research, therefore, is to provide an analytical understanding of the microstructure of the greenware and the deformation resulting from the change of this structure during the binder removal process. The materials and manufacturing of different multilayer ceramic devices vary, but many of the basic principles are similar. In this thesis, the multilayer ceramic capacitor is chosen as an example to study. Attention will be paid to the fundamental physical and chemical mechanisms in order to establish relationships among tape casting, binder removal, and the formation of defects in the final products. This will help in the development of new ceramic forming operations and new binder systems.

This thesis starts with an extensive literature review of the processing of multilayer ceramic devices (chapter 2). It includes powder dispersion, tape casting and drying, microstructure characterization of ceramic green tapes, printing of electrode paste, and binder removal from single and multilayer ceramic greenwares. The microstructure characterization and the thermomechanical properties of ceramic green tapes are described in chapter 3. It focuses on the structure of the adsorption layer on the ceramic particles and on the effects of this adsorbed layer on particle packing and the mechanical properties of the tapes. Chapter 4 is devoted to the observation of the deformation of single layer green tapes during the annealing and binder removal processes. This observation provides information on the structural inhomogeneity and anisotropy of the green tapes. In chapter 5, delamination mechanisms during binder removal from MLC greenware are examined. The factors studied are gas generation rate, stress and strain within the sample from shrinkage mismatch between electrode and dielectric layers, and adhesive strength of interlaminar layers. Binder distribution and the dimensional change of the MLC greenwares are presented in chapter 6. The major conclusions of this project are given in chapter 7, along with suggestions for future development.

## References


1. J.R.H. Black, "Technology and Market Trends in Multilayer Ceramic Devices"; pp. 3-11 in Advances in Ceramics, Vol. 19, *Multilayer Ceramic Devices*. Edited by J.B. Blum and W.R. Cannon, American Ceramic Society, Westerville, OH, 1986.

2. R.R. Tummala, "Ceramics in Microelectronic Packaging"; pp. 3-16 in Advances in Ceramics, Vol. 26, *Ceramic Substrates and Packages for Electronic Applications*. Edited by M.F. Yan, K. Niwa, H.M. O'Bryan, Jr., and W.S. Young, American Ceramic Society, Westerville, OH, 1987.

3. S. Iwanaga, T. Fujita, R. Iwamura, H. Yokono, S. Uena, and S. Suzuki, "Fabrication Process of Air-Fuel Ratio Sensor by Using the Green-Sheet Laminating Method"; pp. 49-68 in Advances in Ceramics, Vol. 19, *Multilayer Ceramic Devices*. Edited by J.B. Blum and W.R. Cannon. American Ceramic Society, Westerville, OH, 1986.

4. S. Majumdar, T. Claar, and B. Flaudermeyer, "Stress and Fracture Behavior of Monolithic Fuel Cell Tapes," *J. Am. Ceram. Soc.*, 69 [8] 628-33 (1986).

5. M.J. Cima, private communication.

6. R.E. Mistler, "High-Strength Alumina Sustrates Produced by a Multiple-Layer Casting Technique," *Am. Ceram. Soc. Bull.*, 52 [11] 850-54 (1973).

7. P. Boch, T. Chartier, and M. Huttepain, "Tape Casting of $Al_2O_3/ZrO_2$ Laminated Composites," *J. Am. Ceram. Soc.*, 69 [8] C191-92 (1986).

8. T. Chartier and J.L. Besson, "Behavior of $ZrO_2/Al_2O_3$ Laminated Composites Loaded at Various Mechanical Arrangements"; pp. 639-44 in *Science of Ceramics*, 14. Edited by D. Taylor. The Institute of Ceramics, Stoke-on-Trent, U.K., 1988.

9. R. Higgins, Ph.D. Thesis, Department of Materials and Engineering, Massachusetts Institute of Technology, 1990.

10. R.E. Mistler, D.J. Shanefield, and R.B. Runk, "Tape Casting of Ceramics"; pp. 411-48 in Ceramic Processing Before Firing. Edited by G.Y. Onoda and L.L. Hench. Wiley, New York, 1978.

11. P.R. Nahass, Ph.D. Thesis, Department of Materials and Engineering, Massachusetts Institute of Technology, 1990.

12. W.D. Kingery, "Firing-The Proof Test for Ceramic Processing"; pp. 291-306 in Ceramic Processing Before Firing. Edited by G.Y. Onoda and L.L. Hench. Wiley, New York, 1978.

# CHAPTER 2

# BACKGROUND

## 2.1 Tape Casting and Drying

Ceramic tapes are made by casting a ceramic slurry on a moving substrate with a doctor-blade. This ceramic slurry is usually made by either a ball milling method[1-3] or by ultrasonic dispersion[4]. A well-dispersed, narrow size distribution powder helps prevent segregation of the particles during the drying process[5] and limits the exaggerated grain growth during sintering[6]. This is desired even though a broad particle distribution promotes a lower slurry viscosity and a higher green tape density[7,8].

The slurry is filtered[9] to remove undissolved polymer or large particle agglomerates. Air bubbles created by ball milling and filtering are removed by subjecting the slip to a vacuum[10]. The deaired slurry, with a viscosity range from 1000 to 5000 mPa-s, is cast onto a substrate surface at a speed of 5 to 100 cm/min[2]. The tape is stripped from the substrate after drying and processed much like a paper or leather product.

### 2.1.1 Powder Dispersion

The state of particle dispersion strongly affects the degree of particle packing and sintering behavior of the tape[11,12]. Dispersion stability is controlled by interparticle forces. The ubiquitous van der Waals forces, which are attractive in nature, are present between particles and cause the particles to flocculate. Repulsive forces between particles must exist to counter the van der Waals forces and to provide suspension stability. This can be accomplished when particles develop common surface charges that will provide

electrostatic repulsion between them. Counter-ions in a polar medium will be attracted preferentially to the particle surface and will produce an equilibrium concentration gradient of ions near the surface which is known as the diffuse double layer. This double layer provides repulsive potential and slurry stability.

The stabilization of particles can also be achieved by adsorption of polymers on particle surfaces to provide steric stabilization. A combination of both the electrostatic and steric stabilization is sometimes adopted by adsorbing polyelectrolytes onto the particle surface. The charged polymer chains provide both steric effect and surface charging due to the polymer chains' inherent ionic character. Such stabilization is referred to as electrosteric stabilization, and it is commonly used in the deflocculation of aqueous suspensions of ceramic powders[13,14] and slip casting[15,16].

Electrosteric stabilization of inorganic powders can also be obtained by using surface active agents referred to as surfactants. These surfactants are usually composed of a hydrocarbon chain and a polar or ionic group. They adsorb on particle surfaces by Lewis acid-base interactions[17]. Mikeska *et al.*[18] studied the effect of about 70 commercial dispersants on the stability of $BaTiO_3$ powder dispersion. They concluded that the three most effective dispersants are phosphate ester, an ethoxylate, and menhaden fish oil. Phosphate and ethoxylate are anionic surfactants and the former was shown[18,19] to prevent the flocculation of ceramic powders by an electrosteric mechanism.

Menhaden fish oil is effective as a dispersant for many kinds of ceramic powders[20-23]. It is a mixture consisting primarily of triglycerides. A significant minor component is lecithin (~10%). It was shown[23] that the triglyceride component of the oil provided steric protection and the lecithin generated a zeta potential on the $Al_2O_3$ surface when p-xylene

was used as a solvent. Fish oil does not dissolve in water, therefore, it is only used with organic solvents.

One problem with steric stabilization is that its effectiveness requires the adsorption of dispersant onto the particle surface. Competitive adsorption occurs between the dispersant and the binder[3]. The properties of slurry often change with time due to this adsorption competition. Two approaches can be adopted to overcome this problem. The first approach is to select a binder which can itself provide good dispersion by a steric or electrosteric mechanism. One of the most popular binders for tape casting, polyvinyl butyral (PVB) has been shown[24,25] to provide good dispersion for ceramic powders. Another popular binder for tape casting, polymethyl methacrylate (PMMA), was shown to act as steric stabilizer for silicon slips[26, 27]. The other approach is to choose a dispersant which chemically reacts with the particle surface. These chemically bound dispersants usually have an organometallic compound that reacts with the powder surface, forming a chemical bond[28, 29]. Therefore, this type of dispersant is not subject to desorption.

### 2.1.2 Tape Casting

Green tapes can be cast from a uniform slurry. The casting procedure is shown schematically in Figure 2.1. The flow behavior of the slurry during tape casting has been analyzed[30, 31]. The flow of slurry in tape casting is considered as a combination of pressure flow and Couette flow in the parallel channel of a casting head. The fluid velocity of these two types of flow is shown in Figure 2.2. The flow under the blade is laminar, and the velocity distribution of a slurry between a blade and a carrier film is :

$$V_z = -\frac{\rho g H(x^2 - hx)}{2\eta l} + \frac{V_0 x}{h} \qquad (2.4)$$

where $V_z$ is the velocity at distance $x$ from the blade, $\rho$ and $\eta$ are the density and viscosity

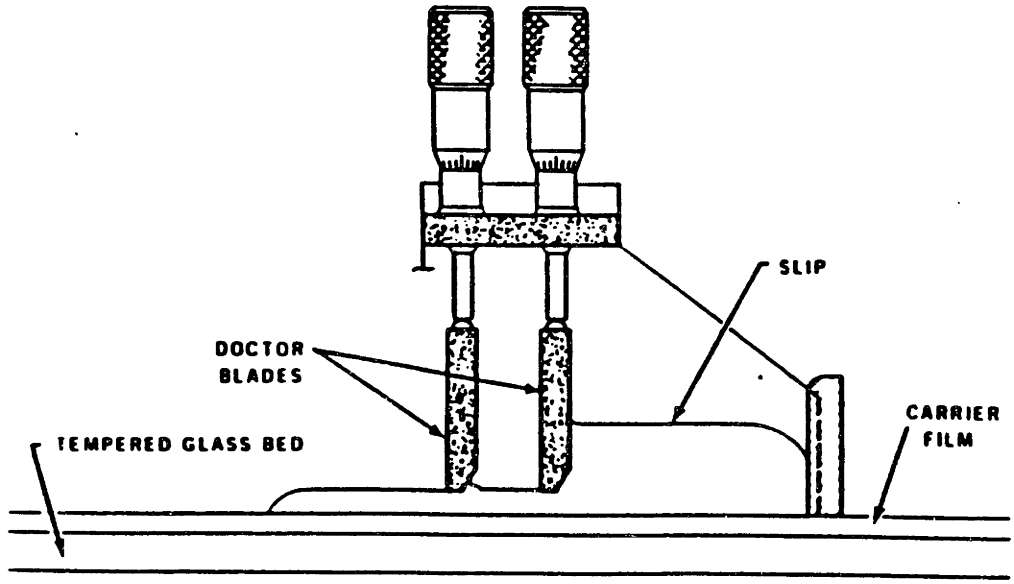


**Figure 2.1. Schematic of the tape casting process (ref. 39)**

of the slurry, $H$ is the height of the slurry between two blades, $h$ and $l$ are the height and length of the blade, respectively, and $V_0$ is the casting speed. The volume flow rate of slurry passing through a unit width of the blade ($Q$) is:

$$Q = \frac{\rho g H h^3}{12\eta l} + \frac{V_0 h}{2} \qquad (2.5)$$

The first terms in 2.4 and 2.5 are related to pressure flow, which is caused by the slurry of height $H$. The second terms are from Couette flow, which is caused by the movement of the doctor blade relative to the substrate. In the precision casting shown in Figure 2.1, $H$ is kept constant by the second blade in contact with the slurry reservoir. The tape thickness is determined by the flow rate, and it is expressed as:

$$\delta_{tp} = \frac{Q}{V_0} = \frac{\rho g H h^3}{12\eta l V_0} + \frac{h}{2} \qquad (2.6)$$

$$\delta'_{tp} = (1-\alpha)\delta_{tp} \qquad (2.7)$$

where $\delta_{tp}$ and $\delta'_{tp}$ are the thickness of wet and dry tape, respectively, and $\alpha$ is linear shrinkage in the thickness during drying. $\alpha$ usually ranges from 0.5 to 0.8[32,33].

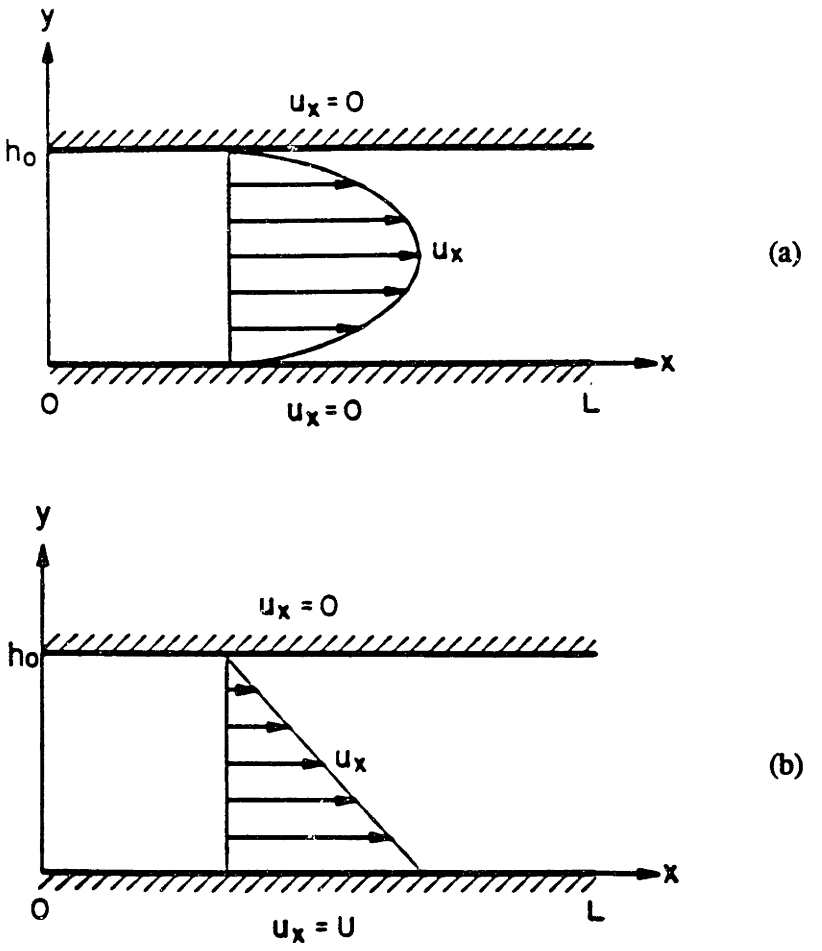


**Figure 2.2. Velocity profile for (a) pressure flow and (b) Couette flow in a parallel channel (ref. 30)**

For a small blade opening or a high casting speed, the pressure flow is insignificant and it can be ignored. Thus, the thickness of the wet tape is approximately half of the height of the doctor blade from the substrate. The velocity gradient (shear rate) is then:

$$D = V_0 / h \qquad (2.8)$$

The casting speed is usually adjusted based on the drying rate and the length of the drying chamber to ensure a dried tape at the end of the drying chamber where the tape is

peeled away continuously. Typical casting speed of thick films (100-500 μm) is 5 to 100 cm/min[2], which corresponds to a 2 to 2000 $min^{-1}$ shear rate. Higher casting speed is usually adopted for thin tapes since shorter drying time is needed. For example, a casting speed of 150 cm/min is chosen for a thin sheet of 35 μm[34], corresponding to a 7000 $cm^{-1}$ shear rate. It is clear that shear rate of thin tapes is higher than thick tapes due to the lower $h$ as well as to the higher $V_0$.

### 2.1.2 Drying of Tape

Drying of the cast tape is usually achieved by either an infrared heater or by convective air while the tape is carried through a chamber on a moving plastic or metal film. In the case of using convective air, the air is blown through the drying chamber in a direction opposite to that of the carrier film motion. This design provides dry air at the end of the chamber where the slip is relatively dry, and nearly solvent-saturated air at the start of the chamber near the doctor blade, where the slip is wet. The design ensures the solvent content of the slip is only slightly higher than the air throughout the whole drying process, so the drying rate is reduced. This slow drying rate has a few advantages. First, it allows the freshly cast wet slip to rearrange itself to a more uniform structure. It has been shown[35] that an uneven surface can be produced from tape casting. This uneven surface has to rearrange itself in order to obtain a uniform and smooth surface in the dried tape. The half-time of the leveling period is[36]:

$$T_{\frac{1}{2}} = C\frac{\eta\lambda^4}{\sigma h^3} \qquad (2.9)$$

where $C$ is a constant, $\eta$ and $\sigma$ are viscosity and surface tension of the slurry, $\lambda$ is the wavelength of the sinusoidal surface profile, and $h$ is the film thickness. Eq. 2.9 shows that the half-time for leveling increases with viscosity. Therefore, it is important to dry slowly at the initial stages to allow the slip enough time to adjust. Another advantage of a

slow drying rate at early stages is to prevent skin formation. Skin formed at the surface from a fast drying rate prohibits air bubbles from floating to the surface, bursting, and disappearing[37,38]. Therefore, it causes defect formation in the green tape.

A two-stage drying is commonly observed[39]. The first stage of drying proceeds at a constant rate, and the second stage at a decreasing rate, as shown in Figure 2.3. The drying process consists of solvent transportation to the sample surface and the evaporation of the solvent at the surface. The first step is liquid transport in the early stage and is fast. Therefore, the drying rate equals the evaporation rate of the slurry, which is close to the evaporation rate of pure solvent[40]. The drying rate rises as the temperature and air flow

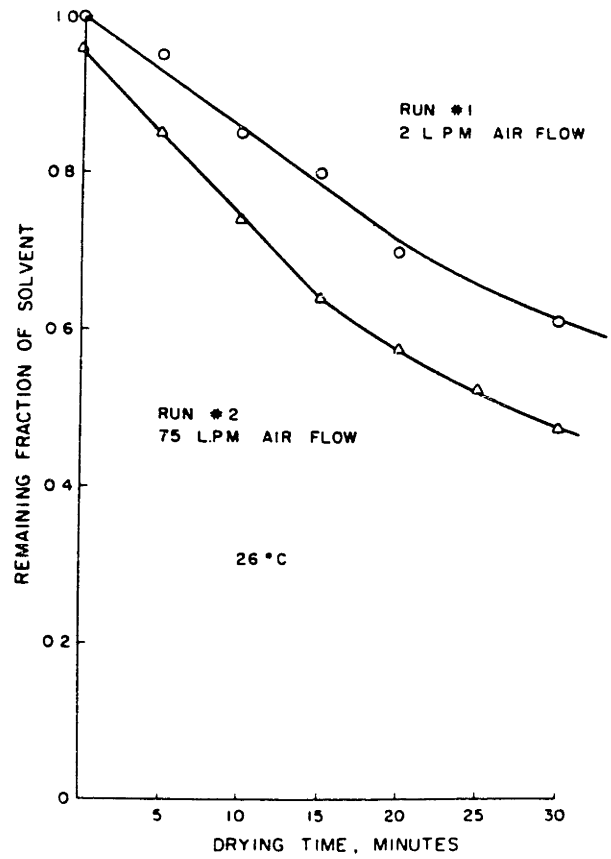


**Figure 2.3. Drying data. Remaining fraction of solvent versus drying time (ref. 39)**

rate increase. A carefully controlled drying experiment conducted by Mistler *et al*[39,41] indicated a drying rate of $1.35\times10^{-5}$ g/cm$^2$·s and $2.22\times10^{-5}$ g/cm$^2$·s at room temperature and at air flow rate of 2 l/min and 75 l/min, respectively. As drying proceeds, the viscosity of the slip increases rapidly, and the transport of the liquid to the surface can no longer keep up with the evaporation from the surface. The drying rate starts to decrease, and it is controlled by the rate at which liquid is transported to the surface.

## 2.2 Characterization of the Green Tape

### 2.2.1 Structure of the Green Tape

Gardner[42] suggested that the packing of particles in a green tape can be divided into two stages as binder content increases. This is shown schematically in Figure 2.4. The first stage is low binder content, and the particle packing density is not affected by the binder content. The particle packing is only determined by the particle size distribution.

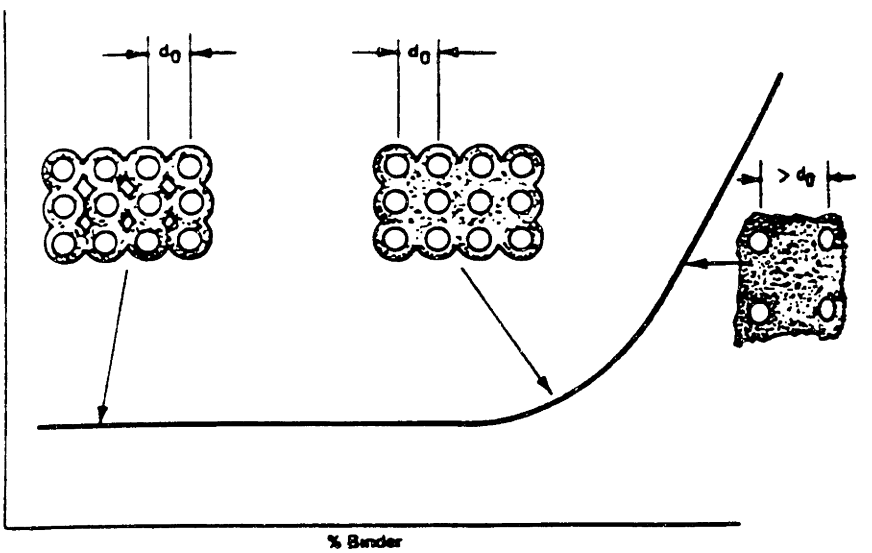


**Figure 2.4. Particle packing versus binder concentration (ref. 42)**

Particle separation increases with binder content in the second stage. The permeability of the tape decreases to a point where the inherent permeability is only governed by the binder.

Asbeck and Van Loo[43] demonstrated that there is a critical particle volume concentration, the CPVC, above and below which many of the physical properties of paint films show dramatic changes. This effect is shown in Figure 2.5. The CPVC corresponds to the particle volume concentration at which the binder just fills the voids between the packed particles. Castells *et al.*[44] extended this concept and proposed a more complete model. A paint film is constituted of particles covered by an adsorption layer, dispersed in a free binder medium. The CPVC of the paint film is the point when particles are in contact through their adsorption layers, and the free binder just fills the interstices between particles. The evidence of an adsorption layer is found in the comparison of experimental

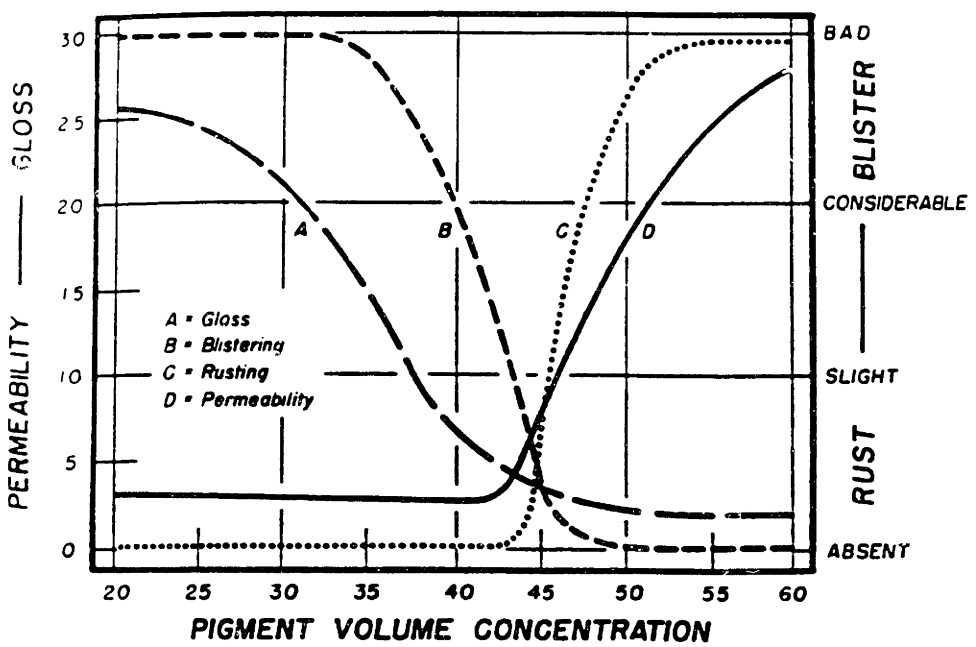


**Figure 2.5. Effect of CPVC on paint characteristics (ref. 43)**

CPVC values with the packing density of dry particles. The adsorption layer prevents particle-particle contacts, and the packing density attainable in paint films is lower than its corresponding dry particle bed.

Increasing particle volume concentration (PVC) above the CPVC cannot promote closer particle approach. There is insufficient free binder to fill the voids between particles, and this volume difference is occupied by air. The adsorbed layer remains unaffected as the increasing of PVC gradually exhausts all the free binder in the system. A point will be reached where the system is only composed of close packed particles with their adsorption layer, and this point is designated as CPVC*. Further increase in the PVC causes the thickness of the adsorption layer to decrease until it reaches zero, where the close packing of dry powder occurs.

### 2.2.2 Properties of the Green Tape

Gardner and Nufer[42] proposed that the following properties of the ceramic tapes are important in the fabrication of MLC substrates: density, tensile strength, and lamination bond strength. (1). Sheet density must be monitored and controlled in order to maintain consistent shrinkage and fired densities when the laminated sample is sintered; (2). High tensile strength is required for dimensional control during sheet processing. Low yield strength materials have large dimensional changes from small applied stresses; these dimensional changes cause misalignments and sheet inhomogeneities; (3). interlaminar bond strength of a laminated MLC structure is important in maintaining substrate integrity after lamination and during binder removal. Metallized ceramic sheets must bond well to each successive layer following lamination, particularly around the edge of the electrode print. Otherwise, viscoelastic recovery of the polymer may cause delamination in the greenware. Good bond strength between the electrode and ceramic

layers is also essential during the initial binder removal process when volatile organics evolve from the electrode paste. These volatiles subject the MLC package to internal pressures capable of causing delamination, if this bond is weak.

The mechanical properties of ceramic green sheets are determined by their composition and by the interaction between ceramic particles and polymer binders. Gardner[42] showed that finer ceramic particles, higher binder content, and higher ratio of polymer to plasticizer result in higher tensile strength of the green tape and higher bond strength. The size distribution of the ceramic particle also affects the properties of the green sheet. Mixing of coarse and fine particles tends to increase the bond strength and decrease the porosity of the green tape[42]. Karas *et al*[45] further showed that both the tensile strength and the elongation to failure of the tape increased with the increasing binder concentration. Addition of dispersant increased the density of green tapes, however, the strength and elongation to failure decreased monotonically with increased dispersant[45].

The strength of the green tape is also affected by drying conditions. It has been shown[46] that a tape dried on the glass substrate had a continually decreasing strength with increasing drying time, whereas if the tape was removed from the substrate 1 hour after the casting, and allowed to dry in air, the strength of the tape increased with the drying time. The detrimental effect of the glass substrate is believed[46] to be caused by the strong bond between the glass and the tape. As the tape dries, its top surface is allowed to shrink but the bottom surface is not, the resulting tensile stresses on the top surface may allow cracks to form during drying. However, no cracks were actually observed in this experiment.

### 2.2.3 Inhomogeneity and Anisotropy of the Tape

Inhomogeneity of the tape has been observed both in the green tape and through the evaluation of firing shrinkage. Shanefield[1] pointed out that after the porosity between ceramic particles is filled, further addition of binder causes segregation of binder to the top surface. A slightly binder-rich top region of the tape was observed by Mistler[39] and Nahass[47], through the TGA results of thin slices cut from top and bottom sections of the tape. Settling of the particles during the drying process is believed[39,47] to be responsible for this inhomogeneity across the thickness direction.

Nahass[47] examined the dimensional change of green sheet under controlled aging conditions and in the firing process. Two kinds of binder systems were used: an aqueous, emulsion-based system and an organic solvent-based slurry. Green tapes from the solvent-based slurry experienced much higher linear shrinkage, and higher anisotropy of shrinkage than tape from the emulsion-based system. Samples from both systems experienced higher shrinkage in the casting direction compared to that in the transverse direction. Shrinkage in all samples was inversely proportional to the amount of the immobile organic phase which is attached to the ceramic particle surface. Shrinkage under controlled aging conditions is believe to be caused by relaxation of residual stresses in the polymer binder that resulted from constrained drying and polymer-ceramic interactions. Firing shrinkage in tapes from solvent-based formulations also showed greater values in the casting direction than that in transverse direction, although the ratio was only 1.01 to 1.02. Tape from the aqueous system had less shrinkage in the casting direction than that in the transverse direction, the ratio was 0.96 to 0.98.

It was found[48,49] that the shape of ceramic particles has a strong effect on the anisotropic properties of the sheet. While tape cast from equiaxed particles has nearly

isotropic firing shrinkage, tape cast from flat platelike particles has much higher shrinkage in the thickness direction than the in-plane directions. This anisotropic sintering shrinkage is caused by the alignment of particles with their large dimensions parallel to the casting surface. Commercially available green tapes[50] also exhibit sintering shrinkage anisotropy. The shrinkage in thickness is 47% higher than that of the in-plane directions. No in-plane anisotropic shrinkage have been observed in these tapes.

Anisotropic properties of green tape are usually undesirable, especially the in-plane properties. It is a common practice, when stacking alternating layers in the laminated structures, to rotate adjacent layers by 90°. This minimizes the differential shrinkage of the laminated package[51]. However, in the production of electromechanical transducers, highly anisotropic properties are desired. Grain-oriented transducer materials can be made from powders with shape anisotropy, by tape casting[52]. The degree of preferred orientation of cast platelike powders is weak in the green tape, but was enhanced greatly by densification and grain growth during sintering[53-56]. The degree of orientation in the fired product can be as high as 98%[54].

The above mentioned limited characterizations of the ceramic green sheets were performed on electronic package substrates, with the thickness of tapes ranging from 100 to 500 μm. No publication has been found in the characterization of the thin films (20-50μm) used as dielectrics in multilayer ceramic capacitors. As more and more effort is directed toward improving and reducing the size of electronic circuitry, the demand for quality and reliability of thin dielectric layers continues to rise. The uniformity of the very thin film becomes a major concern of multilayer manufactures. The shear effect in the casting of thin films is much higher than in thick films since shear rate is inversely proportional to the casting thickness. Also the drying time of the thin film is short, which gives the slip less time to relax to its equilibrium state after the casting. The constraint

from the substrate during drying of the thin film is also a lot higher than that of the thick film. Therefore, a characterization of structure and properties of thin tape-cast sheets is important in order to understand the tape casting and the drying mechanism, so as to optimize the processing conditions.

## 2.3 Binder removal

Binder removal process from MLC greenware is a complex phenomenon which involves simultaneous, coupled chemical and physical processes. Chemical processes involve the degradation of polymers, reactions between polymers and the surface of ceramic powders, and reactions between polymers and surface of metal electrode powders. Physical processes such as mass and heat transport are also important. Previous research has focused on studying the thermolysis process of single layer ceramic sheets[57,58] and injection molded bulk ceramic bodies[59-64]. Little is known, however, about the thermolysis of binders in the electrode print and the transport processes in multilayer greenware such as multilayer ceramic capacitors and multilayer ceramic substrates. This review begins with a discussion of the chemical and physical processes during binder removal from single layer ceramic tape. This discussion will be helpful in understanding the transport processes during binder removal from MLC structures.

### 2.3.1 Thermal Degradation of Polymers

The most effective binder for providing all the required thermoplastic properties and bond strength between layers is polyvinyl butyral (PVB)[65]. Other binders used in certain applications are polymethyl methacrylate (PMMA), polyvinyl chloride acetate, polyisobutylene (PIB), polyalphamethyl styrene (PAMS), nitrocellulose, cellulose acetate, and cellulose acetate butyral. The chemical formula of PVB is shown in Figure 2.6.

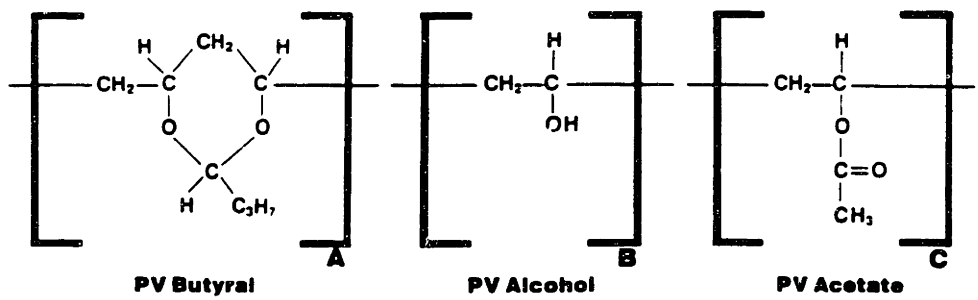


**Figure 2.6 Chemical formula of PVB (ref. 76)**

The pyrolysis mechanism of both pure PVB and PVB/$Al_2O_3$ mixtures has received some amount of study[67-70]. These studies show that the initial degradation of pure PVB occurs by side-chain scission, which involves the loss of water, butanol, and acetic acid. The long organic chains, which are left with appreciable unsaturation and conjugation, subsequently undergo a variety of degradation pathways resulting in the production of many types of volatile substances such as olefinic, aromatic, ketonic, and phenolic compounds. Crosslinking and cyclization reactions also occur during this period, followed by a slow break down of the crosslinking and cyclization byproducts at higher temperatures.

Masia[69] has shown that addition of various oxides decreases the temperature at which both the initial and the subsequent stages of PVB decomposition occurs. The mechanism of this catalysis reaction, however, is unclear. Formation of carbon residue occurs on the ceramic surface which is only removed at very high temperatures (800-1000°C). Howard[70] found that the acetate functionality (C=O) of the PVB polymers interacts with the $Al_2O_3$ surface, which causes a retention of organic species, up to 550°C, on the surface of $Al_2O_3$ powders.

### 2.3.2 Mass Transport

Mass transport in MLC greenware during the binder removal process is very complicated. At low temperature, the evaporation of volatile products occurs. This includes residual solvent, plasticizer, and some low-molecular weight oligomers in the binder systems. As the temperature increases, the degradation of polymers occurs, which produces a large amount of volatile products. These products need to diffuse to the surface of the sample and evaporate. During the binder removal process, the inorganic filling such as ceramic powders and electrode powders are not static either. They are either under tensile or compressive pressure, this pressure can alter their packing density. Therefore, a completely understanding of the binder removal process needs to take into account the following transport phenomena: Capillary flow of liquid, convective flow and diffusion of gas, heat transfer by conduction and convection within the body, and repacking of solid particles.

Although there has not been any publication on mass transport in MLC greenware, mass transport in both single layer cast ceramic tape and injection-molded bulky ceramic bodies have received some attention. The results are summarized below.

The binder removal process from injection molded greenbodies has been divided into three stages[71]. During the first stage, thermal expansion of the liquid binder induces hydraulic pressure in the fully saturated compact. The pressure gradient within the sample serves as a driving force for the flow of the melted binder towards the surface. As the temperature rises, binder evaporation from surface increases. When saturation levels begin to decline, the second stage starts. Capillary pressure brings the binder to the surface where it can evaporate freely. As this process continues, gas pockets begin to coalesce and form a network of interconnected conduits. Eventually, gas flow and

diffusion process will play a part in mass removal. But still, capillary action is expected to remain relatively dominant. When the temperature exceeds the degradation limit for the binder, the third stage starts. The viscosity decreases during this stage, which results in a great increase in removal rates.

Barone[72] and coworkers studied the binder distribution and transient temperature at various sites within injection molded specimens. Two kinds of binders were used separately: a paraffin wax and polyethylene. At low temperature, evaporation or degradation followed by evaporation (in the case of polyethylene) dominated the binder removal process. At high temperature, an oxidation of the binder took place everywhere within the specimen, which raised the peak temperature of the sample to 200°C higher than the furnace temperature. The binder distribution within the specimen remained uniform throughout the binder removal process.

The microstructure of the ceramic compact has a profound effect upon the binder removal. Pore size[58,73,74] and particle size distributions[73,74] have been suggested to directly affect the flow of liquid binder and evolved gases within the material. High particle packing density or small particle size creates small pores, which in turn increases the resistance toward gas diffusion and convection, and thus slows down the binder removal process.

The mass transport mechanisms within tape-cast greenware are not exactly the same as in injection-molded specimens. The viscosity of binder systems in the tape-cast samples is a lot higher($-10^5$p)[75] than that of binder systems in injection-molded samples ($-10^2$p). Despite of the previous suggestion that capillary action requires low viscosity systems such as waxes and oils[76], capillary forces are still shown to influence binder distribution within the tape-cast sample[57]. The flow of dibutyl phthalate (DBP) plasticized PVB

binder under the influence of capillary forces has been directly observed by Cima[77]. Cima and his coworker's work[57,77,78] showed that the distribution of binder within a greenbody can be governed either by diffusion of volatile species within the polymeric phase or by liquid transport driven by capillary pressure. A scaling model was developed to approximate the maximum length scale over which capillary forces dominate:

$$\frac{h}{d} = \frac{\Delta\Phi\varepsilon^3}{18K(1-\varepsilon)^2} \cdot \frac{\gamma}{\upsilon G} \qquad (2.10)$$

where $h$ is the distance over which the fluid binder can flow, $d$ is the particle diameter, $\Phi$ is a factor dependent on the packing arrangement of the particles, $\varepsilon$ is the void fraction of the porous body, $K$ is a constant that accounts for pore geometry, $\gamma$ is the surface tension of the liquid, $\nu$ is the kinematic viscosity ($=\mu/\rho$) and $G$ is the mass flux.

The characteristic length scale for capillary flow, $h$, is large during the initial stage of binder removal, h is very high, usually of the order of the thickness of the tape. Capillary forces dominate the binder removal process. As temperature increases, mass flux ($G$) increases rapidly, which causes $h$ to decrease until it becomes much smaller than the dimensions of tape. At this point, diffusion in the developing polymer film starts to dominate the binder removal process.

The development of quantitative models of the binder removal has been slow, given the extremely complicated system. Some progresses has been made in evaluating basic mechanisms governing mass transport, usually in a simplified model system, although a fundamental description of simultaneously occurring transport phenomena is absent. Started with a water-bound compact containing 10-μm particles, German[79] identified when thermal debinding is controlled by either pressure-driven gas flow, gas permeation, or wicking. Each mechanism was analyzed separately for a one-dimensional compact under steady-state conditions. During gas flow and permeation, the liquid binder was

assumed to recede quasi-statically from the boundary. Wicking, on the other hand, was assumed to occur under fully saturated conditions when flow resistance is minimal. Consequently, the estimated removal rates tend to be considerably higher than anticipated. Later, Calvert and Cima[80] investigated gas flow and permeation of a PMMA binder burnout from a ceramic green body. Assuming a sharp interface of liquid retreats into the green body as the polymer is removed, a steady-state diffusion of volatile monomer in the liquid binder is calculated to determine the concentration of monomer in the green body. The estimated safe removal times were extremely long for any sample exceeding 3 mm in thickness. Calvert and Cima also indicated that transport kinetics are significantly improved if continuous porosity develops in the piece during the early stages of decomposition. A more complete model by Stangle and Aksay[81] considers simultaneous momentum, heat and mass transfer with chemical reaction and evaporation in a disordered porous medium. This model takes into account liquid transport via capillary action, gas transport by convection and diffusion, and phase change by chemical reaction and evaporation. Simulations based on the model can predict the local temperature and mass distribution of the porous body as a function of time and position. Combining this information with known mechanical properties of the body, one can also predict internal stresses generated during removal of liquid from the body. Stangle employed paraffin wax as an example binder system to evaluate this model. Due to the low viscosity of paraffin wax, this system is more similar to the drying process than to the binder removal process. The application of this model to an actual viscous, multicomponents binder system is almost impossible, since it requires a large number of physical, kinetic, and thermodynamic properties for each component.

A major assumption in existing models of mass transport, during binder removal from ceramic greenbodies, is that the ceramic compact is a rigid porous media. The pore structure and particle packing are unaltered by the liquids and gases motions within the

sample. This assumption is reasonable only when the loading of solid particles is very high ($V_{ceramics} \sim V_{max}$), in which case the solid particles are close packed before binder removal starts. But in most of the cases, the initial packing density of solid particles is far below the close packing density, a substantial particle repacking occurs under the capillary pressure. Wright[56] showed that the linear shrinkage of an injection-molded body can be as high as 5.8% in the binder removal process. Tang and Cima[82] showed that in the early stages of binder removal, the shrinkage of the greenware is equal to the volume of the binder lost by evaporation. Apparently, the rigid skeleton assumption is not applicable in these circumstances.

### 2.3.3 Defect Formation in Binder Removal Process

As mentioned before, the major defects which form during the binder removal process are voids, cracks, and delaminations. It is believed that during the binder removal process, the rate of gas generation in the ceramic compact has to be controlled to keep it within the transport capability of the porosity of the compact[83,84]. Otherwise, the increasing gas pressure will cause defects such as delamination and/or voids in the ceramic greenbody.

The formation of bubbles during the binder burnout process has been directly observed by Dong[85]. Her work with a PMMA binder showed that bubbles formed from both residual solvent and polymer degradation. The ceramic particle surfaces act as heterogeneous nucleation sites for the formation of bubbles; the nucleation temperature increases as the heating rate increases. Other factors that affect the nucleation of bubbles on the particle surfaces are the wetting angle of the fluid on the surface, the interface tension, and the curvature of the particle surface. The growth of bubbles is mainly controlled by viscosity, surface tension of the molten binder, and the diffusivities of the

various volatile species. All these properties are functions of temperature and heating rate[86]. It is believed[87] that the growth of the delamination is first controlled by the surface tension of the liquid binder. As the process continues, the liquid viscosity starts to dominate the growth rate[87]. After the binder is partially removed, the bubbles start to shrink. The shrinkage of the gas bubble is mainly controlled by gas diffusion out of the bubbles[88].

The major defect which occurs in MLC's is delamination. A typical quality control procedure involving a destructive physical analysis (DPA) defines a major delamination defect as either (1) any delamination or void which is greater than one half of the dielectric thickness, or (2) any delamination or void which leaves adjacent electrodes in contact with each other. An extreme case was reported[89] with a DPA test of 2000 multilayer ceramic capacitors which revealed 61% of the samples were delamination-free, 19% of the samples had minor delaminations, and 20% of the samples had major delaminations. Delamination is affected by both the gas pressure within the electrode layer and by the adhesive and cohesive bond strength of the paste[41]. The gas pressure is determined by the local temperature, the local oxygen partial pressure, the physical properties of the binder systems, and the pore structure of both the ceramic tape and the electrode layer. Pepin[90] described four electrode-based causes of delamination in multilayer ceramic capacitors. They are: high amounts of organic resins in the electrode vehicle, green-state delaminations due to lack of adhesion of the dried electrode print to the dielectric tape, catalytic reactions of the electrode precious metal powders with the organics during burnout, and mismatch of the densification characteristics of the electrode and dielectric during firing. Since delamination occurs either on the interface of the electrode and dielectric or within the electrode layer, a complete understanding of the physical and chemical process that occur in both the electrode and dielectric, and the interaction between them, is necessary to eliminate delamination.

## 2.4 Screening of Electrode paste and Binder Removal

The application of electrode paste to the ceramic tape is achieved by screen printing. This method enables the printing of many components with the single stroke of a squeegee. Electrode inks used for screen printing have complicated rheological behavior[91]. The inks are usually highly pseudoplastic, or binham. They have low enough viscosity during screening but high viscosity once deposited, so that the slip does not run and level out throughout the surface area[92,93]. A schematic of the viscosity change of an ink during screen printing is shown[94] in Figure 2.7. The paste has a relatively high initial viscosity prior to printing, which is reduced by stirring and transferring to the stencil screen. Further reduction in viscosity is caused by the swiping action of the squeegee. The paste is subjected to a high shear rate when it is forced through the screen, and the viscosity drops rapidly. The viscosity starts to increase immediately after the paste being transferred to substrate, as the material recovers its structure.

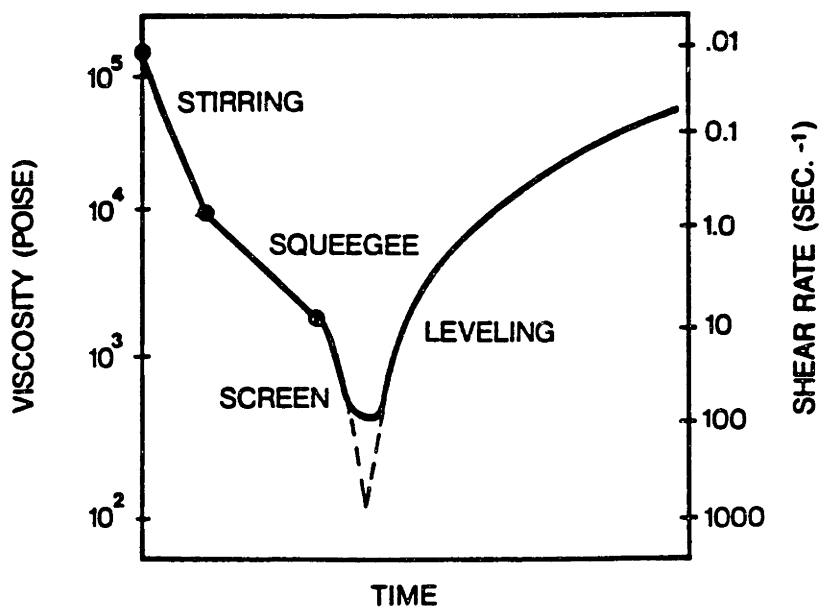


**Figure 2.7. Viscosity changes of a paste during screen printing (ref. 94)**

The binder system based on cellulose and its derivatives satisfies the above requirements[95]. The binder provides the viscosity required for screen printing, and it has to be burned out prior to sintering. While an extensive literature on the degradation of cellulose itself exists, only comparatively few studies have been done on cellulose derivatives.

Cellulose has been shown to degrade and give a complex mixture of compounds; the mechanisms of formation of these compounds are not well understood. Ethyl cellulose[96] is shown to degrade in vacuum, initially by scission of glycoside C-O bonds, followed by a number of competing reactions including depropagation, random scission, and dehydration. These reactions lead to crosslinking of polymer chains. A variety of volatile products such as $H_2O$, CO, $CO_2$, $C_2H_4$, $C_2H_6$, $C_2H_5OH$, $CH_3CHO$, unsaturated aliphatic compounds and furan derivatives are produced. The thermal degradation of one of the widely used ink binders, EHEC, has not been studied. Research on the pyrolysis of cellulose and its derivatives in the presence of metal powders, is lacking.

## REFERENCE


1. D.J. Shanefield, "Casting Ceramic-Polymer Sheets," pp. 69-76 in *Mat. Res. Soc. Symp. Proc.*, vol.40, 1985.

2. R.E, Mistler, "Tape Casting: The Basic Process for Meeting the Needs of the Electronics Industry," *Am. Ceram. Soc. Bull.*, [69], 1022-26, 1990.

3. J.B. Blum and W.R. Cannon, "Tape Casting of $BaTiO_3$," pp.77-82 in *Mat. Res. Soc. Symp. Proc.*, vol.40, 1985.

4. R.J. Mackinnon and J.B. Blum, "Ultrasonic Dispersion of $BaTiO_3$ Tape Casting Slurry," pp.158-63 in Advances in Ceramics, vol. 9, *Forming of Ceramics*, Edited by J.A. Mangels and G.L. Messing, American Ceramic Society, Columbus, Ohio, 1984.

5. E.S. Tormey, R.L. Pober, H.K. Bowen, and P.D. Calvert, "Tape Casting--Future Development," pp140-49 in Advances in Ceramics, Vol.9, *Forming of Ceramics,* Edited by J.A. Mangels, and G.L. Messing, American Ceramic Society, Columbus, Ohio, 1984.

6. M.F. Yan, "Microstructural Control in the Processing of Electronic Ceramics," *Mater. Sci. Eng.*, 48, 53-72 (1981).

7. R.J. Mackinnon and J.B. Blum, "Particle Size Distribution Effects on Tape Casting Barium Titanate," pp. 150-57 in Advances in Ceramics, Vol. 9, *Forming of Ceramics*, Edited by J.A. Mangels, and G.L. Messing, American Ceramic Society, Columbus, Ohio, 1984.

8. J.S. Chong, E.B. Christiansen, and A.D. Baer, "Rheology of Concentrated Suspensions," *Journal of Concentrated Suspensions,* 15, 2007-2021, (1971).

9. D.J. Shanefield, R.E. Mistler, "Filter for Ceramic Slips," *Am. Ceram. Soc. Bull.*, 55 [2], 213, 1976.

10. E.P. Hyatt, "Making Thin, Flat Ceramics-A Review," *Am. Ceram. Soc. Bull.*, 65 [4], 637, 1986.

11. Roosen, "Basic Requirements for Tape Casting of Ceramic Powders", PP. 675-92 in Ceramic Transactions, Vol. 1, *Ceramic Powder Science II, B/* Edited by G.L. Messing, E.R. Fuller, and H.Hausner. American Ceramic Society, Westerville, OH, 1988.

12. T. Ueyama and N. Kaneko, "Effect of Agglomerated Particles on Properties of Ceramic Green Sheets"; pp. 1451-58 in *High Tech Ceramics.* Edited by P. Vincenzini. Elsevier, Amsterdam, Netherlands, 1987.

13. J. Cesarano III, I.A. Aksay, and A. Bleier, "Stability of Aqueous $\alpha$-$Al_2O_3$ Suspensions with poly (Methacrylic Acid) Polyelectrolyte," *J. Am. Ceram. Soc.*, 71 [4] 250-55 (1988).

14. N. Ushifusa and M.J. Cima, "Aqueous Processing of Mullite-containing Green Sheets," *J. Am. Ceram. Soc.*, 74[10] 2443-47 (1991).

15. A.J. Ruys and C.C. Sorrell, "Slip Casting of High-Purity Alumina Using Sodium Carboxymethylcellulose as Deflocculant/Binder," *Am. Ceram. Soc. Bull.*, 69 [5], 828-32 (1990).

16. J. Cesarano III and I.A. Aksay, "Processing of Highly Concentrated Aqueous $\alpha$-$Al_2O_3$ Suspensions Stabilized with Polyelectrolytes," *J. Am. Ceram. Soc.*, 71 [12] 1062-67 (1988).

17. F.M. Fowkes, "Dispersion of Ceramic Powders in Organic Media"; pp. 411-21 in Advances in Ceramics, Vol. 21, *Ceramic Powder Science.* Edited by G.L. Messing, K.S. Mazdiyasni, J.W. McCauley, and R.A. Haber. American Ceramic Society, Westerville, OH, 1987.

18. K. Mikeska and W.R. Cannon, "Dispersants for Tape Casting Pure Barium Titanate"; pp. 164-83 in Advances in Ceramics, Vol. 9, *Forming of Ceramics.* Edited by J.A. Mangels and G.L. Messing. American Ceramic Society, Columbus, OH, 1983.

19. T. Chartier, E. Streicher, and P. Boch, "Phosphate Esters as Dispersants for the Tape Casting of Alumina," Am. Ceram. Soc. Bull., 66[11] 1653-55 (1987).

20. P.D. Calvert, E.S. Tormey, and R.L. Pober, "Fish Oil and Triglycerides as Dispersants for Alumina," *Am. Ceram. Soc. Bull.*, 65 [4] 669-72 (1986).

21. R.E. Mistler, "High-Strength Alumina Substrates Produced by a Multiple-Layer Casting Technique," *Am. Ceram. Soc. Bull.*, 52 [11] 850-54 (1973).

22. V.L. Richards II, "Adsorption of Dispersants on Zirconia Powder in Tape-Casting Slip Compositions," *J. Am. Ceram. Soc.*, 72 [2] 325-27 (1989).

23. R.E. Johnson, Jr. and W.H. Morrison, Jr., "Ceramic Powder Dispersion in Nonaqueous Systems"; pp32-48 in Advances in Ceramics, Vol. 21, *Ceramic Powder Science.* Edited by G.L. Messing, K.S. Mazdiyasni, J.W. McCauley, and R.A. Haber. American Ceramic Society, Westerville, OH, 1987.

24. H. Watanabe, T. Kimura, and T. Yamaguchi, "Particle Orientation During Tape Casting in the Fabrication of Grain-Oriented Bismuth Titanate," *J. Am. Ceram. Soc.*, 72 [2] 289-93 (1989).

25. M.D. Sacks, C.S. Khadilkar, G.W. Scheiffele, A.V. Shenoy, J.H. Doe, and R.S. Sheu, "Dispersion and Rheology in Ceramic Processing"; pp. 495-515 in Advances in Ceramics, Vol. 21, *Ceramic Powder Science.* Edited by G.L. Messing, K.S. Mazdiyasni, J.W. McCauley, and R.A. Haber. American Ceramic Society, Westerville, OH, 1987.

26. A.V. Kerkar, R.J.M. Henderson, and D.L. Feke, "Steric Stabilization of Nonaqueous Silicon Slips: I, Control of Particle Agglomeration and Packing," *J. Am. Ceram. Soc.*, 73 [10] 2879-85 (1990).

27. A.V. Kerkar, R.J.M. Henderson, and D.L. Feke, "Steric Stabilization of Nonaqueous Silicon Slips: II, Pressure Casting of Powder Compacts," *J. Am. Ceram. Soc.*, 73 [10] 2886-91 (1990).

28. R. Laible and K. Haman, "Formation of Chemically Bound Polymer Layers on Oxide Surfaces and Their Role in Colloidal Stability," *Adv. Colloid Interface Sci.*, 13, 65-99 (1980).

29. M. Green, T. Kramer, M. Parish, J. Fox, R. Lalanandham, W. Rhine, S. Barclay, P. Calvert, and H.K. Bowen, "Chemically Bonded Organic Dispersants"; pp. 449-65 in Advances in Ceramics, Vol. 21, *Ceramic Powder Science.* Edited by G.L. Messing, K.S. Mazdiyasni, J.W. McCauley, and R.A. Haber. American Ceramic Society, Westerville, OH, 1987.

30. Y.T. Chou, Y.T, Kom and M.F. Yan, "Fluid Flow Model for Ceramic Tape Casting," *J. Am. Ceram. Soc.*, 70 [10], c-280-82, (1987).

31. K. Otsuka, Y.Ohsawa, and K. Yamada, "A study on the Alumina Ceramic Casting Conditions by the Doctor-Blade Method and Their Effect on the Properties of Green Taps (Part 1)," *Yogyo Kyokaishi*, 94 [3] 49-57 (1986).

32. K.E. Burnfield and B.C. Peterson, "Cellulose Ethers in Tape Casting Formulations"; pp. 191-96 in Ceramic Transactions, vol. 26, Forming Science and Technology for Ceramics, Edited by M.J. Cima. The American Ceramic Society, Westerville, Ohio, 1991.

33. E. Streicher, T. Chartier, and P. Boch, "Study of Cracking and Microstructural Evolution During Drying of Tape Cast Aluminum Nitride Sheets," *J. Mater. Sci.*, 26, 1659-65 (1991).

34. A.D. Devoe, Private communication, MIT, 1992.

35. M. Yasrebi, "Microstructural Development in Ceramic-Polymer Systems"; Ph.D. Thesis. Dept. Mat. Sci. Eng., University of Washington, pp.47, 1988.

36. S.E. Orchard, "On Surface Leveling in Viscous Liquids and Gels," *Appl. Sci. Res.*, Sect. A, 11, 451-464 (1962).

37. D.J. Shanefield, "Competing Adsorption in Tape Casting," pp. 155-160 in Advances in Ceramics, Vol. 19, Multilayer Ceramic Devices, Edited by J.B. Blum and W.R. Cannon. American Ceramic Society, Westerville, Ohio, 1986.

38. E.B. Gutoff, "Avoid Coating and Drying Defects," *Chem. Eng. Prog.*, [1], 49-55 (1993).

39. R.E. Mistler, D.J. Shanefield, and R.B. Runk, "Tape Casting of Ceramics," pp. 411-48 in *Ceramic Processing Before Firing*. Edited by G.Y. Onoda and L.L. Hench. Wiley, New York, 1978.

40. R.K. Dwivedi, "Drying Behavior of Alumina Gels", *J. Mater. Sci. Lett.*, 5, 373-76 (1986).

41. D.J. Shanefield, Rutger University, private communication, 1993.

42. R.A. Gardner and R.W. Nufer, "Properties of Multilayer Ceramic Green Sheets," *solid state technol.*, 17, 38 (1974)

43. W.K. Asbeck, and M. Van Loo, "Critical Pigment Volume Relationships," *Ind. Eng. Chem.*, 41, 1470-75 (1949).

44. R. Castells, J. Meda, J.Caprari, and M. Damia, "Particle Packing Analysis of Coatings Above the Critical Pigment Volume Concentration," *Journal of Coatings Technology,* 55, No. 707, 53-59 (1983).

45. A. Karas, T. Kumagai, and W.R. Cannon, "Casting Behavior and Tensile Strength of Cast $BaTiO_3$ Tape," pp. 374-77 in Advanced Ceramic Materials, 3 [4], 1988.

46. S. Forte, J.R. Morris, Jr., and W.R. Cannon, "Strength of Tape Casting Tape," *Am. Ceram. Soc. Bull.*, 64 [5], 724-25, 1985.

47. P.R. Nahass, Ph.D. Thesis, Department of Materials and Engineering, Massachusetts Institute of Technology, 1990.

48. S. Ohtomo, M. Kato, and K. Korekawa, "Firing Shrinkage of Alumina Green Sheets," *Yogyo-Kyokai-Shi,* 94 [2], 23-29, 1986.

49. F.V. Dimarcello, P.L. Key, and J.C. Williams, "Preferred Orientation in $Al_2O_3$ Substrates," *J. Am. Ceram. Soc.*, 55 [10], 509-14 (1972).

50. Du Pont Electronics, "Green Tape Materials for Ceramic Circuits," Ceramic circuit materials and technology catalog. 1989.

51. J.I. Steinberg, S.J. Horowitz, and R.J. Bacher, "Low Temperature Cofired Tape Dielectric Materials Systems for Multilayer Interconnections"; pp. 302-16 in Processing of the 5th European Hybrid Microelectronics Conference, Stresa, Italy, 1985.

52. G.O. Dayton, W.A. Schulze, T.R. Shrout, S. Swartz, and J.V. Biggers, "Fabrication of Electromechanical Transducer Materials by Tape Casting"; pp. 115-139 in Advances in Ceramics, Vol.9, *Forming of Ceramics*, Edited by J.A. Mangels, and G.L. Messing, American Ceramics Society. Columbus, Ohio, 1984.

53. T. Kimura, M.H. Holmes, and R.E. Newnham, "Fabrication of Grain-Oriented $Bi_2WO_6$ Ceramics," *J. Am. Ceram. Soc.*, 65 [4] 223-6 (1982).

54. S.H. Lin, S.L. Swartz, W.A. Schulze, and J.V. Biggers, "Fabrication of Grain Oriented $PbBI_2Nb_2O_9$ Ceramics," *J. Am. Ceram. Soc.*,

55. R.H. Arendt, "The Molten Salt Synthesis of Single Magnetic Domain Barium Iron Oxide ($BaFe_{12}O_{19}$) and Strontium Iron Oxide ($SrFe_{12}O_{19}$) Crystals," *J. Solid State Chem.*, 8 [4] 339-47 (1973).

56. R.H. Arendt, J.H. Rosolowski, and J.W. Szymasek, "Lead Zirconate Titanate Ceramics from Molten Salt Solvent Synthesized Powders," *Mat.Res. Bull.*, 14 [5] 703-9 (1979).

57. M.J. Cima, J.A. Lewis, and A.D. Devoe, "Binder Distribution in Ceramic Greenware During Thermolysis," *J. Am. Ceram. Soc.*, 72, 1192-99 (1989).

58. D.W. Sproson and G.L. Messing, "Organic Removal Processes in Closed Pore Powder-Binder System," pp. 528-37 in Ceramic Transactions: Ceramic Powder Processing Science. Edited by G.L. Messing, E.R. Fuller, Jr., and H. Hausner. American Ceramic Society, Westerville, OH, 1988.

59. T. Zhang, Z. Chen, Z. Jiang, and J. Wu, "The Mechanism of the Thermal Extraction of Organic Binders From Injection Molded Ceramic Bodies"; pp. 219-26 in *Ceramic Materials and Components for Engines*. Edited by V.J. Tennery. The American Ceramic Society, Westerville, OH, 1989.

60. J.K. Wright, M.J. Edirisinghe, J.G. Zhang, and J.R.G. Evans, "Particle Packing in Ceramic Injection Molding," *J. Am. Ceram. Soc.*, 73, 2653-8 (1990).

61. C.A.Sundback, M.A. Costantini, and W.H. Robbins, "Part Distortion During Binder Removal"; pp. 191-200 in *Ceramic Materials and Components for Engines*. Edited by V.J. Tennery. The American Ceramic Society, Westerville, OH, 1989.

62. J.K. Wright, J.R.G. Evans, and M.J. Edirisinghe, "Degradation of Polyolefine Blends Used for Ceramic Injection Molding," *J. Am. Ceram. Soc.*, 72, 1822-28 (1989).

63. Woodthorpe, M.J. Edirisinghe, and J.R.G. Evans, "Properties of Ceramic Injection Molding Formulation III. Polymer Removal," *J. Mater. Sci.*, 24, 1028-49 (1989).

64. B.C. Mutsuddy, "Oxidative Removal of Organic Binders from Injection-Molded Ceramics," pp. 397-408 in Processing of the International Conference on Non-oxide Technological and Engineering Ceramics, N.I.H.E., Limerick, Finland, 1985.

65. R.R. Tummala, "Ceramics in Microelectronic Packaging"; pp. 3-16 in Advances in Ceramics, Vol. 26, *Ceramic Substrates and Packages for Electronic Applications*. Edited by M.F. Yan, K. Niwa, H.M. O'Bryan, Jr., and W.S. Young, American Ceramic Society, Westerville, OH, 1987.

66. Butvar, Polyvinyl Butyral Resin, Tech. Bull. No. 8084A, Monsanto Chemical Co., St. Louis, Mo., 1991.

67. W.-K. Shih, M.D. Sacks, G.W. Scheiffele, Y.-N. Sun, and J.W. Williams, "Pyrolysis of Poly(Vinyl Butyral) Binders: I, Degradation Mechanisms"; pp. 549-58 in Ceramic Transactions: Ceramic Powder Processing Science. Edited by G.L. Messing, E.R. Fuller, Jr., and H. Hausner. American Ceramic Society, Westerville, OH, 1988.

68. G.W. Scheiffele and M.D. Sacks, "Pyrolysis of Poly (Vinyl Butyryl) Binders: II, Effects of Processing Variables"; pp. 559-566 in Ceramic Transactions: Ceramic Powder Processing Science. Edited by G.L. Messing, E.R. Fuller, Jr., and H. Hausner. American Ceramic Society, Westerville, OH, 1988.

69. S. Masia, P. Calvert, W. Rhine, and H.K. Bowen, "Effect of Oxides on Binder Burnout During Ceramics Processing," *J. M. Sci.*, 24, 1907-12, (1989).

70. K.E. Howard, C.D.E. Lakeman, and D.A. Payne, "Surface Chemistry of Various Poly(vinyl butyryl) Polymers Adsorbed onto Alumina," *J. Am. Ceram. Soc.*, 73, 2543-46 (1990).

71. M.R. Barone and J.C. Ulicny, "Liquid-Phase Transport During Removal of Organic Binders in Injection-Molded Ceramics," *J. Am. Ceram. Soc.*, 73, 3323-33 (1990).

72. M.R. Barone, J.C. Ulicny, R.R. Hengst, and J.P. Pollinger, "Removal of Organic Binders in Ceramic Powder Compacts"; pp.575-83 in Ceramic Transactions:

Ceramic Powder Processing Science. Edited by G.L. Messing, E.R. Fuller, Jr., and H. Hausner. American Ceramic Society, Westerville, OH, 1988.

73. R.R. Gilisen and A. Smolders, "Binder-Removal from Injection-Molded Ceramic Bodies"; pp. 591-94 in *High Tech Ceramics*. Edited by P. Vincenzini. Elsevier, Amsterdam, 1987.

74. D.J. Rhee, G.C. Stangle, and I.A. Aksay, "The Influence of Microstructure, Degradation, and Internal Stresses on Binder Removal," submitted to *J. Am. Ceram. Soc.*

75. J.A. Lewis, "Binder Distribution Processes in Ceramic Green Tapes During Thermolysis"; Ph.D. Thesis, Dept. Mat. Eng., MIT, Oct. 1990.

76. M.J. Edirisinghe and J.R.G. Evans, "Review: Fabrication of Engineering Ceramics by Injection Molding. I. Materials Selection," *Int. J. High Technology Ceramics*, 2, 1-31 (1986).

77. M.J. Cima, M.Dudziak, and J.A. Lewis, "Observation of Poly(Vinyl Butyryl)-Dibutyl Phthalate Binder Capillary Migration," *J. Am. Ceram. Soc.*, 72, 1087-90 (1989).

78. J.A. Lewis and M.J.Cima, "Diffusivities of Dialkyl Phthalates in Plasticized Poly(vinyl butyryl): Impact on Binder Thermolysis," *J. Am. Ceram. Soc.*,73 [9] 2702-7 (1990)

79. R.M. German, "Theory of Thermal Debinding," *Int. J. Powder Metall.*, 23 [4] 237-45 (1987).

80. P. Calvert and M.J. Cima, "Theoretical Models for Binder Burnout," *J. Am. Ceram. Soc.*, 73[3], 675-79 (1990).

81. G.C. Stangle and I.A. Aksay, "Simultaneous Momentum, Heat and Mass Transfer with Chemical Reaction in a Disordered Porous Medium: Application to Binder Removal from a Ceramic Green body," *Chemical Engineering Science,* vol.45, No.7, 1719-31 (1990).

82. Y. Tang and M.J. Cima, "Deformation During Binder Removal from Multilayer Ceramic Greenware"; pp. 115-124 in Ceramic Transactions, Vol. 26, Forming Science and Technology for Ceramics. Edited by M.J. Cima. The American Ceramic Society. Westerville, OH, 1991.

83. M. Kahn, "Effects of Partial Oxygen Pressure During Burnout of Multilayer Structures"; pp. 185-188 in Advances in Ceramics, Vol.19, Multilayer Ceramic Devices, Edited by J.B. Blum and W.R. Cannon. American Ceramic Society, Westerville, Ohio, 1986.

84. D.L. Hipps and J.J. Brown, Jr., "Internal Pressure Measurements for Control of Explosive Spalling in Refractory Castables," *Am. Ceram. Soc. Bull.*, 63[7] 905-10 (1984).

85. Dong and H.K. Bowen, "Hot-stage study of Bubble Formation During Binder Burnout," *J. Am. Ceram. Soc.*, 72, 1082-87 (1989).

86. J.R. Street, A.L.Fincke, and L.P. Reiss, "Dynamics of Phase Growth in Viscous, Non-Newtonian Liquids," *Ind, Eng. Chem. Fund.* 10 [1] 54-64 (1971).

87. I.S. Wichman, "A Model Describing the Steady-State Gasification of Bubble-Forming Thermoplastics in Response to an Incident Heat Flux," *Combust. Flame*, 63, 217-19 (1986).

88. R.H. Doremus, "Diffusion of Oxygen from Contracting Bubbles in Molten Glass," *J. Am. Ceram. Soc.*, 43 [12] 655-61 (1960).

89. A.F. Dyson, "Improvements in Multilayer Ceramic Capacitors," *Electrocomponent Science and Technology, 11, 53-63 (1983)*

90. J.G. Pepin W. Borland, P. O'Callaghan, and R.J.S. Young, "Electrode-Based Causes of Delaminations in Multilayer Ceramic Capacitors," *J. Am. Ceram. Soc.*, 72 [12] 2287-91 (1989)

91. L.F. Miller, "Screenability and Rheology," *Solid State Technol.*, 17, 54-60 (1974).

92. G.Y. Onoda, Jr., "The Rheology of Organic Binder Solutions"; pp. 235-251 in Ceramic Processing Before Firing. Edited by G.Y. Onoda and L.L. Hench. Wiley, New York, 1978.

93. R.A. Vogel, "Fine Line Printing for Consumer Electronics," *Solid State Technol.*, 15, 51-54 (1972).

94. R.E. Trease, "Rheology of Pastes in Thick-Film Printing," *Solid State Technol.*, 15, 39-43 (1972).

95. A.V. Fraioli, "Yield Values in Thick-Film Rheology," *Solid State Technol.*, 17, 48-50 (1974).

96. W.P. Brown and C.F.H. Tipper, "The Pyrolysis of Cellulose Derivatives," *J. Appl. Polymer Sci.*, 22, 1459-68 (1978).

# CHAPTER 3

# INTERFACIAL STRUCTURE AND MECHANICAL PROPERTIES OF TAPE CAST CERAMIC GREEN SHEETS

## 3.1 Introduction

A ceramic green tape is generally viewed as a composite of ceramic particles, polymer binder, and gas filled pores. A major hypothesis of this thesis is that this conventional model is oversimplified; a complete understanding of the system should take into consideration a fourth phase: an adsorption layer of polymers on the ceramic particle surface. This interfacial layer has been shown to play an important role in the particle packing and mechanical properties of paint[1-3]. It was also shown[4-6] that the adsorption layer affects the mechanical properties over a wide temperature range in particle reinforced rubber. However, a systematic study of the structure and the thickness of the interfacial layer and its effect on particle packing and on the mechanical properties of ceramic green tape has not being reported.

Production of MLC devices requires specific mechanical properties of the ceramic green tapes for dimensional control during sheet processing. Low yield strength materials have large dimensional changes from a small applied stress, and these dimensional changes cause misalignment and sheet inhomogeneities[7]. High strength of the tape at elevated temperatures is essential for maintaining the integrity of the MLC structure during binder burnout when internal pressure is high due to the evolution of volatile organics. Thermomechanical properties of green tapes also affect the lamination and punching processes.

The mechanical properties of a green tape are determined by its composition and

microstructure. These factors include the chemical composition of the organic binder[8], the level of ceramic loading[8,9], the particle size distribution of the ceramics[10], and the chemical reaction between particle surface and organic binders. The interfacial structure determines the particle packing and the mechanical properties of green tapes at room and elevated temperatures, after the composition of the slurry is optimized.

The thickness and composition of adsorption layers in a ceramic green tape depend on the surface chemistry of filler particles and on the chemical structure of dispersant, polymer, plasticizer, and solvent (s). The adsorbed layer composition also depends on the interaction among all organics, and the sequence of these components being added to the ceramic slurry[11-13]. Dispersant adsorbs on the particle surface and prevents particle agglomeration through either a steric or an electrosteric stabilization mechanism. It tends to lower the strength of the green tape even though it may increase the particle packing density[9]. Competitive adsorption between the binder and the dispersant also occurs[13] which results in a change of slurry properties with time. An alternative is to select a polymer which functions as both binder and dispersant. Polyvinyl butyral (PVB) has been shown[14,15] to provide good dispersion for ceramic powders, and it is also the most effective binder for providing all the required thermoplastic properties in tape casting and the high bond strength between layers in MLC greenware[16,17].

The packing of particles in a green tape is shown schematically in Figure 3.1. When particle volume concentration (PVC) is low, particles with their adsorption layers are dispersed in a continuous free binder network. The thickness of free binder between particles decreases as PVC increases, and it reaches zero at critical particle volume concentration (CPVC). There is just enough free binder to fill the interstices between particles with adsorbed layer at CPVC. Porosity develops when PVC is greater than the CPVC and the properties of green tapes change considerably. Both the tensile strength

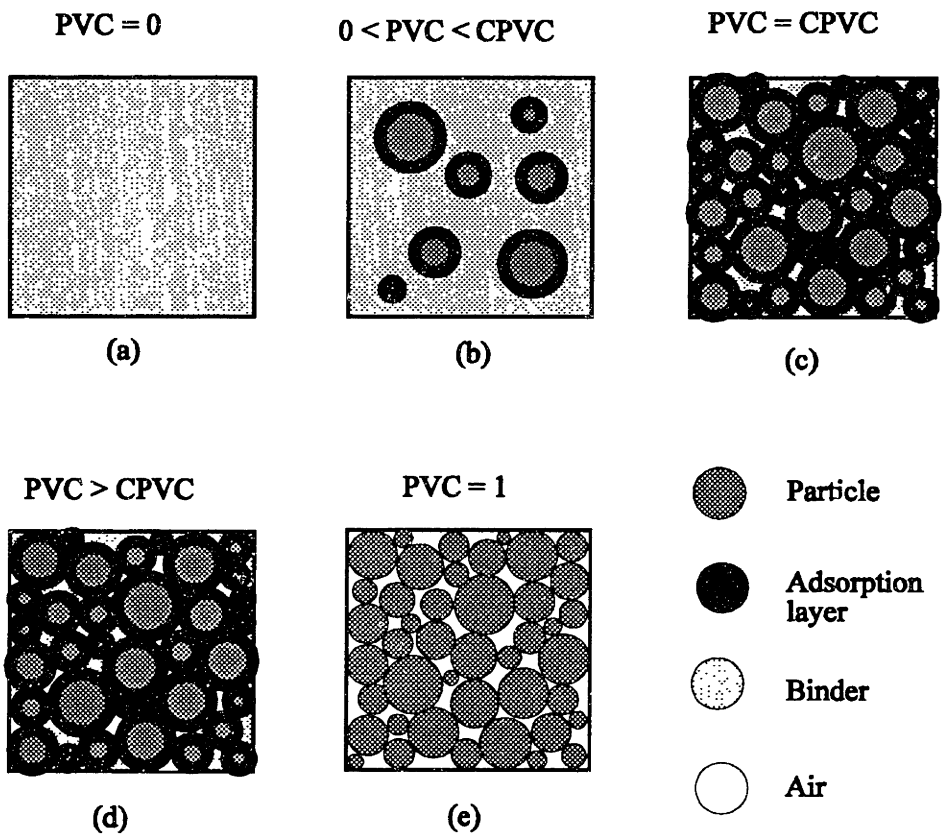


**Figure 3.1 Schematic of particle packing at different stages**

and flexibility of the green tapes are expected to decrease rapidly beyond CPVC, due to the porosity in the tape and to the lack of free binder layer between particles. CPVC is influenced by factors such as the size and shape of particles[18], type of binder used, and dispersability of the particle in the binder system.

This chapter focuses on the interfacial structure of green tapes as well as its effects on the particle packing and mechanical properties of the tape. The chemical composition and thickness of the organic adsorption layer on the ceramic particle surface is characterized using diffuse reflectance infrared transformation and thermalgravimetric analysis. The effect of the adsorption layer on particle packing density is evaluated. Dynamic mechanical properties of the green tapes over a wide temperature range are examined.

## 3.2 EXPERIMENTAL PROCEDURE

Commercially produced green tapes were used in this research. $BaTiO_3$ powders were dispersed in a benzyl butyl phthalate (BBP) plasticized polyvinyl butyral (PVB)# binder network. The loading of $BaTiO_3$ powders varied from 48 to 60 vol%. The composition of the binder was kept constant at PVB/BBP = 60/40. The thickness of the tapes was 34 μm.

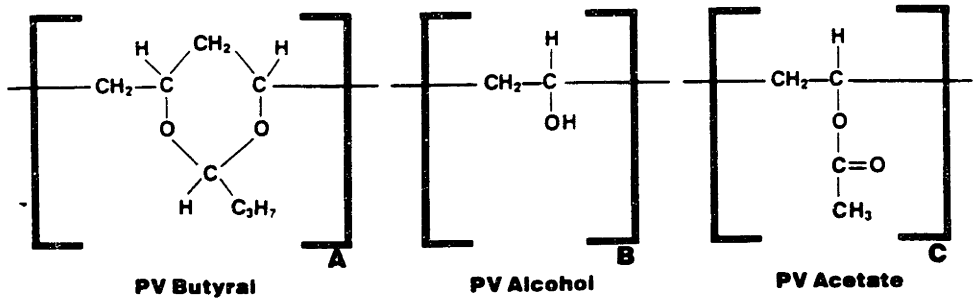


**Figure 3.2 Structure of the PVB. A = 0.88, B = 0.11-13, and C = 0.0-0.015 for B-76[19]**

The structure of PVB (B-76) is shown in Figure 3.2. PVB is a terpolymer of polyvinyl butyral, polyvinyl alcohol, and polyvinyl acetate. These three groups are randomly distributed along the macromolecule. They are designated as PVBu, PVA, and PVAc in this chapter. The number average[20] and weight average[19] molecular weight of PVB (B-76) are 32,000 g/mol and 105,000 g/mol, respectively.

A 120 mm × 40 mm piece was cut from a large roll of tape and dissolved in 50 ml solvent for 24 hours. The solvent was a mixture of methyl ethyl ketone (MEK) and ethyl

# Butvar B-76™, Monsanto Plastics, St. Louis, MO

alcohol at a 80/20 ratio. It was stirred with a magnetic stir bar for three hours. The slurry was then filtered and continuously washed with the same solvent five more times. Fourier transformed infrared (FTIR) spectroscopy was performed on the supernatant after solvent extraction to make sure there was no free polymer in the solution. The residual powders were dried overnight under a hood and then vacuumed at 50°C for 24 hours. Thermogravimetric analysis (TGA)* was performed on the washed powders to determine the amount of organics adsorbed on the particle surface. Diffuse reflectance infrared Fourier transformation (DRIFT) was used to characterize the composition of the adsorption layer. The powder was diluted with KBr, and then pressed into a pellet. DRIFT spectra were acquired at a resolution of 4 $cm^{-1}$ using 100 scans.

A slurry was made by first dispersing 10 g $BaTiO_3$ in 20 g MEK/ethanol solvent, and then adding 1g BBP. This slurry was mixed with a magnetic stir bar for three hours and allowed to sit for 24 hours. The slurry was then dried under the hood overnight, followed vacuuming for 24 hours. The dried powder was washed with MEK/ethanol solvent and then dried, following the same procedures as washing and drying the green tape. DRIFT was performed on the washed powder to determine the reactivity between the $BaTiO_3$ surface and the BBP molecules.

10 g $BaTiO_3$ powder was heated at 10°C/min to 1000°C, and then quenched. The quenched powder was immediately dispersed in 20 g ethyl acetate, the monomer of the PVAc group. 10 g as-received $BaTiO_3$ powder was also dispersed in 20 g ethyl acetate. Both samples were mixed for 3 hours, and allowed to sit for 24 hours. They were then dried under the hood for three days, and vacuumed at room temperature for a week. It is assumed that only the ethyl acetate molecules adsorbed on powder surface remain after

* TAS 7, Thermal Analysis System, Perkin-Elmer, Hartford, CT

the vigorous vacuuming. DRIFT spectra of the above samples were collected.

Dynamic mechanical analysis (DMA)* of the green tapes was conducted under tension mode of deformation. Rectangular samples of 20 mm × 5 mm were used. A 1 HZ single frequency and a 20 μm amplitude were used throughout the experiment. The samples were heated at 5°C/min to the desired temperature. The tensile force exerted on the tape varied from 50 to 500 g, which was automatically adjusted based on the stiffness of the samples.

## 3.3 RESULTS AND DISCUSSION

### 3.3.1 Surface Reaction Between $BaTiO_3$ and Binders

Figure 3.3 shows the TGA results of a green tape before and after solvent extraction. Two distinctive stages of binder removal were observed in a green tape, corresponding to the evaporation of plasticizer between 120°C and 140°C and to the decomposition of PVB between 200°C and 400°C. The rapid weight loss between 120°C and 140°C was no longer observed after solvent extraction. A slow weight loss between 50 and 200°C was observed, corresponding to a 0.2% weight loss. This was followed by a 1.5% weight loss between 200°C and 400°C, and a further weight loss of 0.23% between 400°C and 700°C.

DRIFT results of the tape before and after solvent extraction are shown in Figure 3.4. The DRIFT spectra of pure PVB and BBP are shown in Figure 3.5 as references. The existence of PVB in the solvent washed sample was indicated by C-H stretching peaks

* Seiko DMS 200 Dynamic Mechanical Rheology Station

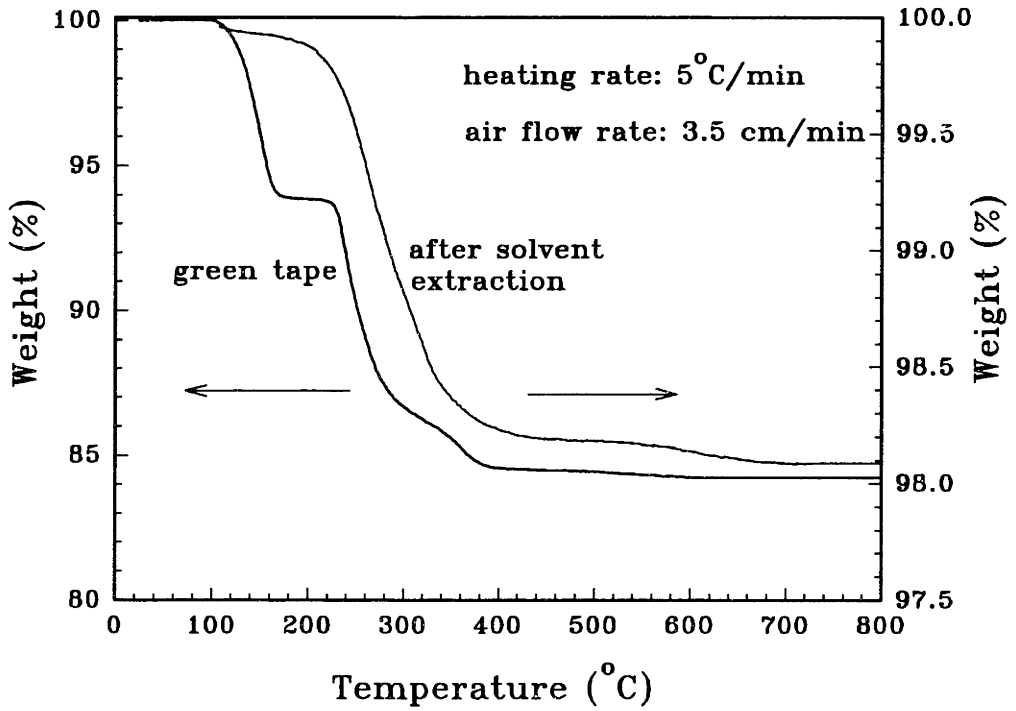


**Figure 3.3 Thermalgravimetric analysis of a green tape before and after solvent extraction**

at 2950 and 2870 $cm^{-1}$, C-H bending at 1378 $cm^{-1}$, and C-O-C stretching at 1136 $cm^{-1}$[21]. C=O stretching at 1732 $cm^{-1}$ from the PVAc segment of PVB was also observed. No shifting of the C=O peak was observed in the adsorption layer compared to pure PVB, even though a 20 $cm^{-1}$ shift toward lower energy had been observed in the $Al_2O_3$-PVB system[22]. A broadened O-H stretching band between 3000 and 3700 $cm^{-1}$ was observed after solvent extraction, indicating that the alcohol groups of the PVA segment interact with the ceramic surface through hydrogen bonding[15].

It is unclear from Figure 3.4 whether there is any BBP chemically adsorbed on the $BaTiO_3$ surface after solvent extraction, since all major peaks of BBP molecules overlap with those of PVB. The DRIFT spectra of the $BaTiO_3$ and the $BaTiO_3$-BBP systems after solvent washing are shown in Figure 3.6. The lack of BBP after solvent extraction

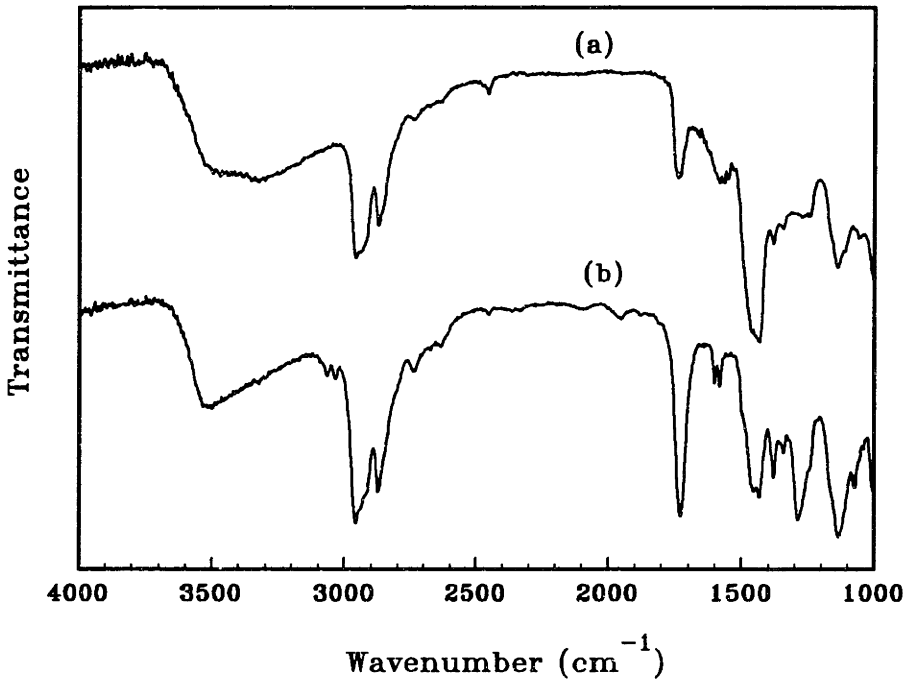


**Figure 3.4 DRIFT spectra of: (a) green tape after solvent extraction and (b) green tape**

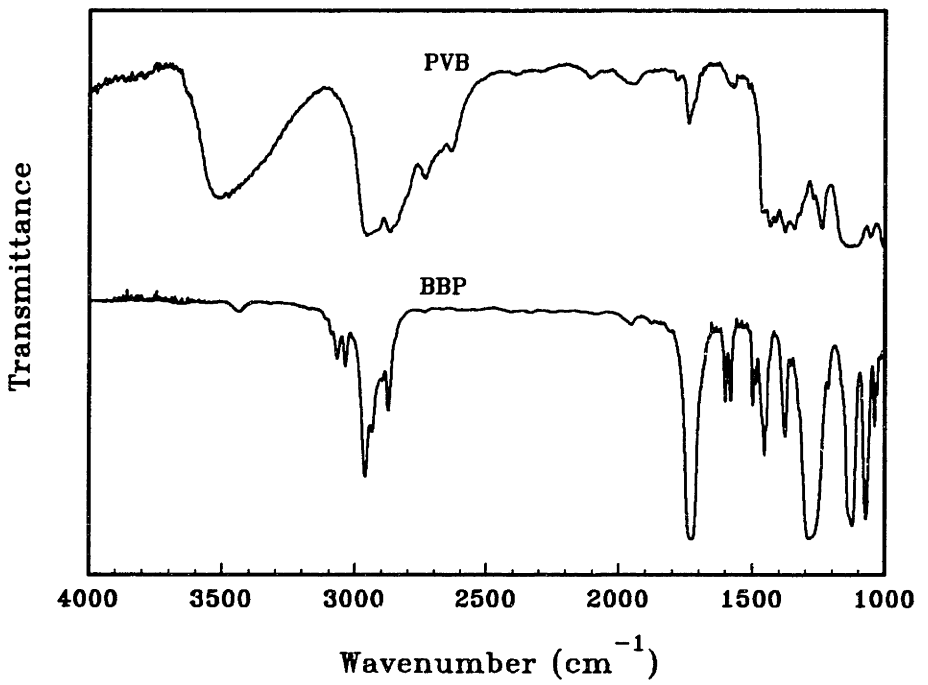


**Figure 3.5 DRIFT spectra of PVB (B-76) and BBP**

indicates that BBP does not chemically bond to the $BaTiO_3$ surface.

The DRIFT spectra of $BaTiO_3$ powders showed hydroxyl stretching of bonded water between 2700 and 3700 $cm^{-1}$. $BaCO_3$ was detected in the $BaTiO_3$ powders, as indicated by the adsorption peaks at 1437, 1750, and 2454 $cm^{-1}$. $BaCO_3$ is likely to be formed by $CO_2$ chemically adsorbed on $BaTiO_3$ powder surface. The adsorption peaks

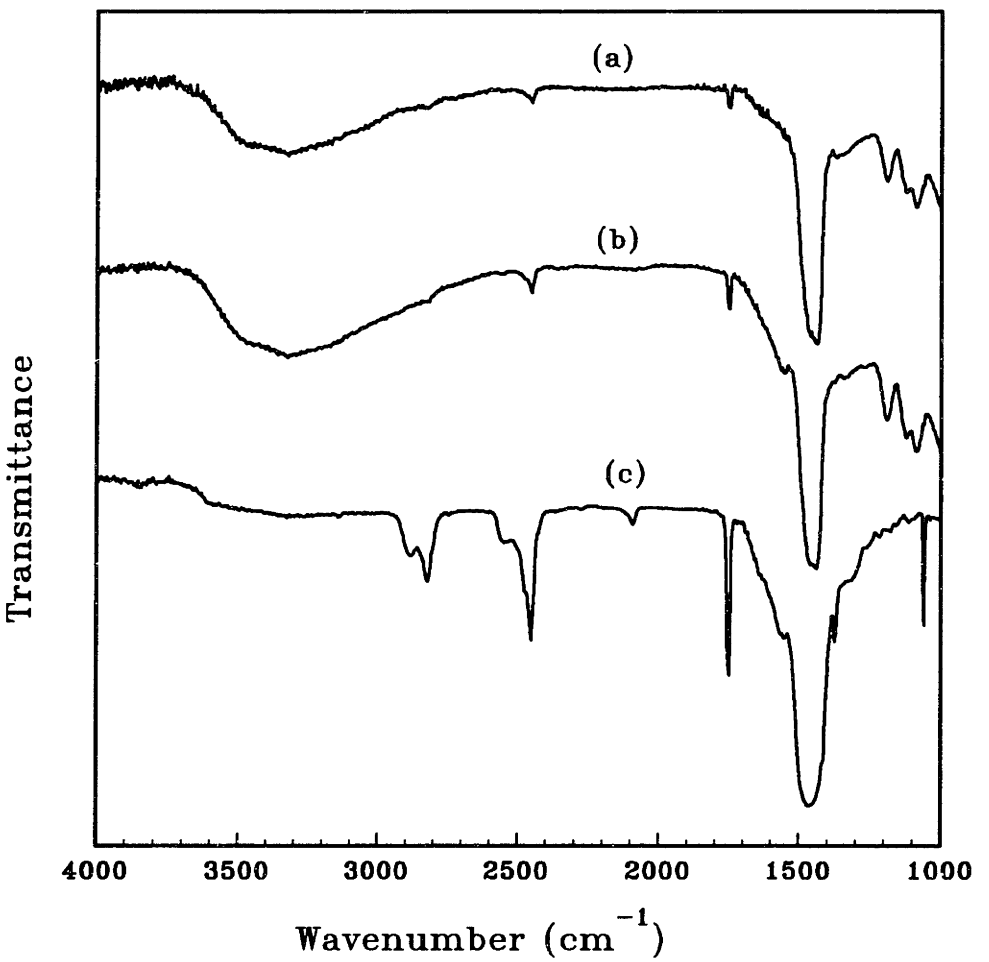


**Figure 3.6 DRIFT spectra of: (a) as-received $BaTiO_3$ powder, (b) $BaTiO_3$-BBP after solvent extraction, and (c) $BaCO_3$ powder**

of $BaCO_3$ were no longer observed after the $BaTiO_3$ powder was heated to 1000°C and quenched, as indicated in Figure 3.7. DRIFT spectra of $BaTiO_3$ powder and $BaTiO_3$ heated to 1000°C, after being exposed to ethyl acetate and dried, are also shown in Figure 3.7. Ethyl acetate was not detected in the dried $BaTiO_3$-ethyl acetate sample, indicating that the carbonyl group in ethyl acetate does not react with $BaTiO_3$ powder surface that is covered with a $BaCO_3$ surface layer. The $BaTiO_3$ powder that was heated to 1000°C and quenched, however, interacted with ethyl acetate. The presence of ethyl acetate is

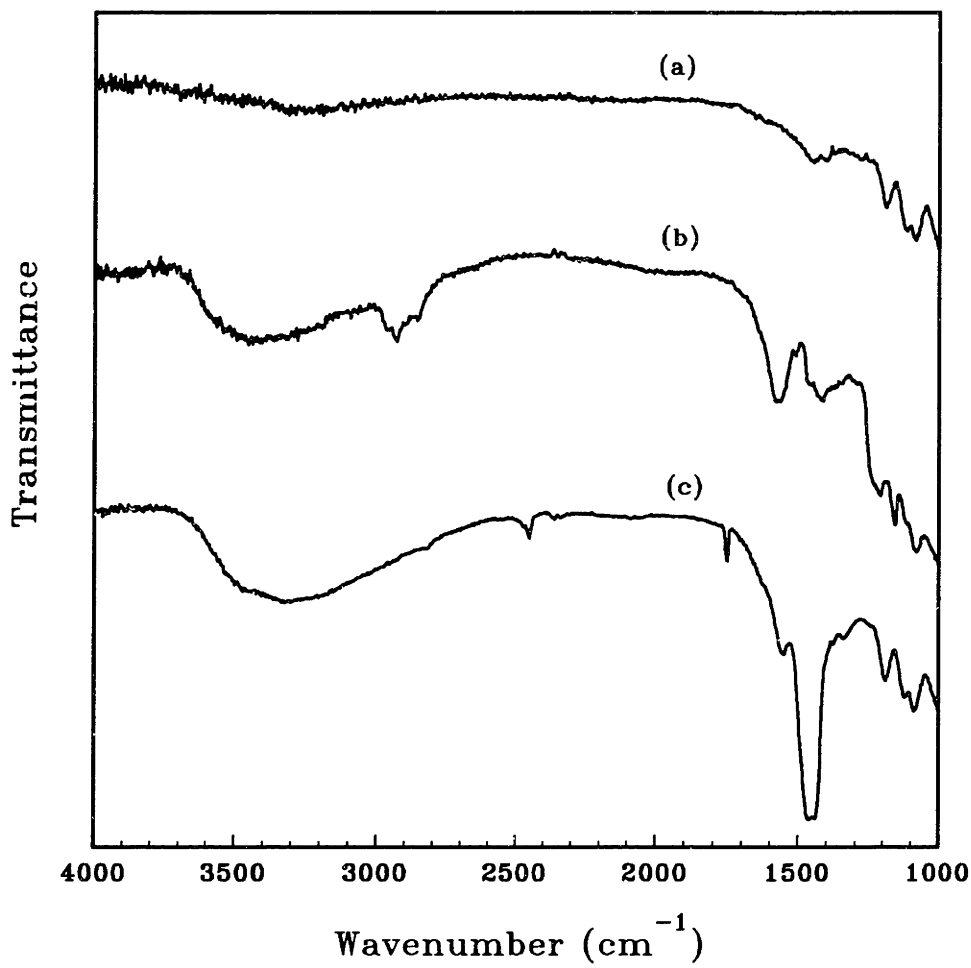


**3.7 DRIFT spectra of: (a) $BaTiO_3$ immediately after heated to 1000°C and quenched, (b) dried above powder after exposed to ethyl acetate, and (c) dried as-received $BaTiO_3$ powder after exposed to ethyl acetate.**

indicated by the C-H bending peaks at 2932 and 2855 $cm^{-1}$. The adsorption peak of the C=O group around 1734 $cm^{-1}$ in ethyl acetate, however, was not observed. A strong adsorption peak at 1574 $cm^{-1}$, which is not present in ethyl acetate, was detected. This band has been observed in the $Al_2O_3$/methyl methacrylate system and can be attributed to the formation of metal carboxylate species at the oxide surface[23, 24]. The metal carboxylate is formed by the reaction between ester groups of ethyl acetate and the $BaTiO_3$ surface. Therefore, the adsorption peak of the free ester group could no longer be observed in the adsorbate.

The TGA of $BaTiO_3$ powder is shown in Figure 3.8. The adsorbed water desorbed and evaporated before 200°C, resulting 0.2% weight loss. The decomposition of $BaCO_3$ on the $BaTiO_3$ surface occurred between 400 and 700°C, which caused 0.23% weight loss.

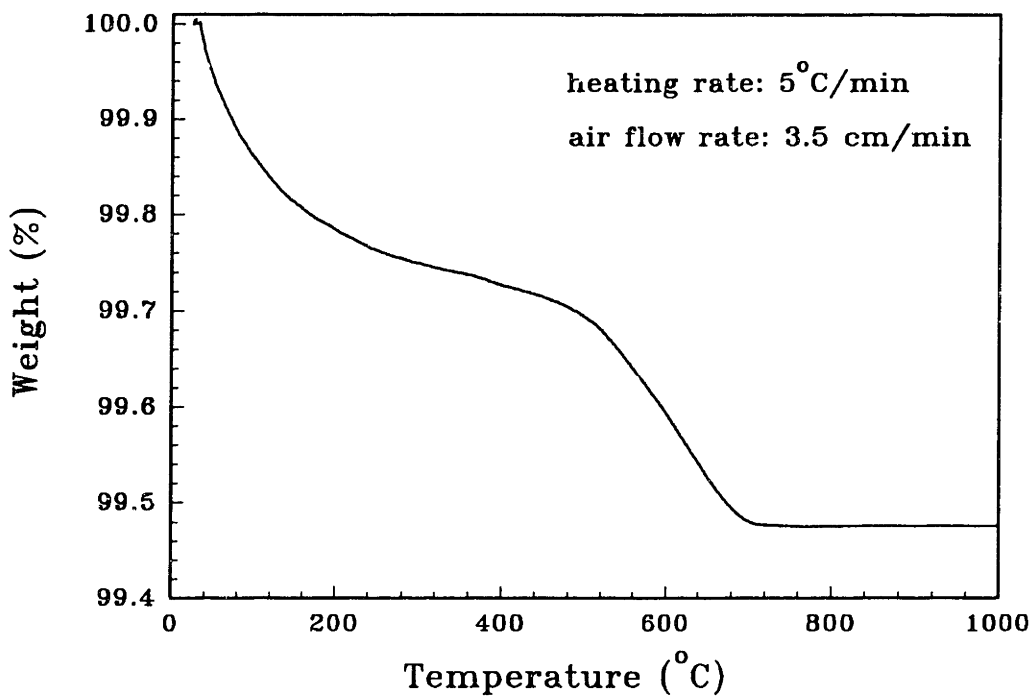


**Figure 3.8 TGA of $BaTiO_3$ powder**

It has been shown[25-28] that polymers and other organic species interact with ceramic surfaces by Lewis acid-base interactions. The strength of polymer adsorption onto particles is determined by the enthalpy of acid-base interactions between the acidic or basic sites of polymers and the acidic or basic sites on particle surface[25,26]. Both $BaTiO_3$ and $BaCO_3$ are basic materials. Therefore, their strongest reactions are with acid organics. Hydrogen bonding is a subset of the Lewis acid-base interaction and it has been observed between organic binders and ceramic oxides[22, 29-32]. Hydrogen bonding occurred between the basic $BaTiO_3$ and $BaCO_3$ surface and the acidic COH group in PVA segments of PVB polymers.

Another commonly observed surface reaction is the chemical reaction between carbonyl groups in organic binders and the surface of ceramic powders[23,24,33]. This reaction causes a shift of the C=O peak in a polymer toward lower energy and the formation of metal carboxylate species on the particle surface. The C=O peak vanishes if a carbonyl group containing monomer is used[23]. This reaction occurred between thermally treated $BaTiO_3$ and ethyl acetate, monomer of the PVAc segment. However, neither the shifting of the C=O peak nor the barium carboxylate was observed in the $BaTiO_3$-PVB system. This indicates that the presence of $BaCO_3$ layer at the surface of $BaTiO_3$ powder prevents the chemical reaction between carbonyl group and $BaTiO_3$. This is confirmed by the lack of adsorbence of ethyl acetate on the surface of as-received $BaTiO_3$ powder.

### 3.3.2 Particle Packing in a Green Tape

The particle size distribution of $BaTiO_3$ powders is shown in Figure 3.9. The surface area and average particle size of $BaTiO_3$ powder are 3.1 $m^2/g$ and 1.04 μm. respectively. TGA results showed that there were 0.2 wt% water and 1.5 wt% PVB

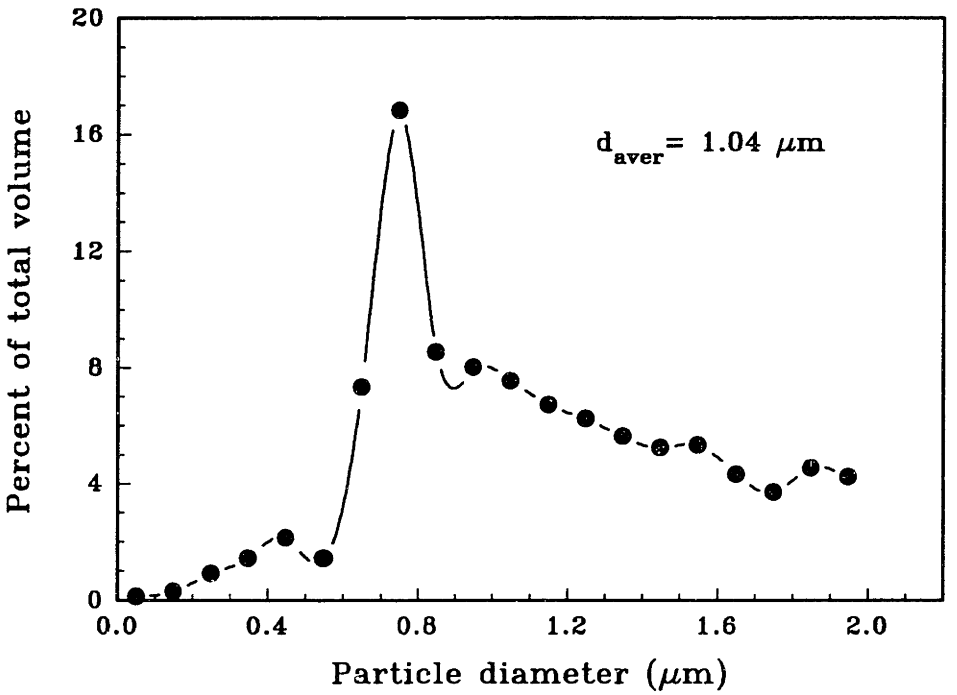


**Figure 3.9. Particle size distribution of $BaTiO_3$ powders (by volume)**

adsorbed on $BaTiO_3$ surface (Fig. 3.2). This accounts for 1.2% and 8.4% of the volume of $BaTiO_3$ particles, assuming the density of water and PVB in the adsorption layer was the same as free water and free PVB. The thickness of the adsorption layer is then:

$$\delta = \frac{V_{adsorb}}{S_{BaTiO_3}} \qquad (\delta << d) \qquad (3.1)$$

where $\delta$ and $V_{adsorb}$ are thickness and volume of the adsorption layer, respectively. $S_{BaTiO_3}$ and $d$ are the surface area and diameter of $BaTiO_3$ powders. Eq. 3.1 yields a 0.6 nm water layer and a 4.5 nm PVB adsorption layer.

The end to end distance ($h$) of a polymer chain in solution is[34]:

$$h = \beta n^{\frac{1}{2}} \qquad (3.2)$$

where $\beta$ is a constant and is determined by the nature of the polymer, $n$ is the number of links per chain. $\beta \approx 3l$ for a typical synthetic organic polymer. $l$ is the length of bond. The end to end distance in a melt is expected to be similar to that in solution. The number of links per PVB chain is:

$$n = n_1 + n_2 + n_3 = m_1 \frac{Mx_1}{M_1} + m_2 \frac{Mx_2}{M_2} + m_3 \frac{Mx_3}{M_3} \qquad (3.3)$$

where the subscripts *1*, *2*, *3* represent PVBu, PVA, and PVAc respectively, $M$ is the molecular weight of PVB, $x_i$ is the weight fraction of $i$ segment in PVB, $m_i$ is the number of links per $i$ monomer, and $M_i$ is the molecular weight of $i$ monomer. Eq. 3.2 and 3.3 yield an $h$ value of 26 nm and 14 nm for Mw = 105,000 g/mol and Mn = 32,000 g/mol, respectively, taking $l$ as 1.54 Å[34] and $x_1$, $x_2$, and $x_3$ as 0.88, 0.11, 0.01[19], respectively.

An adsorbed polymer chain consists of trains which are in contact with the surface, loops (segments in the solution) of which both ends are on the surface, and two tails. This is shown schematically in Figure 3.10. Bridges in which a chain adsorbs on more than one particle may also occur if large tails and loops are present[35, 36]. The average end to end distance of PVB molecules is 5.8 (from Mw) and 3.1 (from Mn) times the thickness of

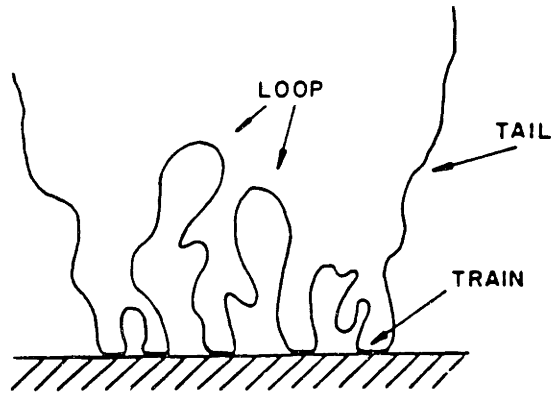


**Figure 3.10 Schematic of an adsorbed polymer chain at a particle surface**

the PVB adsorption layer. This indicates that there is more than one adsorption train for an average PVB molecule. 20% of the chain segments are in tails in a semidilute solution[37] such as the binder solution in tape casting, and short trains and long loops alternate in the middle. The number of trains ($N$) can be roughly estimated as:

$$N = \frac{(1-0.2)n}{n_l} + 1 \qquad (3.4)$$

where $n_l$ is the number of links in a loop. A loop assumes random coil state if it is long enough that the restriction from the powder surface is negligible. Therefore, $n_l = h_l^2 / \beta$, and $n = h^2 / \beta$. The number of trains is then:

$$N = \frac{(1-0.2)h^2}{h_l^2} \qquad (3.5)$$

Eq. 3.5 yields an $n$ value of 27 and 8 for Mw=105,000 g/mol and Mn=32,000 g/mol, taking $h_l$ as the thickness of the adsorption layer. The actual number of trains is expected to be greater than the value estimated from Eq. 3.5 since the configuration of a loop is constrained by the surface.

The adsorption layer is considered immobile[4-6] and, therefore, behaves as if it were part of the solid particle. We define the effective particle volume as the volume of $BaTiO_3$ particles plus the volume of the adsorption layer:

$$V_{eff} = V_{BaTiO_3} + V_{ads} \qquad (3.6)$$

where $V_{eff}$, $V_{BaTiO_3}$, and $V_{ads}$ represent the effective particle volume, the volume of $BaTiO_3$ powder, and the volume of PVB adsorption layer in a green tape, respectively. The volume of adsorbed water is included in $V_{BaTiO_3}$ since as-received $BaTiO_3$ powder contains adsorbed water layer. The packing of particles in the green tapes should be evaluated in terms of the effective particle volume instead of the volume of $BaTiO_3$ powders. Table 3.1 lists the comparison of these two values.

**Table 3.1 Particle packing in ceramic green tapes**

| $\frac{V_{BaTiO_3}}{V_{BaTiO_3}+V_{binder}}$ | 0.40 | 0.45 | 0.50 | 0.55 | 0.60 | 0.65 |
|---|---|---|---|---|---|---|
| $\frac{V_{eff}}{V_{eff}+V_{binder}}$ | 0.43 | 0.49 | 0.54 | 0.60 | 0.65 | 0.71 |

The loading of ceramic particles in a green tape is generally selected to be near or a few percent below the CPVC. Obviously, it is important to know the CPVC and use it as a reference point in tape casting. The determination of the CPVC is achieved by an oil-adsorption test (ASTM D-281) or by a modification of this technique in painting[3] and injection molding[38]. This measurement is based on the assumption that the thickness of the adsorption layer of all types of vehicles is the same as one standard oil such as linseed oil or oleic acid. This simplification is valid when low molecular weight resins are used. In the case of tape casting, however, the adsorption of a high molecular weight polymer would be different from an oil.

The CPVC can also be estimated from the particle size distribution and the thickness of the adsorption layer. This estimation is made by calculating the random dense packing of particles plus its adsorption layer. The expression for spherical particle with any size grouping of particles were as follows[39]:

$$\Phi_{ij} = \Phi_{ii} + [\Phi^{max}(d_i / d_j) - \Phi_{ii}] / 0.265 \quad (\text{if } d_i / d_j \geq 1, \text{i}\geq\text{j}) \tag{3.7}$$

$$\Phi_{ji} = \Phi_{ii} + [\Phi^{max}(d_i / d_j) - \Phi_{ii}] / 0.735 \tag{3.8}$$

$$\Phi_i = \sum_{j=1}^{m} \Phi_{ij} v_j \qquad (\sum \sum_{j=i}^{n} v_j = 1) \tag{3.9}$$

$$\Phi = \min(\Phi_i) \tag{3.10}$$

where

$\Phi_{ii}$: maximum close packing density of monosize spheres

$\Phi_{ij}$: binary packing coefficients of the packing for the size range $i$ and size range $j$ components,

$\Phi^{max}(d_i / d_j)$: maximum packing factor, for spheres of size ratio $d_i / d_j$[39,40]

$d_i$, $d_j$: diameter of particles in size range i and j components,

$v_j$: volume fraction of size range $j$,

$\Phi_i$: possible packing factors of $m$ component system,

$\Phi$: random densest packing factor of a mixture of particles

The above equations can be extended[41] to include the effect of adsorption layer. The geometry for the modified system is:

$$d_i' = d_i + 2\delta \qquad (3.11)$$

$$u_i = v_i(d_i'/d_i)^3 / \sum_{i=1}^{m} v_i(d_i'/d_i)^3 \qquad (\sum_{i=1}^{m} u_i = 1) \qquad (3.12)$$

The densest packing density of particles plus adsorption layers can be calculated by replacing $d_i$ and $v_i$ with $d_i'$ and $u_i$ in Eq. 3.7 to 3.10. The maximum packing density of particles plus adsorption layers was calculated to be 0.646, which corresponds to a CPVC value of 0.596 in this system.

The above calculated CPVC represents an upper limit on packing density of spherical particles. It has been shown that the maximum packing density of multicomponent angular shape particles is lower than its corresponding multicomponent spherical particles[42]. Interparticle friction[43,44] and "wall effect"[45] of substrate can also lower the packing density of particles in a green tape. Thus, the maximum packing density of irregular shaped particles in a greenware is expected to be lower than 0.596. Therefore, the ceramic loading in this system should be lower than 59.6 vol% in order for

the green tape to have enough flexibility. The following DMTA results will provide experimental evidence of the CPVC value in a green tape.

### 3.3.3 Dynamic Mechanical Properties of Green Tapes

Dynamic mechanical analysis (DMA) measures the ability of materials store energy and dissipate energy. The energy stored and dissipated per cycle are proportional to the elastic modulus (E') and to the viscous modulus (E"), respectively. The ratio of the viscous modulus to the elastic modulus (tanδ) represents the damping of the materials, and this ratio reaches maximum when materials go through glass transition.

Figure 3.11 shows the DMA of a ceramic green tape with 50 vol% ceramic loading.

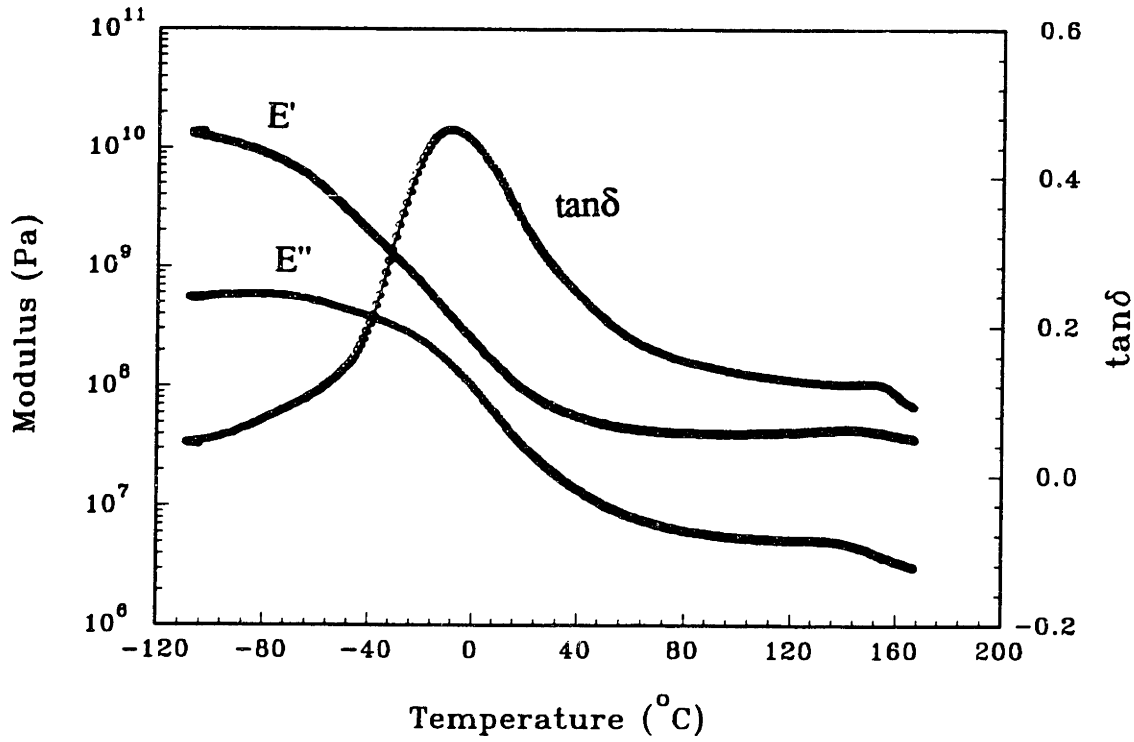


**Figure 3.11 DMA of the green tape with 50 vol% $BaTiO_3$ powder**

The glass transition of the tape starts from -70°C and finishes at about 70°C. The elastic modulus of the tape (E') started to increase slightly when the temperature exceeds 120°C, due to the loss of the plasticizer from the sample. Further loss of the plasticizer caused the tape to break at 180°C. The damping of PVB and PVB-BBP films and a ceramic green tape is shown in Figure 3.12. The glass transition temperature of PVB was 51°C. It was lowered to -11°C when 40% plasticizer was added to the system. Further addition of 50 vol% of $BaTiO_3$ to the PVB-BBP system lowered the magnitude of damping, and it broadened the glass transition region from -70–20°C to -70–70°C. The damping of the ceramic tapes with different ceramic loadings is shown in Figure 3.13. The magnitude of damping decreased when the ceramic loading in a green tape increased. A dramatic change occurred in the tape loaded with 60 vol% of ceramic powders: the tanδ peak became very broad and shifted toward higher temperatures. The effects of particles on

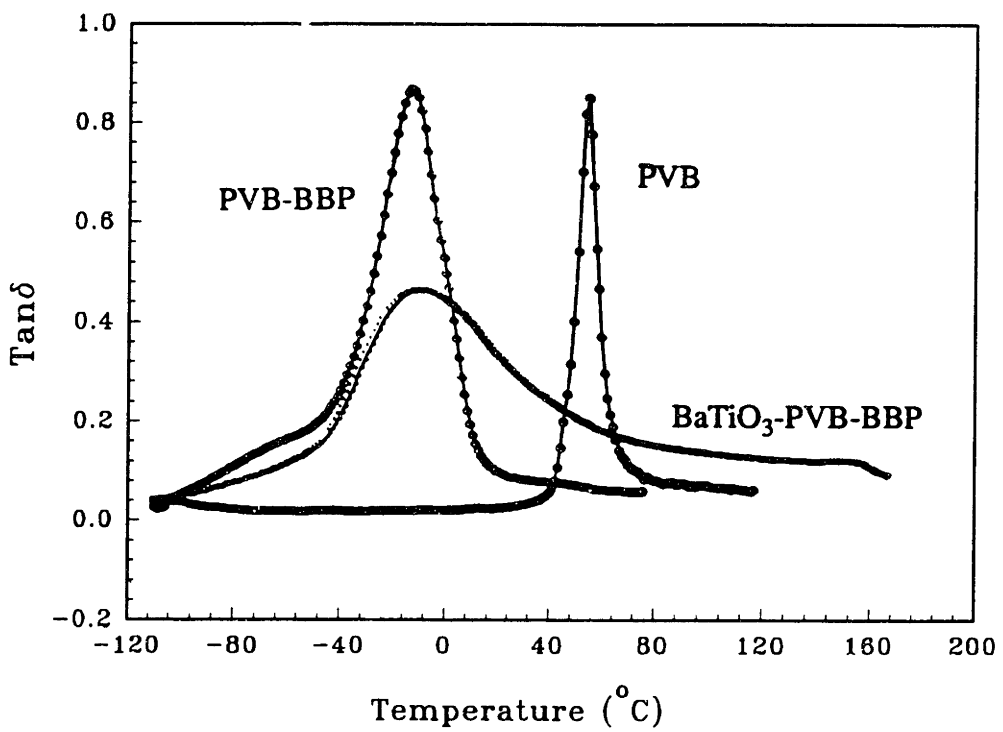


**Figure 3.12 Damping of PVB, PVB-BBP, and PVB-BBP-$BaTiO_3$ systems**

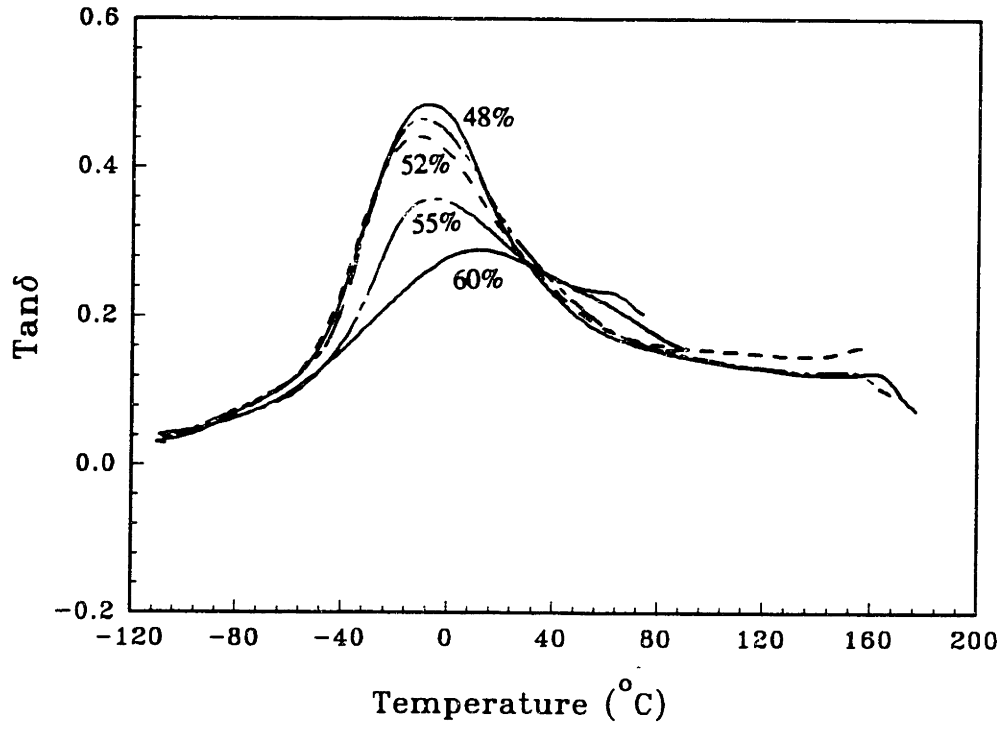


**Figure 3.13 Damping of the ceramic tapes with different ceramic loadings**

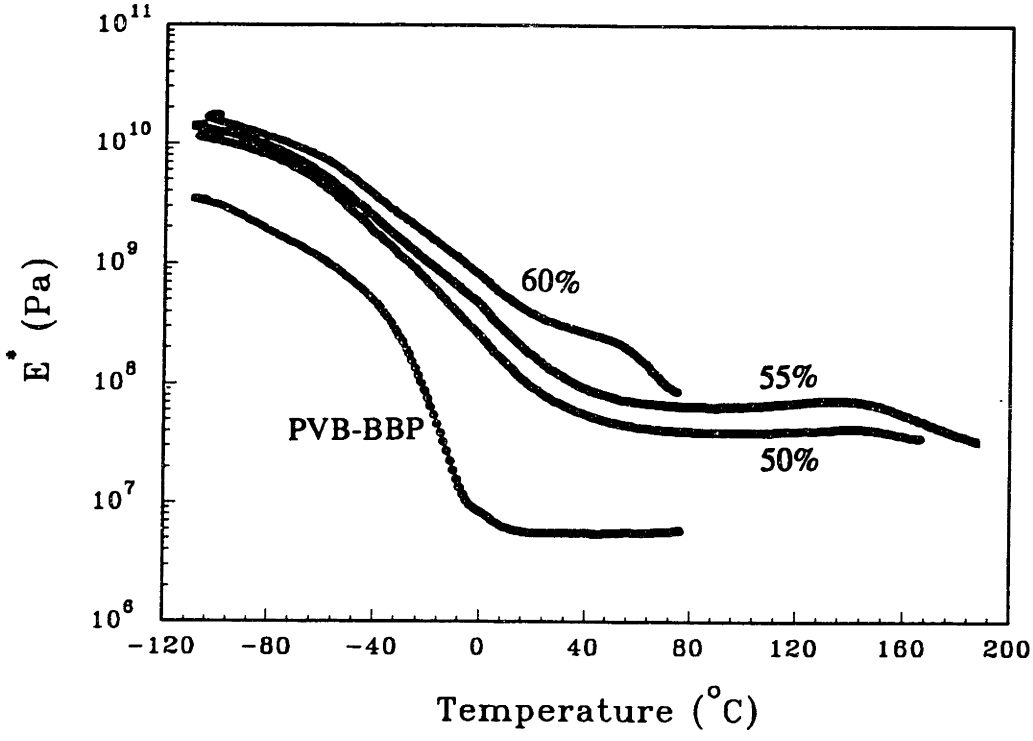


**Figure 3.14 Complex modulus of the ceramic tapes**

complex modulus are shown in Figure 3.14. The particles raised the modulus of the binder matrix, and this effect was greater above $T_g$ than below it. The modulus also increased with the increase of ceramic loading in the green tape.

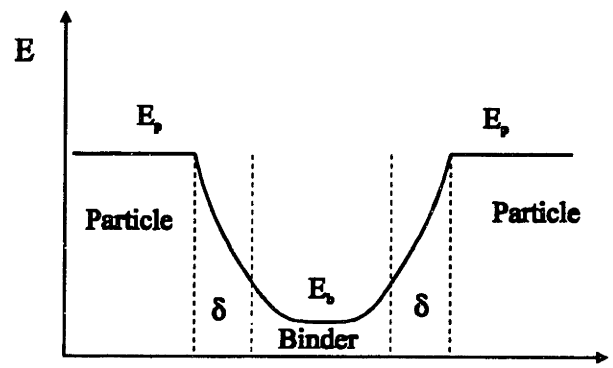


(a) PVC < CPVC

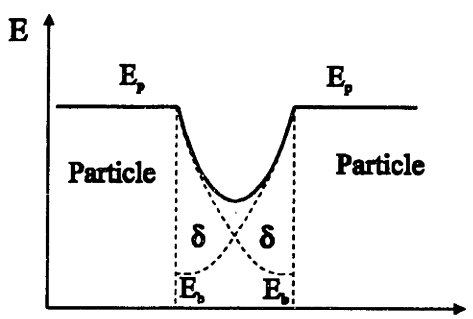


(b) PVC = CPVC

**Figure 3.15 Schematic of the modulus of interparticle binder layer**

A ceramic green tape can be considered as a composite and consists of a dissipative binder phase, a nondissipative dispersed phase, and a transition layer which lies in between. The mobility of the binder near the particle surface is greatly reduced[46], as illustrated in Figure 3.15. The amorphous polymer behaves as free polymers only at a distance far from the particle surface. The low mobility interfacial layers caused the broadening of the glass transition region toward higher temperatures. The glass transition regions were not shifted by particles for tapes below the CPVC, since free binder layers

still remain between the particles. Shifting of the glass transition towards higher temperatures occurred above the CPVC, when the interparticle layers were only composed of two adsorption layers with reduced mobility. Discrete glass transition peaks for adsorbed and free polymer are not observed since the polymer mobility changes continuously with distance from the particle surface.

The shifting of $T_g$ in the tape with 60 vol% ceramic powders indicates that the particle volume concentration has exceeded the CPVC of this system. For the tapes with ceramic loading equal or higher than 60 vol%, low flexibility is expected due to the depletion of free binder in the interparticle layers. Low strength is also expected due to the formation of porosity in the green tapes.

**Conclusion**

The interfacial structure of the green tapes was characterized. $BaCO_3$ was found in the as-received $BaTiO_3$ powders; this is believed to be caused by chemically adsorbed $CO_2$ on the $BaTiO_3$ powder surface. 0.2 wt % water and 0.23 wt% $CO_2$ were released from the $BaTiO_3$ powder between 25 to 200°C and 400 to 700°C, respectively. 1.5wt% PVB was adsorbed on the surface of $BaTiO_3$ powder through hydrogen bonding in the green tape.

The thickness of adsorbed water and PVB was 0.6 nm and 4.5 nm, respectively. This accounted for 1.2% and 8.6% of the volume of $BaTiO_3$ powders. The adsorption layer is considered immobile and, therefore, behaves as part of the particles. It increases the effective volume of particles in the green tape. The maximum packing density of particles plus adsorbed PVB was calculated to be 0.646, which corresponded to 0.596 critical particle volume concentration (CPVC).

$BaTiO_3$ powder broadened the glass transition region of PVB-BBP binder network from -70–20°C to -70–70°C. This broadening was caused by the low mobility binder near the particle surface. Shifting of the glass transition region as well as broadening toward higher temperatures occurred when the particle volume concentration was increased to 60 vol%, due to the lack of free binder layers between particles. Ceramic particles increased the modulus of binder matrix. This effect was greater above the glass transition temperature than below it.

The calculation of CPVC based on particle size distribution and on the thickness of adsorption layer agrees well with the mechanical property measurement. It provides guidelines for determining the loading of ceramic powder in a green tape, which has been determined empirically. We recommend the loading of the ceramic powders to be kept a few per cent below CPVC of the system in order to ensure a strong and flexible green tape. This is particularly important for thin green sheets such as the tape used in MLC capacitors.

## References


1. R. Castells, J. Meda, J.Caprari, and M. Damia, "Particle Packing Analysis of Coatings Above the Critical Pigment Volume Concentration," *Journal of Coating Technology*, 55, No. 707, 53-59 (1983).

2. W.J. Culhane, D.T. Smith, and C.P. Chiang, "Characterization of Pigment Volume Concentration Effects in Latex Paints," *Journal of Coatings Technology*, 55, No. 698, 53-58 (1983).

3. T.K. Hay, "Reaching an Objective in Oil Adsorption Measurement," *J. Paint Technol.*, 46 [591] 44-9 (1974).

4. K.D. Ziegel, "Role of the Interface in Mechanical Energy Dissipation of Composites," *Journal of Colloid and Interface Science*, 29 [1], 72-80 (1969).

5. I. Pliskin and N. Tokita, "Bound Rubber in Elastomers: Analysis of Elastomer-Filler Interaction and Its Effect on Viscosity and Modulus of Composite Systems," *Journal of Applied Polymer Science*, 16, 473-92 (1972).

6. M. Sumita, H. Tsukihi, K. Miyasaka, and K. Ishikawa, "Dynamic Mechanical Properties of Polypropylene Composites Filled with Ultrafine Particles," *Journal of Applied Polymer Science*, 29, 1523-30 (1984).

7. R.A. Gardner and R.W. Nufer, "Properties of Multilayer Ceramic Green Sheets," *Solid State Technol.*, 17, 38-43, (1974).

8. A. Karas, T. Kumagai, and W.R. Cannon, "Casting Behavior and Tensile Strength of Cast $BaTiO_3$ Tape" pp. 374-77 in Advanced Ceramic Materials, 3 [4], 1988.

9. Y. Tang and M.J. Cima, unpublished work.

10. R.J. MacKinnon and J.B. Blum, "Particle Size Distribution Effects on Tape Casting Barium Titanate"; pp. 150-57 in Advances in Ceramics, Vol.9, Forming of Ceramics, Edited by J.A. Mangels and G.L. Messing, American Ceramic Society, Columbus, OH, 1984.

11. W.R. Cannon, J.R. Morris, and K.R. Mikeska, "Dispersants for Nonaqueous Tape Casting"; pp. 161-174 in Advances in Ceramics, Vol. 19, Multilayer Ceramic Devices. Edited by J.B. Blum and W.R. Cannon. American Ceramic Society, Westerville, OH, 1986.

12. W.R. Cannon and R. Becker, "Interactions Among Organic Additives Used for Tape Casting"; pp. 525 in Advances in Ceramics, vol. 26, Ceramic Substrates and

Packages for Electronic Applications. Edited by M.F. Yan, K. Niwa, H.M. O'Bryan, Jr., and W.S. Young. American Ceramic Society, Westerville, OH, 1989.

13. J.B. Blum, and W.R. Cannon, "Tape Casting of $BaTiO_3$"; pp. 77-82 in Mat. Res. Soc. Symp. Proc., vol. 40, 1985.

14. H. Watanabe, T. Kimura, and T. Yamaguchi, "Particle Orientation During Tape Casting in the Fabrication of Grain-Oriented Bismuth Titanate," *J. Am. Ceram. Soc.*, 72 [2] 289-93 (1989).

15. M.D. Sacks, C.S. Khadilkar, G.W. Scheiffele, A.V. Shenoy, J.H. Dow, and R.S. Sheu, "Dispersion and Rheology in Ceramic Processing"; pp.495-515 in Advances in Ceramics, Vol. 21, Ceramic Powder Science. Edited by G.L. Messing, K.S. Mazdiyasni, J.W. McCauley, and R.A. Haber. American Ceramic Society, Westerville, OH, 1987.

16. R.R. Tummala, "Ceramic Packaging"; pp.455-521 in Microelectronics Packaging Handbook. Edited by R.R. Tummala and E.J. Rymaszewski, Van Nostrand Reinhold, New York, 1989.

17. R. Moreno, "The Role of Slip Additives in Tape Casting Technology: Part II-Binders and Plasticizers," *Am. Ceram. Soc. Bull.*, 71, [11], 1647-57 (1992).

18. R. Moreno, "The Role of Slip Additives in Tape Casting Technology: Part I-Solvents and Dispersants," *Am. Ceram. Soc. Bull.*, 71, [10], 1521-30 (1992).

19. Information provided by G. J. Wiener from Monsanto Chemical Co., Springfield, Mass., 1993.

20. Butvar, Polyvinyl Butyral Resin, Tech. Bull. No. 8084A, Monsanto Chemical Co., St. Louis, Mo., 1991.

21. W.-K. Shih, M.D. Sacks, G.W. Scheiffele, Y.-N. Sun, and J.W. Williams, "Pyrolysis of Poly(Vinyl Butyral) Binders: I, Degradation Mechanisms"; pp.549-58 in Ceramic Transactions: Ceramic Powder Processing Science. Edited by G.L. Messing, E.R. Fuller, Jr., and H. Hausner. American Ceramic Society, Westerville, OH, 1988.

22. K.E. Howard, C.D.E. Lakeman and D.A. Payne, "Surface Chemistry of Various Poly(vinyl butyral) Polymers Adsorbed onto Alumina," *J. Am. Ceram. Soc.*, 73 [8] 2543-46 (1990).

23. R. Higgins, Ph.D. Thesis, Department of Materials and Engineering, Massachusetts Institute of Technology, 1990.

24. Y. Sun, M. Sacks, and J. Williams, "Pyrolysis Behavior of Acrylic Polymers and Acrylic Polymer/Ceramic Mixtures"; pp. 538-48 in Proc. First Intl. Conf. on Ceramic Powder Processing Sci.: Ceramic Powder Sci. II; Edited by G. Messing, E. Fuller, and H. Hausner. The American Ceramic Society, Columbus, OH, 1988.

25. F.M. Fowkes, "Dispersion of Ceramic Powders in Organic Media"; pp. 411-21 in Advances in Ceramics, Vol. 21, *Ceramic Powder Science.* Edited by G.L. Messing, K.S. Mazdiyasni, J.W. McCauley, and R.A. Haber. American Ceramic Society, Westerville, OH, 1987.

26. F.M. Fowkes and D.O. Tischler, "Acid-Base Complexes of Polymers," *Journal of Polymer Science: Polymer Chemistry Edition*, Vol. 22, 547-66 (1984).

27. F.M. Fowkes, "Donor-Acceptor Interactions at Interface"; pp.43-52 in Adhesion and Adsorption of Polymers, Part A; Edited by L.-H. Lee. Plenum, New York, 1980.

28. F.M. Fowkes and M.A. Mostafa, *Ind. Eng. Chem. Prod. Res. Dev.*, 17, 3 (1978).

29. D.J. Shanefield, "Competing Adsorptions in Tape Casting"; pp. 155-60 in Advances in Ceramics, Vol. 19, Multilayer Ceramic Devices. Edited by J.B. Blum and W.R. Cannon, American Ceramic Society, Westerville, OH, 1986.

30. A. Roosen, F. Hessel, H. Fischer, and F. Aldinger, "Interaction of Polyvinylbutyral With Alumina"; pp. 451-459 in Ceramic Powder Science III. The American Ceramic Society, Westerville, OH, 1090.

31. K. Nakamae, K. Sumiya, T.Taii, and T. Matsumoto, "Studies on Adsorption of Poly(Vinyl Butyral) and Dispersibility of $\gamma$-$Fe_2O_3$ in Magnetic Paints," *J. Polym. Sci.: Poly. Symp.*, 71, 109-19 (1984).

32. M.D. Sacks, and G.W. Scheiffele, "Polymer Adsorption and Particulate Dispersion in Nonaqueous $Al_2O_3$ Suspensions Containing Poly(vinyl butyral) Resins"; pp. 175-84 in Advances in Ceramics, Vol. 19, Multilayer Ceramic Devices. Edited by J.B. Blum and W.R. Cannon, American Ceramic Society, Westerville, OH, 1986.

33. L. Bellamy, The Infrared Spectra of Complex Molecules: Advances in Infrared Group Frequencies, Vol. 2. Chapman and Hall, London, 1980.

34. C. Tanford, Physical Chemistry of Macromolecules, Chapter 3. John Wiley & Sons, INC., New York, 1961

35. B.M. Moudgil and B.D. Shah, "Removal of Particulate Impurities from Ceramic Powders by selective Flocculation," pp. 483-494 in Advances in Ceramics, Vol. 21: Ceramic Powder Science. Edited by G.L. Messing, K.S. Mazdiyasni, J.W. McCauley, and R.A. Haber. The American Ceramic Society, Westerville, OH, 1987.

36. J.M.H.M. Scheutjens and G.J. Fleer, "Statistical Theory of the Adsorption of Interactiong Chain Molecules. 1. Partition Function, Segment Density Distribution, and Adsorption Isotherms," *J. Phys. Chem.*, 83 [12], 1619-35 (1979).

37. J.M.H.M. Scheutjens and G.J. Fleer, "Statistical Theory of the Adsorption of Interacting Chain Molecules. 2. Train, Loop, and Tail size Distribution," J. Phys. Chem., 84 [2], 178-90 (1980).

38. C.J. Markhoff, B.C. Mutsuddy, and J.W. Lennon, "Method for Determining Critical Powder Volume Concentration in the Plastic Forming of Ceramic Mixes"; pp. 246-50 in Advances in Ceramics, Vol. 9, Forming of Ceramics. Edited by J.Mangels and G.L. Messing. American Ceramic Society, Columbus, OH, 1984.

39. Lee, D.I., "Packing of Spheres and its Effect on the Viscosity of Suspensions," *Journal of Paint Technology.*, 42, No. 550, 579 (1970).

40. R.K. Mcgeary, "Mechanical Packing of Spherical Paticle," *J. Am. Ceram. Soc.*, 44 [10], 522 (1961).

41. G.P. Bierwagen, "CPVC Calculations," *Journal of Paint Technology.*, Vol. 44, No.574, 46-55 (1972).

42. J.E. Ayer and F.E. Soppet, "Vibratory Compaction: II, Compaction of Angular Shapes," *J. Am. Ceram. Soc.*, 49 [4] 207-10 (1966).

43. J.K. Wright, M.J. Edirisinghe, J.G. Zhang, and J.R. G. Evans, "Particle Packing in Ceramic Injection Molding," *J. Am. Ceram. SOc.*, 73[9] 2653-58 (1990).

44. J.W. Cahn and R.B. Heady, "Analysis of Capillary Forces in Liquid-Phase Sintering of Jagged Particles," *J. Am. Ceram. Soc.*, 53, 406-9 (1970).

45. L.H.S. Roblee, R.M. Baird, and J.W. Tierney, "Radial Porosity Variations in Packed Beds," *AICHE Journal*, 4 [4] 460-64 (1958).

46. L.C.E. Struik, Physical Aging in Amorphous Polymers and Other Materials, Elsevier Scientific Publishing Company, New York, 1978.

# CHAPTER 4
# INHOMOGENEITY AND ANISOTROPY OF TAPE CAST CERAMIC GREEN SHEETS

## 4.1 Introduction

Tape cast sheets experience a number of processes which cause deformation. For example, thermal expansion of the polymer matrix occurs on heating and shrinkage occurs as binder is removed from particle junctions. Warping, cracking, and delamination can result from these processes during binder removal and sintering. Defects mainly originate from two sources. The first source is the high gas pressure within the ceramic greenware during binder removal, when the gas generation rate exceeds the capacity of the pores to permit diffusion[1-5]. This type of defect can usually be avoided by decreasing the heating rate. The second source is the nonuniform dimensional change of the sample, resulting from the pre-existing structural inhomogeneity and anisotropy of the greenware[6]. This second type of defect cannot be prevented by lowering the heating rate since it is only determined by the microstructure of the greenware. Structural inhomogeneity of the green tapes results in shrinkage gradients within the samples during binder removal and sintering processes. This differential shrinkage within a ceramic greenware creates stresses, which serve as origins for defect formation. Anisotropic shrinkage increases difficulties in dimensional and shape control of the final products. The structure of the tape also determines the strength and flexibility of the tape, which is extremely important for the processing and handling of the thin films[7].

Limited research has been conducted toward understanding the inhomogeneity and anisotropy of the green sheets. Shanefield[8]pointed out that after the porosity between ceramic particles was filled, further addition of binder caused the segregation of the extra

binder to the top surface. A slightly binder-rich top region of the tape has been observed by several researchers[9-12], through the TGA results of thin slices cut from the top and bottom sections of the tape. Settling of the particles[9,10] or migration of the binder towards the surface[11,12] during drying was believed responsible for this inhomogeneity across the thickness. All the observations were made in thick films (h = 200-5000 μm).

Gradient in binder composition has also been observed recently[13]. Cima *et al*[13] found that a $BaTiO_3$ tape with BBP plasticized PVB as binder has higher plasticizer concentration in the top surface region than the bottom surface region. Multicomponent transport phenomena during drying are believed to be responsible for this binder composition inhomogeneity across the tape thickness.

Nahass[10] observed anisotropic shrinkage of green tapes under controlled aging conditions and after firing. His research showed that the tape casting direction experienced higher shrinkage during aging and firing than the transverse direction, even though equiaxed particles were used in the tape. The causes of the inhomogeneity and anisotropy, however, are not well understood.

The previous limited characterization was performed on electronic package substrates, with the thickness of tapes ranging from 100 to 500 μm. No publication has been found on the characterization of the thin films (10-50 μm) used as dielectrics in multilayer ceramic capacitors. As more and more effort is directed toward reducing the size of electronic circuitry, the demand for quality and reliability of thin dielectric layers continues to rise. A systematic study of structural inhomogeneity and the resulting properties of ceramic green sheets is necessary in order to understand the origins of these defects and to design processing conditions to avoid them.

The following properties of the tapes will be examined in this chapter: 1. warping of the single tapes during annealing, and binder removal; 2. shrinkage of the tapes during annealing, binder removal, and sintering; 3. tensile properties of the green tapes along casting direction and transverse direction. The deformation of pure polymer films during annealing will also be examined to understand the origins of residual stresses in the binder matrix of the green tapes.

## 4.2 Experimental Procedure

A large amount of the ceramic tapes used in this study were industrially produced green sheets. They were composed of $BaTiO_3$ powder and benzyl butyl phthalate (BBP) plasticized poly (vinyl butyral) (PVB) as binder. The weight ratio of PVB to BBP was kept constant at 60:40. The volume ratio of $BaTiO_3$ powder to $BaTiO_3$ powder plus binder varied from 50% to 60%. The thickness of the tapes was 22 and 34 μm, respectively.

**Table 4.1. Composition of Tape Casting Slurry**

| Name | wt% | vol% | Function |
|---|---|---|---|
| Barium titanate | 53.4 | 14.0 | Ceramic |
| Polyvinyl butyral | 6.0 | 8.7 | Binder |
| Benzyl butyl phthalate | 4.0 | 5.7 | Plasticizer |
| Methyl ethyl ketone | 29.3 | 57.0 | Solvent |
| Ethyl alcohol | 7.3 | 14.6 | Solvent |

Ceramic green tapes were also produced in a lab under controlled drying conditions in order to study the effect of drying rate on the structural inhomogeneity of the tape. $BaTiO_3$ powers were dispersed in a premade binder solution by ball milling for 16 hours. The composition of the slurry is shown in Table 4.1. The slurry was cast at 0.85 cm/s on a

silicone coated Mylar film. Drying of the slip was achieved by blowing air from the end of a 1.2 meter drying chamber. Three air flow rates were used: 60, 30, and 0 m/min. The tapes were peeled from the substrate after being dried for an hour.

PVB films were cast from its solution on a glass substrate at 2.54 cm/s. The solution was made by dissolving 25% PVB in a mixture of solvents which contained 80 wt% methyl ethyl ketone and 20 wt% ethyl alcohol. The films were dried in stagnant air either for 12 hours or for a week. They were then washed off from the substrate with water and dried again in a vacuum for 48 hours.

An experiment was designed to measure the deformation of green tape *in situ* during binder removal. A piece of tape (L×W×H = 1.2×0.5×H $mm^3$) was cut from a large

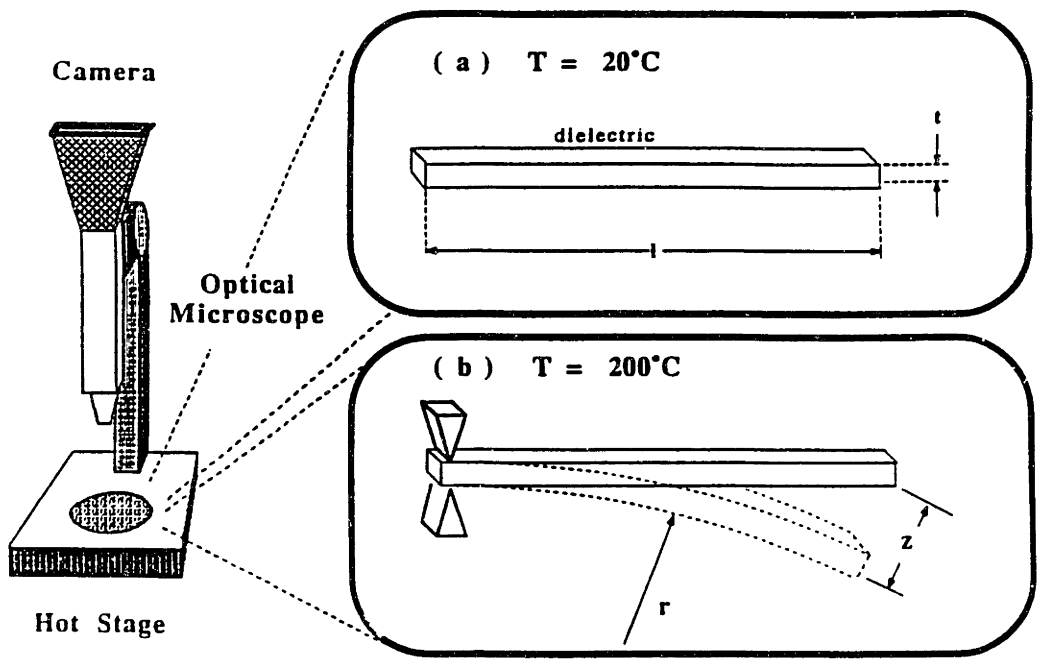


**Figure 4.1 Schematic of the bending measurement of a ceramic tape**

section of sheet using a razor blade, and this piece was then fixed at one end with a copper grip. The other end was free to move, as shown in Figure 4.1. The sample was then heated and observed with the hot-stage/optical microscope. Micrographs were taken at various temperatures. The length of the beam ($\bar{l}$), the deflection of the beam (h), and the displacement of the free end of the beam from its original state ($z$), were measured from the negative using an optical magnifier (10×). The curvature ($1/r$) and the length ($l'$)of the tape are given by (Fig. 4.2):

$$\frac{1}{r} = \frac{8h}{\bar{l}^2 + 4h^2} \qquad (4.1)$$

$$l' = 2r(\pi - 2\tan^{-1}\frac{l}{2|h|}) \qquad (4.2)$$

When the curvature and shrinkage of the tapes are small, the curvature of the tape can be approximated as[6]:

$$\frac{1}{r} = \frac{2z}{l^2} \qquad (z<<l) \qquad (4.3)$$

$z$ and $h$ were randomly chosen to be positive if the tape bent toward the face which was exposed to air during casting (top), and negative if bending was toward the surface which was in contact with the carrier substrate during casting (bottom).

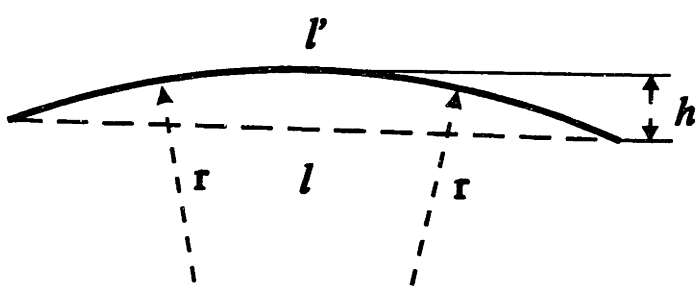


**Figure 4.2 Geometry of the deformation of a single layer ceramic tape**

The ceramic green tapes were heated at 5°C/min to 500°C to remove all the binder. The annealing process, on the other hand, was conducted by heating the samples at 5°C/min to 70°C, and kept at 70°C for the desired period of time. The same annealing temperature was used for both the ceramic tape and for the PVB films.

The shrinkage of the tapes was measured using an optical method. Small pieces ($2\times2mm^2$) were cut from the tapes using a razor blade and they were then placed on spherical particles (proppens). These samples were first annealed at 70°C for 24 hours, then heated at 5°C/min to 500°C to remove all the binders. They were then transferred onto zirconia grogs and were heated at 10°C/min to 1330°C and kept at this temperature for 2 hours. Optical micrographs (50 ×) were taken before and after each stage. The dimensional changes of the samples in the x-y plane were measured from the negatives using an magnifier (15 ×).

A 1 m long and 8 cm wide $BaTiO_3$ tape was cast at 2.54 cm/s on a lecithin coated glass substrate from the slurry described in Table 4.1. The thickness of the dried tape was 34 μm. The tape was cut in half and peeled from the substrate after being dried in stagnant air for 12 hours. One half of the tape was peeled off along the casting direction ($A_1$), which is the conventional way to peel off the tape. The other half of the tape was peeled off along the transverse direction ($A_2$). Small pieces of the tape were cut from the middle of these two large pieces and the shrinkage of these small pieces was measured following the same optical method as described above.

The tensile properties of the green tapes and annealed tapes were measured using an Instron 4505. The annealed tapes were prepared by heating them at 1°C/min to 70°C and keeping them at this temperature for 8 hours. The tapes were weighed before and after annealing, and 0.14% weight loss was detected. Rectangular samples prepared according

to ASTM D882-90 for thin plastic films continuously failed at the grip. Dog bone shaped samples cut with a conventional die contained defects on their cutting edges, which caused a tear of the sample before the maximum strength of the materials was reached. A schematic of the modified sample is shown in Figure 4.3. A razor blade was bent to an arc of radius of 280 cm. The thin film was placed on a glass substrate and cut with the razor blade. Each razor blade only served for two cuts to ensure clean, defect-free edges. Samples produced using this method were checked under an optical microscope, and showed smooth, defect-free cutting edges. A 1 kg load cell was used and the samples were deformed at 0.002 $s^{-1}$. Eight to ten samples were used for each measurement.

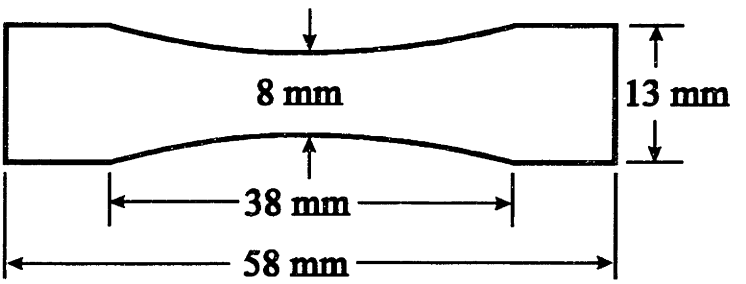


**Figure 4.3 Geometry of the sample for the tensile test**

## 4.3 Results

### 4.3.1 Deformation of the Tapes During the Binder Removal Process

The thermal gravimetric analysis (TGA) of a single layer tape at 5°C/min and 1°C/min heating rates are shown in Figure 4.4. Two distinctive stages of binder removal were observed. At the 5°C/min heating rate, the first weight loss period occurred between 120 and 160°C, corresponding to the evaporation of the BBP plasticizer. The second

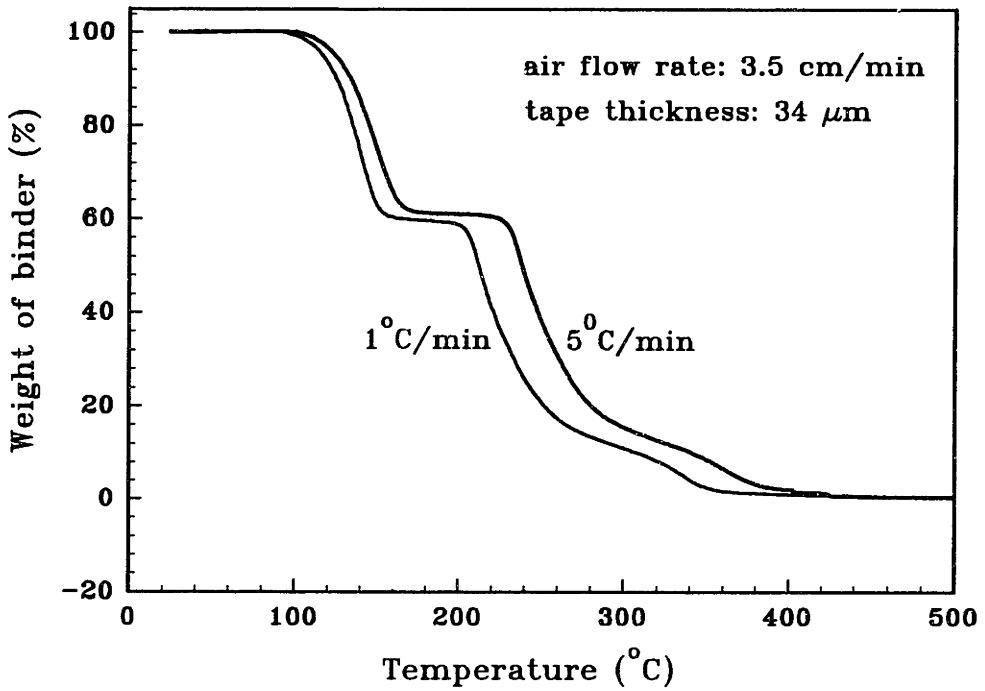


**Figure 4.4 TGA of a ceramic tape at different heating rates**

weight loss period occurred between 200 and 400°C, during which the PVB polymer decomposed. Decreasing the heating rate from 5°C/min to 1°C/min shifted the TGA curve toward lower temperature.

Figure 4.5 shows four optical micrographs of the cross-section of the tape with 50 vol% ceramic powders cut along the casting direction. The tape bent toward the bottom surface at 70°C. The curvature recovered by 100°C and then bent toward the top surface at higher temperatures. Curvature versus the temperature of the tapes loaded with 50 vol% ceramic powders is shown in Figure 4.6. Specimens were cut with long axis along the casting direction, transverse direction, and 45° between these two directions. All specimens bent toward the bottom at low temperature and bent toward the top at high temperatures. The magnitude of the maximum negative curvature was nearly independent of specimen orientation. The curvature became positive as the temperature was raised above 80°C until 160°C where the curvature remained constant until 290°C. The

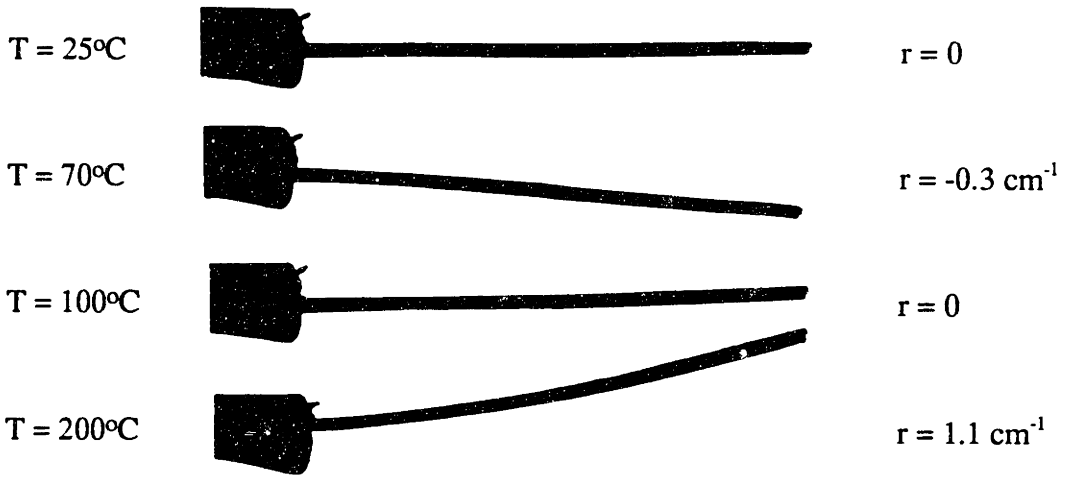


**Figure 4.5 Optical micrographs of the cross-section of a tape at different temperatures**

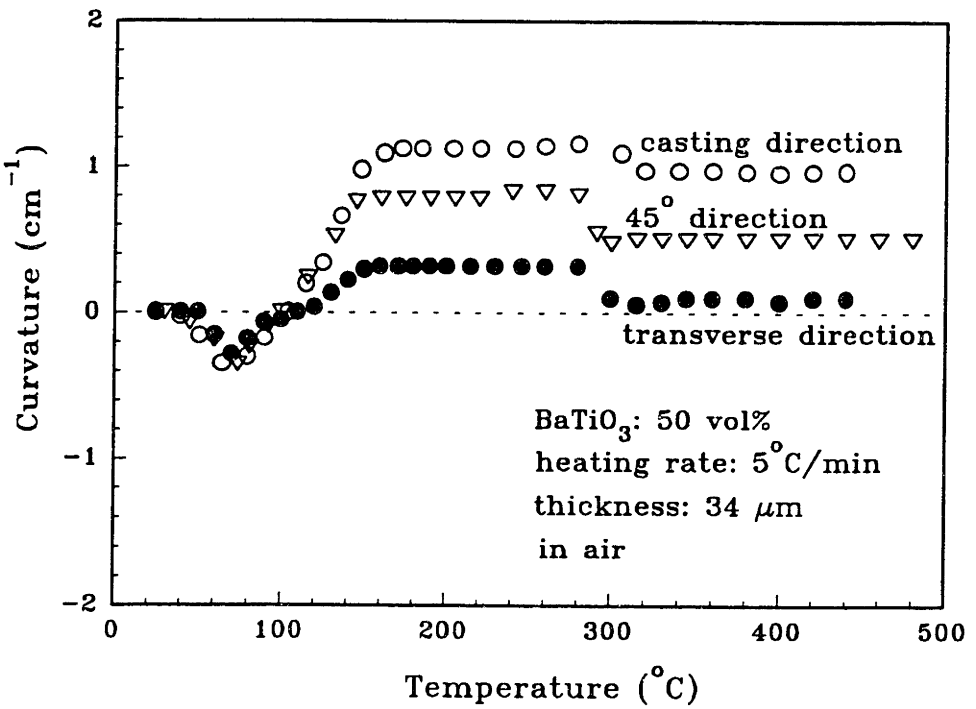


**Figure 4.6 Curvature of the tape with 50 vol% ceramic powders during binder removal**

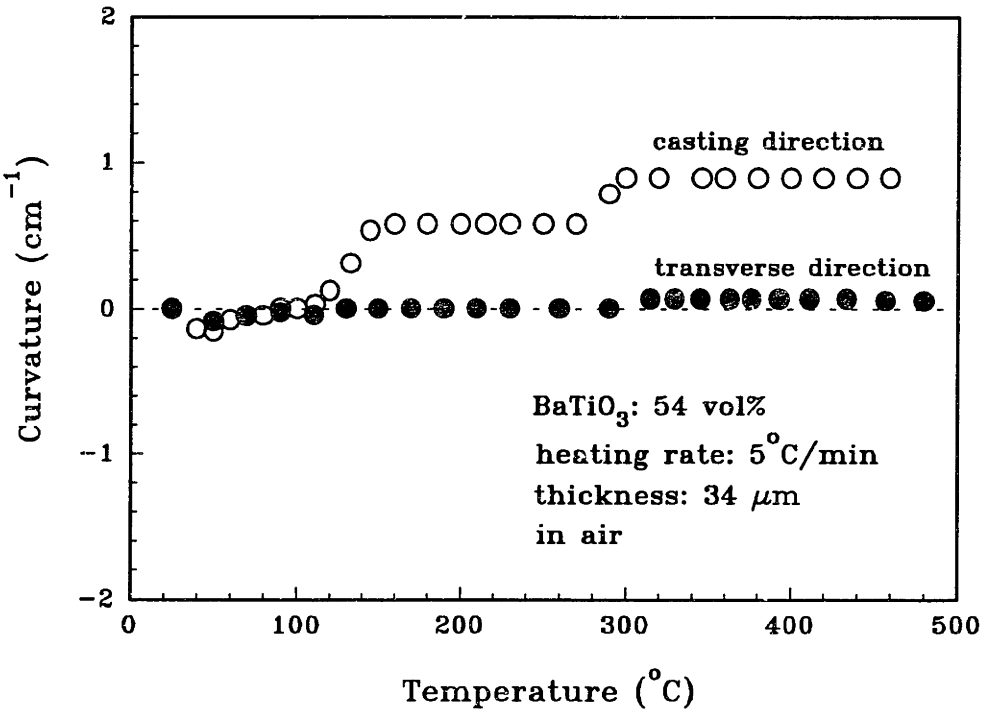


**Figure 4.7 Curvature of the tape with 54 vol% ceramic powders during binder removal**

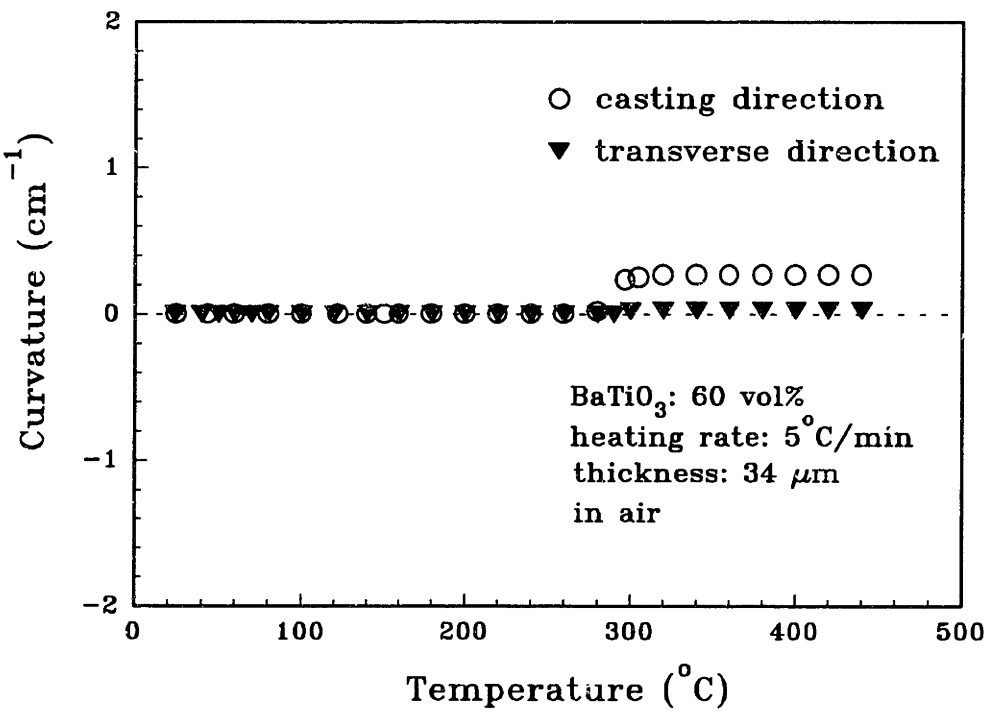


**Figure 4.8 Curvature of the tape with 60 vol% ceramic powders**

maximum positive curvature was, however, anisotropic. The casting direction had the highest curvature, and the transverse direction had the lowest. The curvature of the tape cut 45° between these two directions was intermediate. The curvature in all three directions decreased from 290 to 320°C. It remained constant as the temperature further increased.

The maximum curvature decreased with increasing ceramic loading as shown in Figures 4.7 and 4.8. The sample loaded with 60 vol% ceramics did not deform in either direction until the temperature reached 290°C. It then bent toward top surface between 290 and 320°C. The maximum curvature of the tapes decreased from 1.1 to 0.9 and 0.3 $cm^{-1}$ in the casting direction, and decreased form 0.3 to 0.07 and 0.03 $cm^{-1}$ in the transverse direction as the ceramic loading increased from 50 to 54 and 60 vol%. The

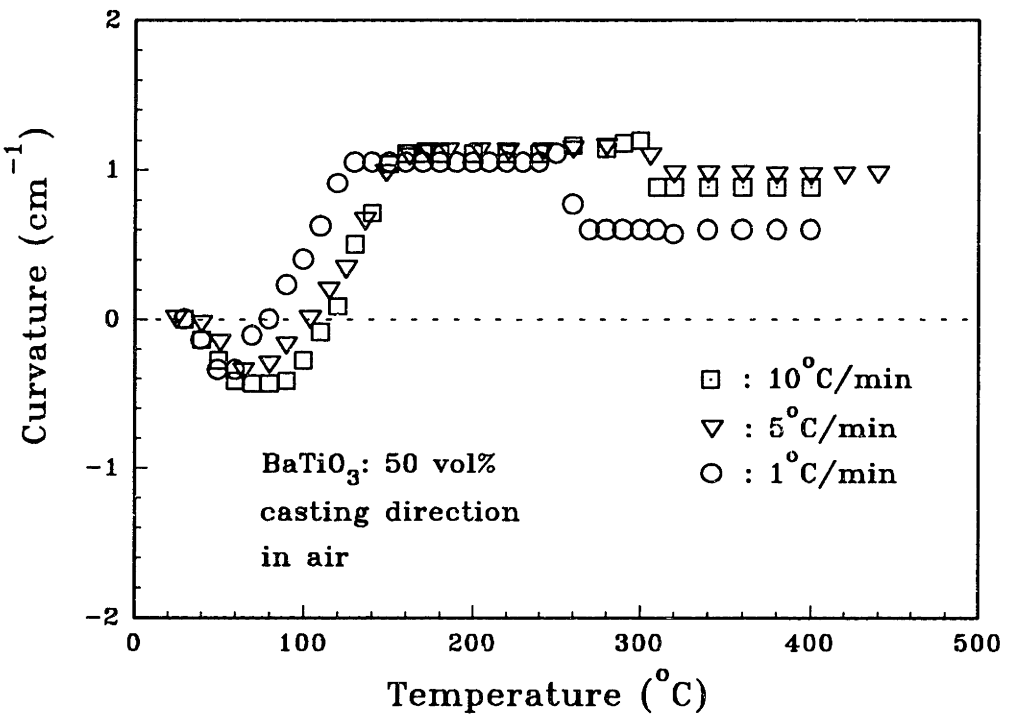


**Figure 4.9 Curvature of the tape with 50 vol% ceramic powders at different heating rates**

curvature of tape with 50 vol% ceramic powders at different heating rates is shown in Figure 4.9. Lowering the heating rate only lowered the temperature at which bending started; it did not change the magnitude of the maximum deflection. Decreasing the film thickness from 34 to 22 μm, however, caused an increase of the curvature from 1.1 to 2.5 $cm^{-1}$, as shown in Figure 4.10.

The shrinkage of the tapes after binder removal and sintering is shown in Figure 4.11. The shrinkage decreased rapidly when the ceramic loading increased from 48 to 50 vol%. It then decreased slowly as the ceramic loading further increased from 50 to 60 vol%. Higher shrinkage occurred in the tape casting direction than in the transverse direction. The differential shrinkage in these two directions, however, decreased with increasing ceramic loading in the green tapes. Thus differential shrinkages after sintering were the same as they

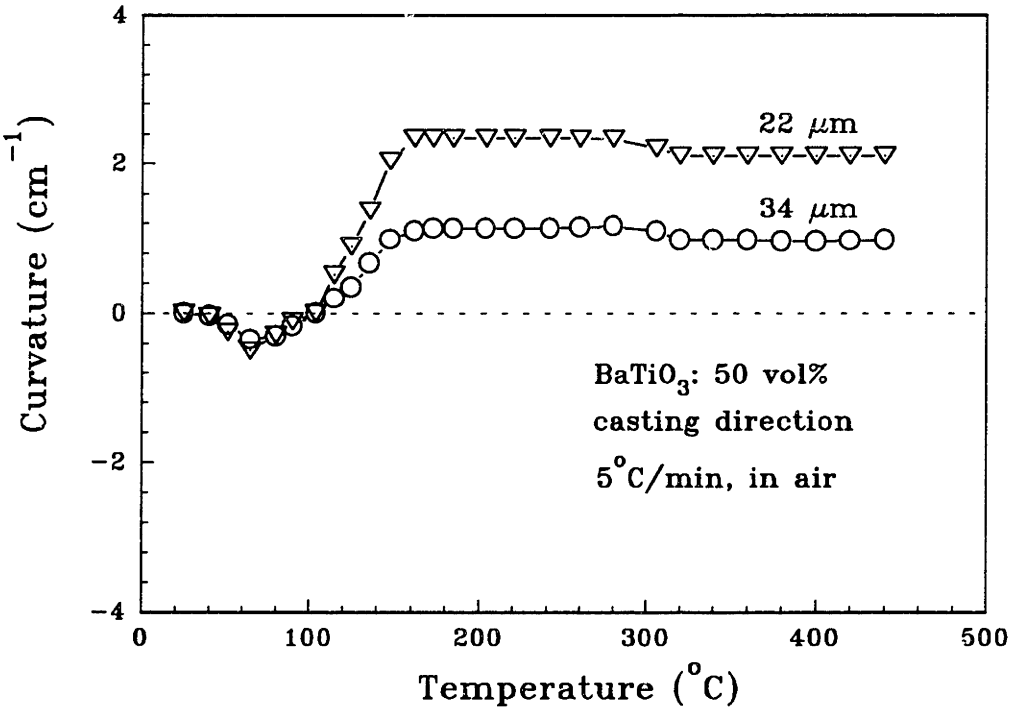


**Figure 4.10 Curvature of the ceramic tapes with different thickness during binder removal**

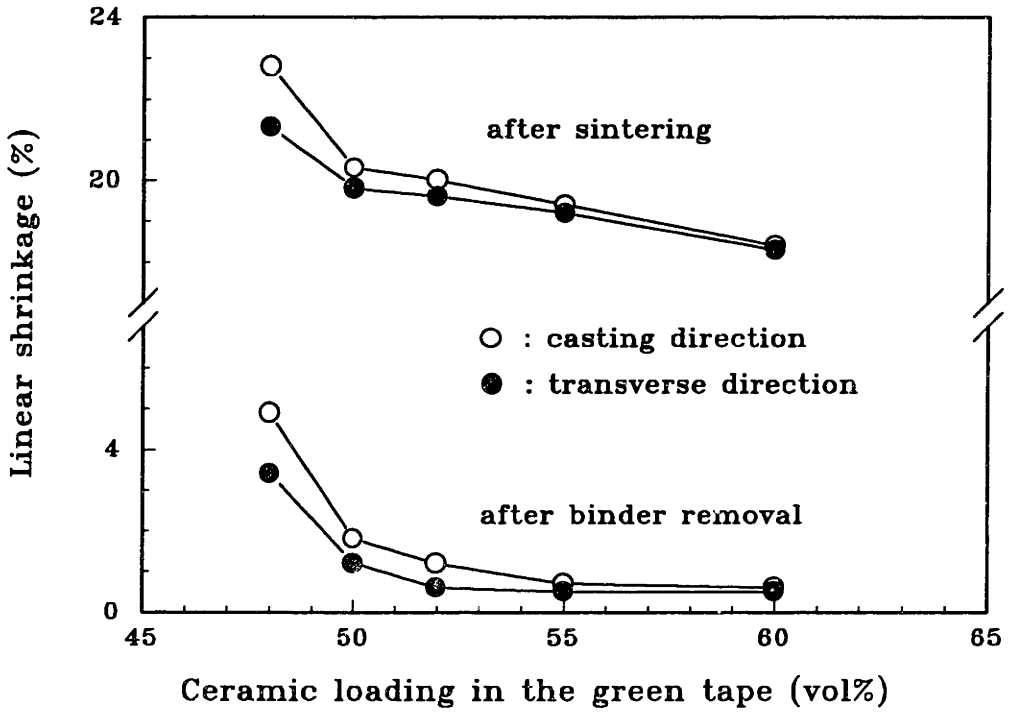


**Figure 4.11 Shrinkage of the green tapes after binder removal and sintering**

were after binder removal, indicating that the sintering process did not create shrinkage anisotropy.

The deformation of the samples dried at three different air flow rates is shown in Figures 4.12 and 4.13. The tapes dried at 60 and 30 m/min air flow rates first bent to the bottom surface direction when they were heated, and the curvature of the fast drying tape was higher. The tape dried in stagnant air, however, bent toward the top surface. This bending slowed down after 100°C. The tapes in all three drying rates bent toward the top surface between 120 and 160°C. Two to three percent shrinkage occurred between 120 and 180°C, and the shrinkage increased as the drying rate of the tape increased. Half a percent shrinkage occurred between 280 and 320°C.

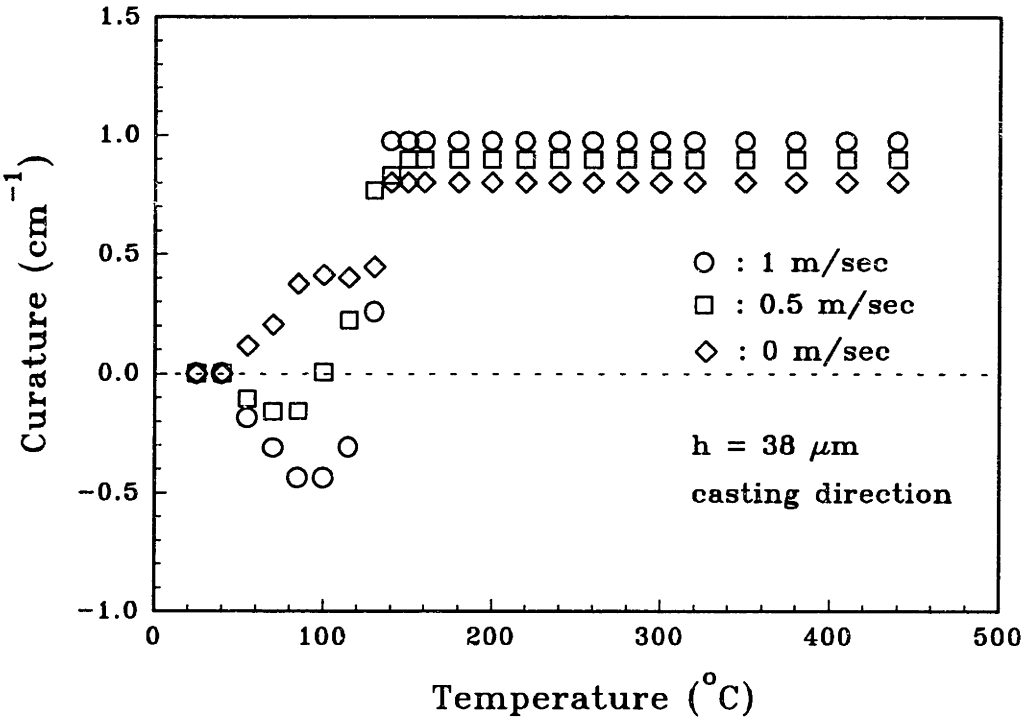


**Figure 4.12 Curvature of the cast tape during binder removal**

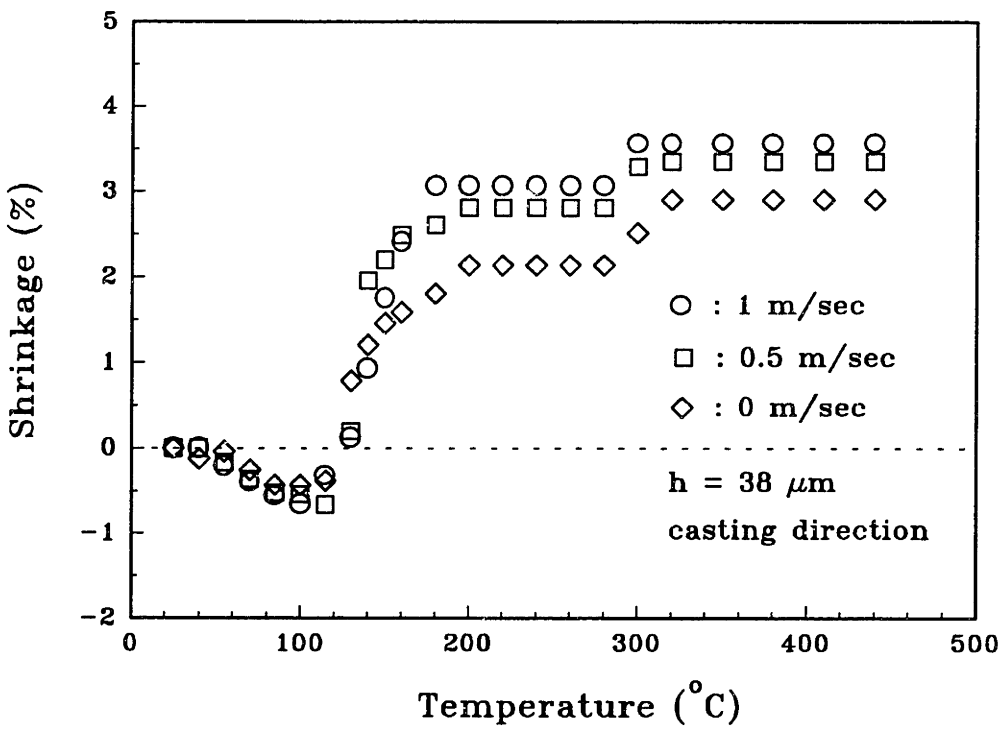


**Figure 4.13 Dimensional change of the cast tape during binder removal**

**Table 4.2 Linear shrinkage of the tape peeled along the casting and transverse directions after binder removal**

| | $A_1$ | $A_2$ | $\varepsilon_{A_1} / \varepsilon_{A_2}$ |
|---|---|---|---|
| $\varepsilon_{casting}$ (%) | 2.92 ± 0.03 | 2.91 ± 0.05 | 1.00 |
| $\varepsilon_{trans}$ (%) | 2.39 ± 0.04 | 2.42 ± 0.05 | 0.99 |

The shrinkage of the $A_1$ and $A_2$ samples after binder removal is shown in Table 4.2. The casting direction experienced higher shrinkage than the transverse direction in both samples. The shrinkages in both the $A_1$ and $A_2$ samples along the casting direction were nearly the same, and this was also true along the transverse direction. Therefore, shrinkage during binder removal was not affected by the way the green tape was peeled off the substrate in the current system. This leads to the conclusion that the stress from peeling in the green tape can either be fully relaxed or is too small to be detected using the current technique.

### 4.3.2 Deformation of Tapes During Annealing

The deformation of the tapes during the annealing process is shown in Figure 4.14. The tapes had negative curvature in both the casting and transverse directions when the temperature had reached 70°C. The deformation was isotropic at this point. The tape along the casting direction returned to its original state after only four minutes, and then continued to bend toward the top surface. This process slowed after 45 minutes. In the transverse direction, however, it took 12 minutes for the tape to return to its original state, and it stayed in that state during the following 33 minutes. It then started to bend toward the top surface slowly. The differential curvature of these two directions remained constant after 45 minutes. The curvatures in both directions reached the same magnitude

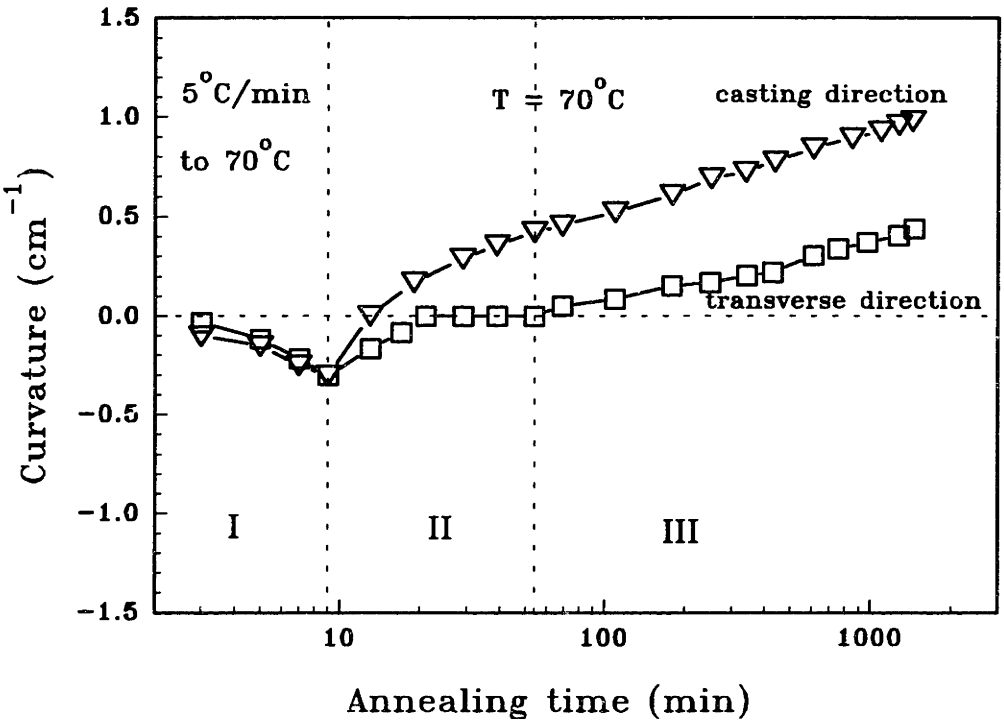


**Figure 4.14 Curvature of the tape with 50 vol% ceramic powders during annealing**

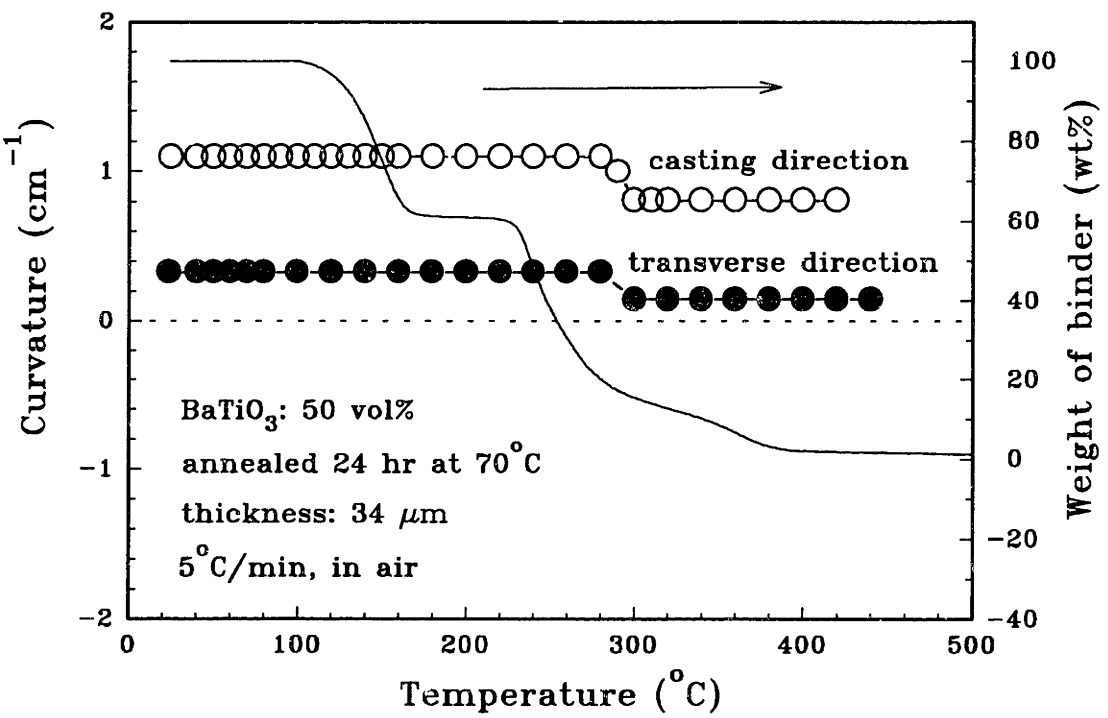


**Figure 4.15 Curvature of the annealed tape during binder removal**

after annealing as did the tapes with their respective values when heated to 280°C.

The annealed samples were heated at 5°C/min to removal the binder. The curvature of these samples during binder removal is shown in Figure 4.15. The curvatures in both directions remained constant until 280°C. Between 280°C and 320°C, the curvature decreased slightly.

The dimensional change of the tape after annealing and binder removal is shown in Figure 4.16. There was 0.3 wt% weight loss in the tapes after them were kept at 70°C for 24 hours. The tape casting direction experienced higher shrinkage than the transverse direction. This differential shrinkage was the same as after binder removal. Two percent and 0.6% linear shrinkages were observed in the casting and transverse directions,

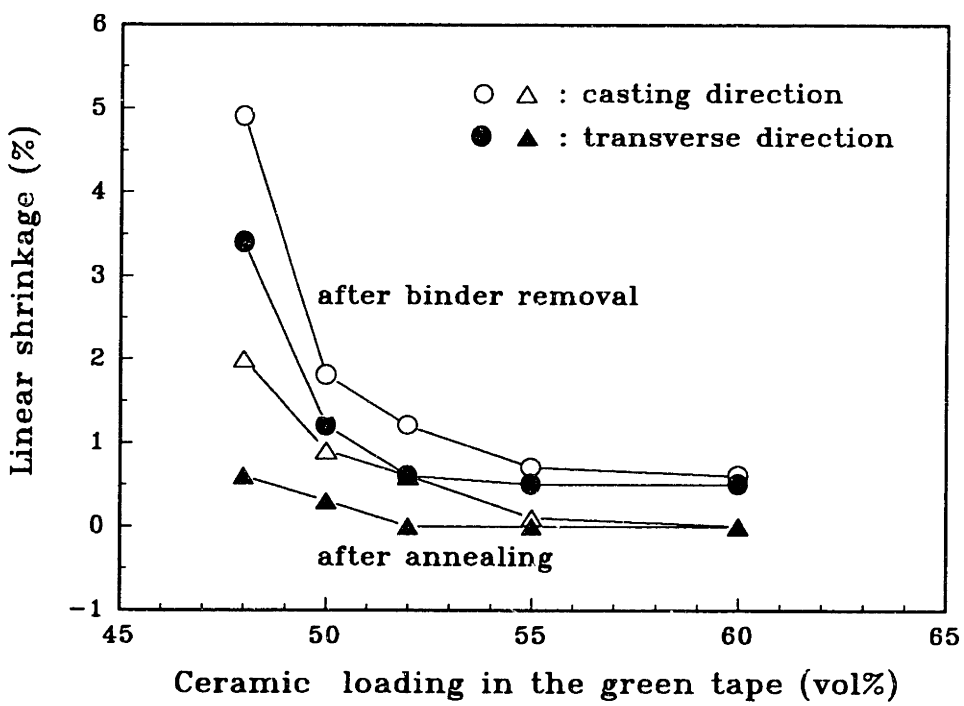


**Figure 4.16 Shrinkage of the tapes after annealing and binder removal**

respectively, after the annealing. This shrinkage would produce a 2.6% volume shrinkage, even if there were to be no shrinkage in the thickness. The 0.3 wt% weight loss can only account for 1 vol% shrinkage in this sample. Therefore, the tape either experienced expansion in its thickness during annealing or/and the porosity in the green tape was eliminated. This will be discussed further later.

### 4.3.3 Deformation of Tape Cast PVB Film During Annealing

The deformation of the PVB film during annealing is shown in Figure 4.17. The film was dried on the glass substrate for 12 hours before it was removed from the substrate. It bent toward the bottom surface slightly when heated and then bent rapidly toward the top

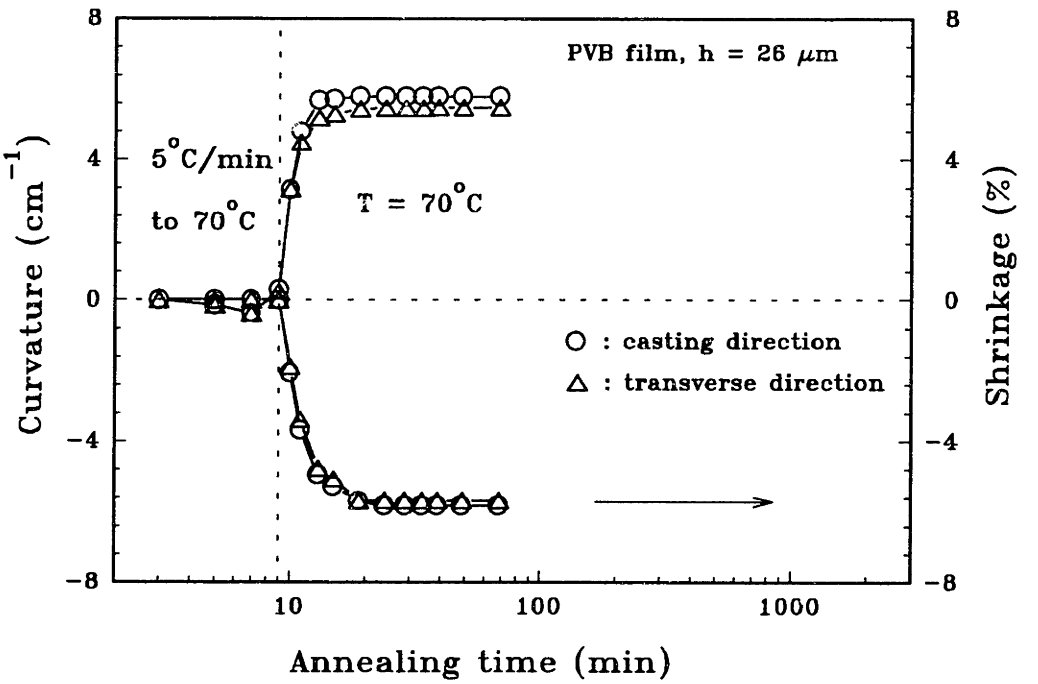


**Figure 4.17 Deformation of the PVB film (dried on substrate for 12 hours) during annealing**

surface. Shrinkage in both the tape casting and the transverse directions also occurred at 70°C. The deformation stopped after the film was kept at 70°C for ten minutes. This annealing process produced 5.8% linear shrinkage and 5.7 $cm^{-1}$ curvature in both the casting and transverse directions. The thickness of the film was measured from its scanning electron micrograph before and after annealing, and 7.6% expansion was observed.

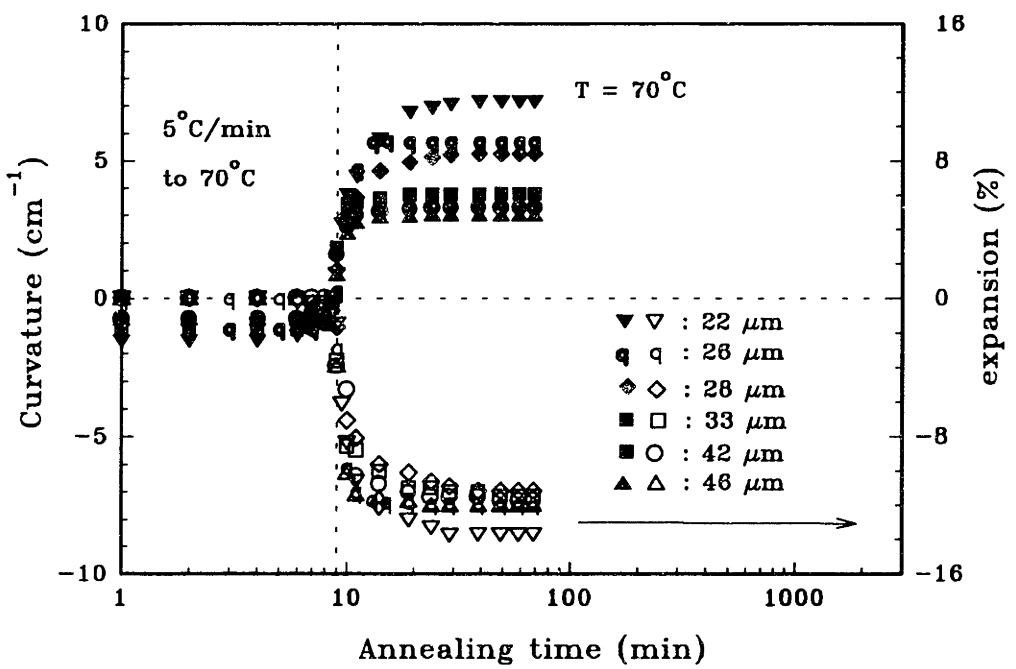


**Figure 4.18 Deformation of the PVB films (dried on substrate for a week) during annealing**

The deformation of the PVB films which dried on glass substrate for a week is shown in Figure 4.18. The thickness of the film varied from 22 to 46 μm. These films bent slightly toward the bottom surface after being washed off and dried. The film bent toward the top surface rapidly at 70°C. A large shrinkage also occurred. The curvature increased from 3.0 to 7.2 $cm^{-1}$ as the film thickness decreased from 46 to 22 μm. The

shrinkage of the films, however, remained at 11.6% as the film thickness decreased from 46 to 26 μm. The 22 μm film experienced slightly higher shrinkage (13.5%) than the rest of the samples.

The linear shrinkage of the PVB film in the x-y plane increased from 5.8% to 11.5% when the drying time of the PVB film on the glass substrate increased from 12 hours to a week. The curvature of the film, however, was not affected by the drying time on glass. TGA results of the 26 μm film stripped away from the substrate indicated 4 wt% residual solvent in this sample. Less than 0.2% solvent was detected after the film was on the glass substrate for a week. No solvent could be detected after storage in vacuum for 48 hours.

### 4.3.4 Tensile Properties of the Ceramic Green Sheet

**Table 4.3. Tensile Properties of Green Tapes**

| | | $\sigma$ (MPa) | $\varepsilon$ (%) | E (MPa) | $\sigma_{\parallel} / \sigma_{\perp}$ | $\varepsilon_{\parallel} / \varepsilon_{\perp}$ | $E_{\parallel} / E_{\perp}$ |
|---|---|---|---|---|---|---|---|
| Ceramic tape | $\parallel$ | 5.08 | 20.4 | 56.08 | 1.07 | 0.88 | 1.40 |
| | $\perp$ | 4.79 | 23.2 | 40.03 | | | |
| Annealed tape | $\parallel$ | 7.31 | 17.3 | 89.09 | 1.01 | 0.91 | 1.16 |
| | $\perp$ | 7.22 | 19.0 | 76.64 | | | |

Table 4.3 lists the mechanical properties of the green tapes and the annealed tapes, along the tape casting direction and transverse directions. The tensile strength and modulus along the tape casting direction were 7% and 40% higher than in the transverse direction. The elongation to failure, however, was 12% lower in the casting direction than in the transverse direction. After the tapes had been annealed at 70°C for 8 hours, the strength and modulus increased and the elongation to failure decreased. Annealing also lowered the anisotropy in the green tapes. The differential strength and modulus

decreased to 1% and 16% in the two directions, and the differential elongation to failure decreased to 9%.

## 4.4 Discussion

The tape cast green ceramic sheet is a mixture of three phases: ceramic powder, polymer binder, and pores. The polymer binder is a continuous network in which ceramic powders are dispersed, and a small amount of trapped porosity (usually 1-5 vol%) is distributed in the tape. Structural homogeneity requires that all the phases uniformly distribute throughout the tape.

One kind structural inhomogeneity is a binder rich top surface which has been previously observed and been contributed to particle settling during drying process[9,10]. A binder-rich surface will cause deflection toward the bottom during heating because of the high thermal expansion coefficient of polymers relative to ceramics. As the plasticizer starts to evaporate from the sample, capillary forces rearrange the ceramic particles to a higher packing density and cause shrinkage of the sample. This shrinkage occurs between 120 and 160°C, and its magnitude increases with increasing binder concentration[14]. Thus, high binder content near the top will cause positive curvature during binder removal.

The particle settling speed ($V_{sett}$) during drying can be estimated by Stokes' law[15]:

$$V_{sett} = \frac{d^2(\rho_s - \rho_l)g}{18\eta_l} \qquad (4.4)$$

where $d$ is the particle diameter, $\rho_s$ and $\rho_l$ are the particle and liquid densities, respectively, $g$ is gravitational acceleration, and $\eta_l$ is the viscosity of the liquid. Eq. 4.4 reveals the

settling speed for a one μm particle is $5.44 \times 10^{-9}$ cm/s, taking $\eta_l$ as 500 cp which is the typical viscosity of a binder solution used in tape casting. This is the maximum settling speed since $\eta_l$ increases rapidly as drying proceeds, which decreases the particle settling speed according to Eq. 4.4.

The tape shrinks in the thickness during drying. The shrinkage rate of the tape along thickness ($V_{shrin}$) can be estimated as:

$$V_{shrin} = \frac{J}{\rho_{sol}} \qquad (4.5)$$

where $J$ is the evaporation rate, and $\rho_{sol}$ is the density of solvent. A typical J value of organic solvents is $2.22 \times 10^{-5}$ g/cm$^2$·s at 25°C and 75 l/min air flow rate[9,16]. This gives a shrinkage rate of the tape along thickness as $2.8 \times 10^{-5}$ cm/s. Comparing the particle settling speed and the shrinkage rate in the thickness indicates that particle settling does not occur during drying in a well dispersed slurry since the shrinkage rate in the tape thickness is four order of magnitude higher than the maximum settling rate of a one μm particle.

A binder-rich surface layer is not consistent with the annealing results either. The temperature of the annealing process is above the glass transition temperature of most of the binder in the ceramic tape, and is below the temperature of binder removal. Therefore, the major process during annealing is the relaxation of residual stresses in the binder matrix. This leads to the conclusion that the relaxation of the residual stresses in the binder matrix causes the bending and the anisotropic deformation of the films since annealing resulted in the same magnitude of curvature in the green tape as in the binder removal. Most of the differential shrinkage in the tape casting and transverse directions also occurs during annealing, indicating that stress relaxation is the cause of shrinkage anisotropy.

The binder network consists of free binder regions apart from particles as well as reduced mobility binders near particles. The free polymer region can not retain any residual stress at room temperature since its glass transition temperature is as low as -11°C. The residual stress can only exist in regions of reduced mobility. Studying the relaxation of the PVB film (which has a $T_g$ of 51°C) during annealing has shed light on the origins of these residual stresses, as discussed below.

Two types of structural inhomogeneities can exist in a solvent cast polymer film. First, the polymer chains tend to align in the plane parallel to the substrate during drying[17-24]. The orientation of the polymer chains is completely random within the x-y plane. This alignment is long range if a high molecular weight polymer is used[24], and the degree of this alignment tends to be higher near the bottom surface of the film. This orientation is caused by the steric/adhesion effects and long-range interactions of the solid surface with the polymer molecules. Secondly, a density gradient across the film thickness might exist. Solvents evaporate from the top surface during drying. As a result, a "skin", or at least a considerable gradient in viscosity can form[25,26]. The polymer chains in the top surface region are "frozen-in", while the polymer chains in the regions away from the top surface can still relax. Therefore, the top layer may trap a higher amount of free volume than the bottom region. The aligned polymer chains will relax back to their random coil state to resume the lowest energy state if the film is annealed at a temperature above its $T_g$, and the extra free volume will also be eliminated. The relaxation of oriented polymer chains in the x-y plane will result in shrinkage in this plane and expansion in the thickness. The higher orientation near the bottom surface region causes higher shrinkage. Therefore, the film will bend toward the bottom surface during annealing. The elimination of the extra free volume will bend the film toward the top surface, and it will also cause a slight shrinkage of the film. The deformation of the film, therefore, is determined by the

combined effects of these two kinds of inhomogeneities. Neither of them, however, will result in anisotropic deformation in the x-y plane.

The shrinkage of the tape in the x-y plane increases when the overall stress rises. The curvature of the tape, however, is only determined by the shrinkage gradient across the film. A small amount of solvent can cause rapid relaxation of stress upon removal of the film from the substrate[14]. This relaxation before the annealing process decreases the residual stress and, therefore, the shrinkage of the film during annealing. The shrinkage of the 26 μm PVB film decreased from 11.6 to 5.8% due to the relaxation caused by the 4% residual solvent. The unaltered curvature of this film indicates that its stress gradient remained the same even though the overall stress decreased.

The two kinds of structural inhomogeneities in pure polymer films exist in a ceramic green tape, although their magnitudes will be different. For example, the shrinkages of the tapes during annealing is lower than the PVB films, due to the existence of ceramic particles and to the different $T_g$ values of the two systems. The high shrinkages in the x-y plane of the tape with 48 vol% ceramic powders is likely to be accompanied by an expansion in the tape thickness, similar to the deformation of PVB films during annealing. Ceramic particles lower the mobility of polymer chains during drying and increase the drying rate, which alters the magnitudes of the residual stresses. The anisotropic deformation observed in the ceramic tape must be caused by a factor other than those which exist in the pure polymer films since these two types of structural inhomogeneities are isotropic in the x-y plane. This third factor is discussed below.

It is well known that a slurry which contains polymer exhibits pseudoplasticity. This means that during shearing, polymer chains line up along the casting direction, which results in a reduced resistance to flow[27]. The alignment of molecules in a liquid polymer

solution may immediately disappear when the shear stress is removed, and no preferred orientation can be observed in the x-y plane of a dried polymer film[17]. For a ceramic-polymer slurry, however, a high percentage of the polymer chains are adsorbed on the ceramic particle surface, and some of these chains may adsorb on more than one ceramic particle. The relaxation time of these polymer chains increases dramatically. Assuming that a polymer chain adsorbs on one particle at each end and that these two particles are separated by shearing, as shown in Figure 4.19, the relaxation time constant ($\tau$) for one particle is[28]:

$$\tau = \frac{3\pi\eta a^3}{kT} \qquad (4.6)$$

where $\eta$ is the viscosity of the suspension, $a$ is the radius of the particle, $k$ is the Boltzmann's constant, and $T$ is the temperature of the suspension. The relaxation time for a 0.5 μm radius particle in a 10 poise suspension at room temperature is 4.7 minutes. The complete drying time for a 34 μm thick green tape is the same order of magnitude[29]. The viscosity of slip rises rapidly as drying proceeds, which increases the relaxation time greatly. Therefore, it is reasonable to assume that the dried green tapes have a residual orientation of polymer chains along the casting direction. The surface region will have a higher orientation than the bottom region since the surface layer dries faster.

The above speculation is consistent with the tensile properties of the green tapes. A preferred orientation of the polymer chains along the tape casting direction will result in higher tensile strength, higher modulus, and lower elongation to failure in that direction than in the transverse direction[30]. The annealing process causes relaxation of the polymer chains and corresponding particle rearrangement. This reduces the anisotropy of the tensile properties of the tape.

The magnitude of the residual stresses in the green tapes is also affected by the drying rate. The slurry has less time to relax at a higher drying rate, which results in higher stresses in the green tape. Therefore, higher curvature and shrinkage of the tape can be observed during binder removal.

The deformation of a tape cast ceramic film during annealing and binder removal is then determined by the combination of the following three types of structural inhomogeneities: the alignment of polymer chains in the x-y plane during drying, a free volume concentration gradient across the tape thickness, and the residual orientation of the polymer chains in the casting direction from shearing. The deformation of the ceramic tape during annealing can then be divided into three stages. The first stage ranges from room temperature to 70°C, during which the relaxation of the aligned polymer chains in the x-y plane dominates the deformation. The tape is bent in the bottom surface direction, and this bending is isotropic. The second stage ranges from zero time to 45 minutes at 70°C, during which the relaxation of shearing induced orientation controls the tape deformation. In the casting direction, the tape is bent rapidly toward the top surface. In the transverse direction, however, the tape returns to its original state and remains in that state for the rest of the time. The third stage starts from 45 minutes at 70°c goes to the end of the annealing process, during which the elimination of the extra free volume from drying determines the deformation. The tapes in both directions are bent slowly toward the top surface, and the net curvature produced in this stage is the same in both directions.

The annealing process eliminates the residual stresses of the binder whose $T_g$ is lower than 70°C. A small portion of the binder in the ceramic tape has a glass transition temperature higher than 70°C, which can be observed from Figure 3.12. This portion of the polymer corresponds to the layer of polymer adsorbed onto the surface of the ceramic particles. It can be considered immobile until the temperature reaches its degradation

point. The polymer degradation started at 200°C, which caused shrinkage in the tapes. A nonuniform shrinkage across the tape thickness resulted in the bending of the tapes between 250 and 320°C.

The interparticle layers are composed of only two adsorbed polymer layers as the loading of the ceramic powders reaches or exceeds its critical particle volume concentration (CPVC)[31]. The adsorption layer does not relax. Therefore, the tapes with ceramic loading equal to or greater than CPVC do not deform until the temperature exceeds the degradation temperature of the polymer. The deformation of the tape with 60 vol% ceramic particles during binder removal confirmed this analysis.

Bending of the tape is undesirable in the production of both single layer films and MLC devices. After its origins are understood, steps can be taken to minimize the camber. A low shear rate is preferred to a high one in order to lower the orientation of polymer chains from shearing. A slow drying rate is recommended to give the polymer matrix a longer time to relax toward a uniform and equilibrium state. An extremely slow drying process might not be the best, since it lowers the production rate. A reasonable drying rate can be chosen after taking into consideration the relaxation of polymers and the production rate.

## 4.5 Conclusions:

A new experimental strategy was designed to observe the deformation of unconstrained ceramic tapes *in situ* during binder removal. This experiment resulted in the first measurement, using a hot-stage/optical microscope, of the curvature of the tapes. The tapes bent toward the bottom surface between 40°C and 100°C, and this bending was isotropic in the x-y plane. The tapes then bent toward the top surface as temperature

increased, and the casting direction had higher curvature than the transverse direction. The curvature of the tapes after binder removal decreased as the ceramic loading in the tape increased. Decreasing the tape thickness from 34 to 22 μm caused an increase of the curvature from 1.1 to 2.5 $cm^{-1}$. A higher air flow rate during the tape drying process caused an increase in both tape curvature and shrinkage during binder removal. Annealing at 70°C for 24 hours resulted in the same magnitude of curvature as binder removal.

Shrinkage of the green tapes after annealing, binder removal, and sintering was measured. The tapes had higher shrinkage in the casting direction than in the transverse direction after annealing. The differential shrinkages remained the same after the binder removal and sintering processes.

Tensile properties of the green tapes along the casting and transverse directions were measured at room temperature. The tapes had higher tensile strength, higher modulus, and lower elongation to failure in the casting direction than in the transverse direction. The difference in these properties decreased after the tapes were annealed at 70°C for eight hours.

The bending and the anisotropic properties of the green tapes were associated with the relaxation of residual stresses in the polymer matrix. Three types of residual stress in the tapes were speculated: 1. the alignment of polymer chains in the plane parallel to the substrate, which causes the tape to bend toward the bottom surface upon relaxation; 2. preferred orientation of polymer chains in the tape casting direction, which causes the tape in the casting direction to bend toward the top surface; 3. density gradient across the tape thickness, which causes the tape in both directions to bend toward the top surface.

**References**


1. D.L. Hipps and J.J. Brown, Jr., "Internal Pressure Measurements for Control of Explosive Spalling in Refractory Castables," *Am. Ceram. Soc. Bull.*, 63[7] 905-10 (1984).

2. M. Kahn, "Effects of Partial Oxygen Pressure During Burnout of Multilayer Structures"; pp. 185-88 in Advances in Ceramics, Vol. 19, Multilayer Ceramic Devices. Edited by J.B. Blum and W.R. Cannon. American Ceramic Society, Westerville, OH, 1992.

3. P. Calvert and M.J. Cima, "Theoretical Models for Binder Burnout," *J. Am. Ceram. Soc.*, 73 [3] 575-79 (1990).

4. M. Kahn and M. Chase, "Effects of Heat Treatments on Multilayer Piezoelectric Ceramic-Air Composites," *J. Am. Ceram. Soc.*, 75 [3] 649-56 (1992).

5. H. Verweij and W.H.M. Bruggink, "Reaction-Controlled Binder Burnout of Ceramic Multilayer Capacitors," *J. Am. Ceram. Soc.*, 73 [2] 226-31 (1990).

6. Y.Tang and M.J. Cima, "Inhomogeneity and Anisotropy of Tape Cast Ceramic sheets"; pp.14. CPRL report #22, MIT, 1992.

7. R.A. Gardner and R.W. Nufer, *Solid State Technol.*, 117, 38 (1974).

8. D.J. Shanefield, "Casting Ceramic-Polymer Sheets", pp. 69-76 in Mat. Res. Soc. Symp. Proc., vol. 40, 1985.

9. R.E. Mistler, D.J. Shanefield, and R.B. Runk, "Tape Casting of Ceramics"; pp. 411-48 in Ceramic Processing Before Firing. Edited by G.Y. Onoda and L.L. Hench. Wiley, New York, 1978.

10. P.R. Nahass, "The Effect of Changes in Chemistry and Ceramic Slurry Processing on Alumina Green Tapes"; Ph.D. Thesis, Department of Materials Science and Engineering, Massachusetts Institute of Technology, 1990.

11. M. Yasrebi, "Microstructural Development in Ceramic-Polymer Systems"; Ph.D. Thesis, Department of Materials Science and Engineering, University of Washington, 1988.

12. Y. Zhang, X.X. Tang, N. Uchida, and K. Uematsu, "Mathematical Simulation for Segregation of PVA During Drying," *J. Ceram. Soc. Japan*, 101 [2] 180-83 (1993).

13. M. Liu, and M.J. Cima, unpublished work, CPRL, MIT (1993).

14. J.K. Wright, M.J. Edirisinghe, J.G. Zhang, and J.R.G. Evans, "Particle Packing in Ceramic Injection Molding," *J. Am. Ceram. Soc.*. 73 [9] 2653-58 (1990).

15. For example, see M.M. Denn, *Process Fluid Mechanics*, Prentice-Hall Inc., NJ, 1980.

16. D.J. Shanefield, Rutger University. private communication, 1993.

17. J.S. Machell, J. Greener, and B.A. Contestable, "Optical Properties of Solvent-Cast Polymer Films," *Macromolecules*, 23, 186-194 (1990)

18. W.M. Prest, Jr. and D.J. Luca, "The Origin of the Optical Anisotropy of Solvent Cast Polymeric Films," *J. Appl. Phys*, 50[10], 6067-71(1979).

19. W.M. Prest, Jr. and D.J. Luca, "The Alignment of Polymers During the Solvent-Coating Process," *J. Appl. Phys.*, 51[10], 5170-74 (1980)

20. T.P. Russel, H.Gugger, and J.D. Swalen, "In-Plane Orientation of Polyimide," *Journal of Polymer Science*, vol.21, 1745-56 (1983).

21. K. Nakagawa, "Optical Anisotropy of Polyimide," *J. Applied Polymer Science*, vol.41, 2049-58 (1990)

22. R.D. Sudduth and C.E. Rogers, *Polym. Lett.*, 11, 603 (1973)

23. T.P. Sosnowske and H.P. Weber, "Thin Birefringent Polymer Films for Integrated Optics," *Appl. Phys. Lett.* vol.21, [7] 310-11 (1972).

24. Y. Cohen and S. Seich, "Ordering Phenomena in Thin Polystyrene Films," *Journal of Polymer Science: Polymer Physics Edition*, vol.19, 599-608 (1981).

25. T. Krzyzanowska, and Z., Hippe, *Prog. Org. Coat.*, 3, [4], 349 (1975).

26. S.G. Croll, "Internal Stress In a Solvent-Cast Thermoplastic Coating," *Journal of Coatings Technology*, Vol. 50, No. 638, 33-38 (1978).

27. G.Y. Onoda, Jr. "The rheology of organic binder solutions," pp. 235-251 in Ceramic Processing Before Firing. Edited by G.Y. Onoda, Jr. and L.L. Hench, Wiley, New York, 1978.

28. P. Lindner, I. Markovic, R.C. Oberthür, R.H. Ottewill, and A.R. Rennie, "Small Angle Neutron Scattering Studies of Polymer Lattices, " *Progr. Colloid Polym. Sci.*, 76, 47-50 (1988).

29. A.D. Devoe, private communication, 1992.

30. L.E. Nielson Mechanical Properties of Polymers; p. 243. Reinhold Publishing Corporation, Chapman & Hall, Ltd., London, 1962,

31. R. Castells, and J. Meda, "Particle Packing Analysis of Casting Above the Critical Pigment Volume Concentration," *J. Coating Tech.*, 55[707], 53-59 (1983).

# CHAPTER 5

# DELAMINATION DURING BINDER REMOVAL FROM MULTILAYER CERAMIC GREENWARES

## 5.1 Introduction

Multilayer ceramic (MLC) devices such as MLC capacitors and MLC packages must have excellent physical integrity in order to maintain good electrical properties. Delamination, which is defined[1] as the separation of the electrode and the ceramic dielectric in the MLC structures, must be avoided in order to achieve a high degree of reliability.

Delamination occurs in binder burn out and/or sintering process. During the binder burn out process, delamination can be caused by low adhesion between the electrode and dielectric layers, high gas generation rate, and stresses in both dielectric and electrode layers. These factors are shown schematically in Figure 5.1.

Adhesive strength between the dielectric-electrode and dielectric-dielectric layers is important in maintaining sample integrity during processing. This strength between dielectric layers has to be high enough to withstand viscoelastic recovery of the polymers after the delamination, especially around the electrode line[2]. High bond strength between the dielectric and electrode layers is essential when the laminated greenware is cut into individual pieces. It is also important during the binder burn out when the evolution of volatile organics subjects the sample to internal stresses.

Particles are initially bound together by polymer binders in both the ceramic dielectrics and the metallic electrodes. These binders have to be burned out prior to

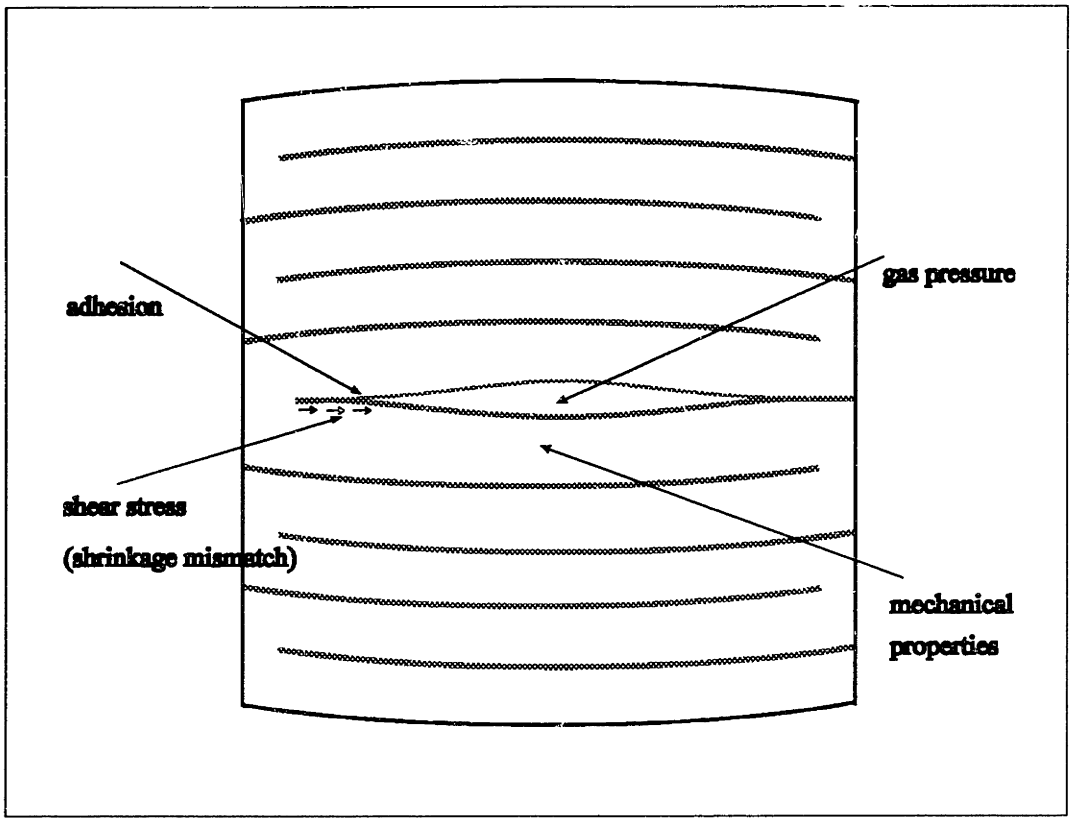


**Figure 5.1 Schematic of a delamination in an MLC capacitor**

sintering. It is believed[3] that during this process, the rate of gas generation within the green compact has to be controlled to keep it within the capability of the porosity in the sample to diffuse it. Otherwise, the increasing gas pressure will cause defects such as delamination and/or voids in the compact.

A shrinkage mismatch between the dielectric and electrode layers, during the binder burn out and sintering, can create substantial stresses in the sample. Different kinds of binders are usually used for the dielectric and electrode layers to satisfy their processing needs. The binder for the dielectric tape has to provide the green tape with high tensile strength, sufficient flexibility, and high adhesive strength. Polyvinyl butyral[4] is the most effective binder for meeting these requirements. The binder used for electrode print should be highly pseudoplastic, so the electrode paste can have low viscosity during

printing, and high viscosity once printed to prevent the electrode area from running or leveling out[5]. Cellulose and its derivatives are usually employed to meet these requirements. The binders in the dielectric and the electrode layers are burned out at different temperature range. Therefore, the shrinkage of the dielectric and electrode layers from binder removal can occur at different temperatures. The overall shrinkage of the electrode layer may also differ from that of the dielectric layer. Delamination can originate from the interface or from the electrode layer where stress from shrinkage mismatch is high.

Pepin[6,7] suggested electrode-based causes of delamination in multilayer ceramic capacitors. The causes included (1) high amount of organic resins in the electrode vehicle, (2) green state delamination due to a lack of adhesion of dried electrode print to dielectric tape, (3) catalytic reactions of the electrode precious metal powders with the organics during burnout, and (4) mismatch of the densification characteristics of the electrode and dielectric during firing. A solution was also suggested in each case. These included lowering the concentration of the electrode binder, and passivating the surface of metal powder to avoid the catalyzing reaction. Kahn[3,8] suggested that control of the partial oxygen pressure during binder burnout was effective at controlling and preventing exothermic reactions of binder. This, then, would help to eliminate delamination. Verweij and Bruggink[9] described a reaction-control process of binder burnout of MLCs in which a weight-time program was used to control the temperature such that a linear rate of weight loss was obtained.

A major assumption of previously published work on binder removal was that the weight loss rate was the prime factor in determining the defect formation during binder burnout. Based on this assumption, thermal gravimetric analysis (TGA) became an exclusive method in monitoring the binder removal process. Using the weight loss rate to

control the binder removal process suffers a few disadvantages. Throughout the binder burnout process, the porosity of the greenware for gas transport changes continually, usually from an initial 1 to 5 vol% to 35 to 50 vol% after all the binders are removed. Permeability of the sample increases rapidly as binder removal proceeds[3,10-14]. In addition, the dominant binder removal mechanism changes as the binder removal process proceeds[15,16]. Resistance to binder removal, therefore, varies constantly throughout the whole process. In the case of MLC structures, additional complexity such as shrinkage mismatch of different layers exists. Therefore, a universal liner weight loss control system is not the best choice for preventing defect formation. Previous research also focused on correlating the processing conditions and defects in the final products. The samples were not viewed during heating and thus the point at which defects occurred could not be identified[17].

This chapter evaluates three aspects of the delamination mechanism: adhesive strength between the electrode and dielectric layers, gas pressure distribution in the electrode layers during binder removal, and stress and strain in the electrode and dielectric layers. Delamination during binder removal was observed *in situ*. Four kinds of green samples were used for the direct observation: pure laminated dielectric tapes, cast electrode greenware, MLC greenware, and MLC with two layers of electrode prints instead of one layer. Comparison of delamination or the lack of it in the above four kinds of samples provides insight into the delamination mechanism.

## 5.2 Experimental Procedure

Commercial products were used for the characterization in this project. The dielectric green tape used is composed of $BaTiO_3$ ceramic powders, and benzyl butyral

phthalate (BBP) plasticized polyvinyl butyral (PVB) binder. The loading of $BaTiO_3$ powders varied from 50 to 55 vol%. The thickness of a single layer dielectric tape was 34 μm. An approximately 3 μm thick palladium electrode paste was silk screened onto the surface of the dielectric green tape. Ethyl hydroxyethyl cellulose (EHEC) was used as the binder for palladium electrode print. The loading of Pd powder in the dried electrode print was about 41 vol%.

A peeling test was conducted to reveal some information about the adhesion between (1) the dielectric-electrode and, (2) the dielectric-dielectric layers, after lamination. An approximately 3μm thick electrode ink vehicle was silk-screened onto the bottom surface of a 50×10 $mm^2$ commercial dielectric green tape. After drying of the electrode ink, another dielectric green tape was placed on top of the ink layer. A thin teflon film was placed between these two layers, which covered approximately 20 mm of the length from one end. The sample was then laminated at 70°C and 20 $kg/cm^2$ for five minutes. After lamination, the teflon film was removed, uncovering the edge for peeling test. The dielectric-dielectric layers were prepared the same way, but omitting the electrode print between them. Each sample was then mounted on an Instron 45 and peeled at 180° and 2 mm/min. The peeling forces were recorded.

An MLC sample was composed of forty layers of ceramic tape, of which the middle thirty layers were printed with palladium electrode paste. The dimensions of the sample were L×W×H=1.62×1.32×1.34 $mm^3$. Greenwares of the same dimensions were also made out of laminated ceramic tapes and cast electrode paste. A model system was made to compare the effect of electrode thickness on delamination. This sample was composed of ten layers of ceramic tape, of which the third and eighth layers had either one or two layers of electrode paste printed on them. In the following discussion, we will refer to these samples with one or two layers of electrode print as $E_1$ and $E_2$, respectively.

Thermal gravimetric analysis (TGA) was conducted to monitor the mass change during the binder removal process. About 5 mg of sample was used for each analysis, except for the 12 mg MLC sample. Differential thermal analysis (DTA) was used to measure the energy change during the binder removal process. A hot-stage/Fourier transformed infrared (FTIR) spectroscopy was used to monitor the gas products *in situ* during binder removal.

The deformation of single layer ceramic tape with and without the presence of electrode print was observed *in situ* with a hot-stage/optical microscope, during the binder removal process. A strip (L×W×T = 2×0.5×H $mm^3$) was cut from a large piece of ceramic tape using a razor blade. *L* was chosen to be perpendicular to the casting direction of the dielectric tape since the pure dielectric tape has the least deformation in this direction during binder removal (Chapter 4). This strip was then held at one end with a small copper grip. The other end was free to move, as shown in Figure 5.2. The sample was heated and observed with a hot-stage/optical microscope. Micrographs were taken at various temperatures, and the displacement of the free end of the sample from its original state, *z*, was measured from the negatives using an optical magnifier (10×). The approximate curvature of the tape is given by:

$$\frac{1}{r} = \frac{2z}{l^2} \qquad (z<<l) \qquad (5.1)$$

in which *l* is the original length of the tape. The parameter, *z*, was chosen to be positive if the tape bent toward the surface which was exposed to air during casting (top), and negative if it bent toward the surface which was in contact with the substrate during casting (bottom). The length of the tape during binder removal was calculated from Eq.4.2 and the shrinkage of the tape versus temperature was obtained.

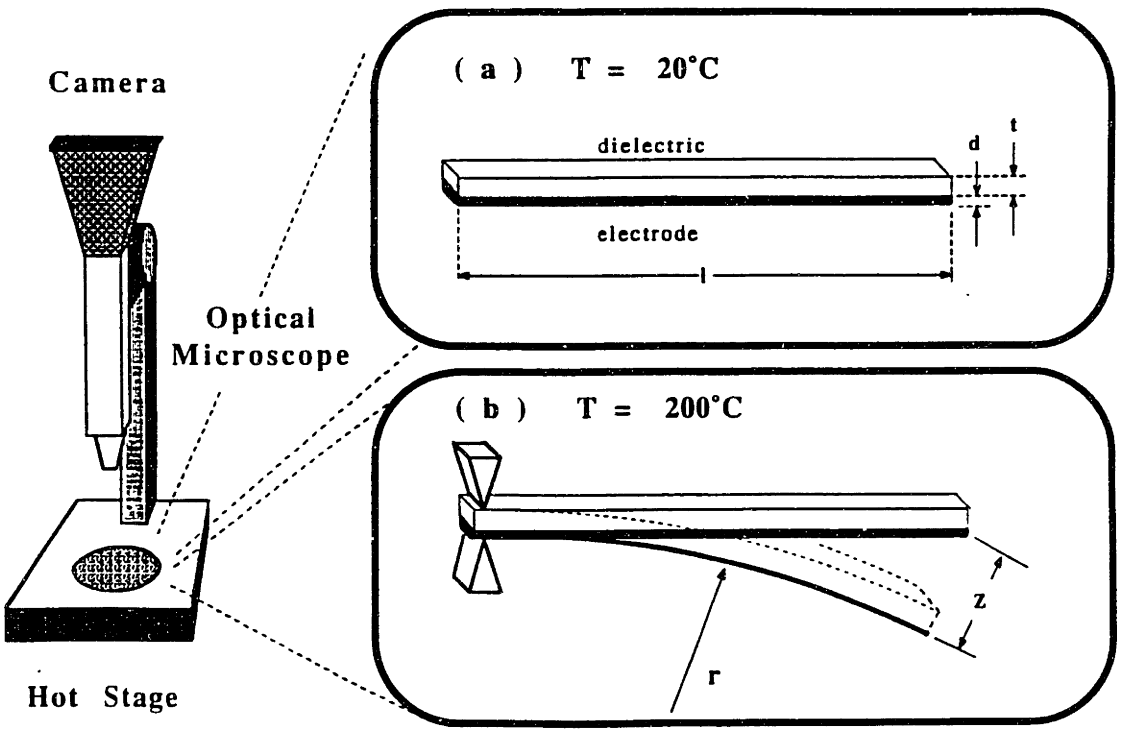


**Figure 5.2. Schematic of the bending measurement of an electrode-dielectric strip**

A 50 μm palladium electrode green sheet was made by spreading the electrode paste onto a teflon film using a glass slide. It was then dried under a hood for 48 hours and peeled from the teflon substrate. A strip ($L \times W \times T = 2 \times 0.5 \times 0.05$ mm$^3$) was cut from the dried electrode film. The dimensional change of this strip during binder removal was measured *in situ* using the same optical method as for the dielectric tape.

Delamination produces gaps in the electrode layers of the sample. The thickness of these gaps indicates the degree of delamination. This delamination was monitored by two methods. In the first method, a hot-stage/optical microscope equipped with a charge-

couple device (CCD) camera was used to monitor the development of delamination of an MLC *in situ*. The optical microscope was focused on the exterior surface of the MLC where the electrode termination was clearly visible. The thickness of the delamination could be measured from the TV screen at different temperatures. The second method was used to examine the interior defects of the MLC. The binder was burned out to different extents in a series of samples by monitoring the mass removed via thermalgravimetric analysis and quenching the sample at the desired amount of removal. The sample was then fractured through the middle, perpendicular to the electrodes. The fracture surface, thus produced, was then observed using scanning electron microscopy (SEM).

## 5.3 Results and Discussion

### 5.3.1 Adhesion of Interlaminar Layers

Figure 5.3 shows peel forces between the dielectric-electrode and the dielectric-dielectric layers, respectively. Adhesive failure was observed between the dielectric and electrode layers, and it always occurred along the interface of the electrode and the bottom surface of the dielectric tape. Peeling of laminated dielectric-dielectric layers, on the other hand, could only proceed for a limited length. Further movement caused elongation of the tape until it finally broke. The strength at which the tape broke reflected the intrinsic tensile strength of the tape, and this force was much higher than the peeling force of the electrode-dielectric layers.

Figure 5.4 shows the atomic force microscopy (AFM) images of the top and bottom surfaces of a dielectric tape. The bottom surface was flatter than the top surface. Therefore, the actual contact area between the bottom surface and the electrode ink layer was lower than the interfacial area between the top surface of the tape and the electrode

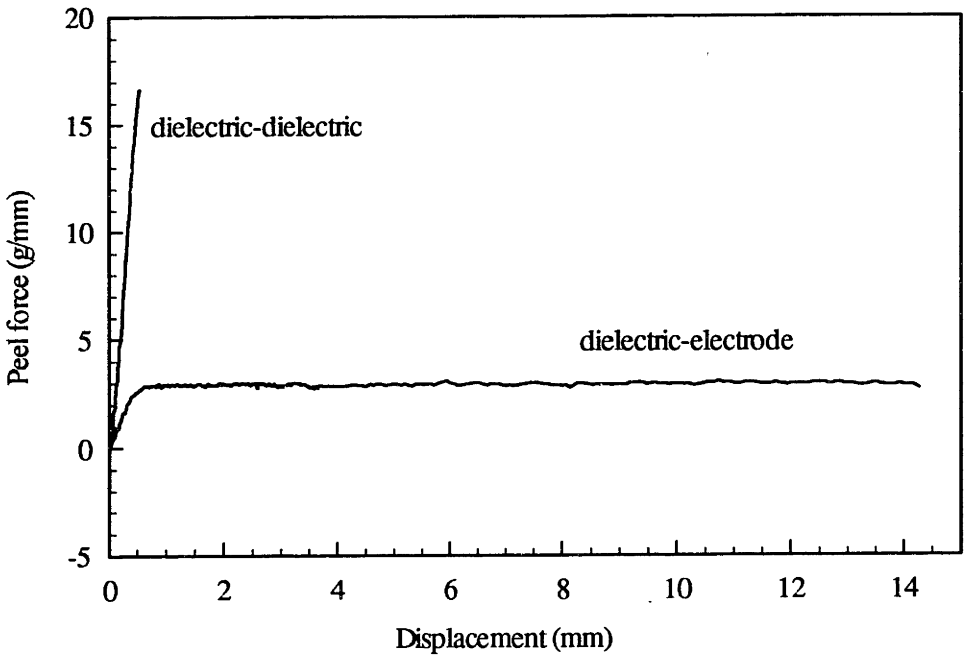


**Figure 5.3 Peel force of laminated dielectric-electrode and dielectric-dielectric layers**

ink layer. A higher stress existed on ink layer. A higher stress existed on the interface of the electrode and the bottom surface of the tape, which caused the propagation of peeling along this interface.

Two dielectric layers joined together and formed one single piece during lamination. No distinguishable interface exists between these two layers after lamination. The intrinsic tensile strength of the tape instead of adhesive strength was measured during the peel test. It appeared that this intrinsic strength was much higher than the dielectric-electrode adhesive strength at room temperature.

The peel test conducted at room temperature reveals information of adhesive strength after lamination. The peel force can be compared with the shear force during cutting and punching to determine whether green state delamination may occur. Its

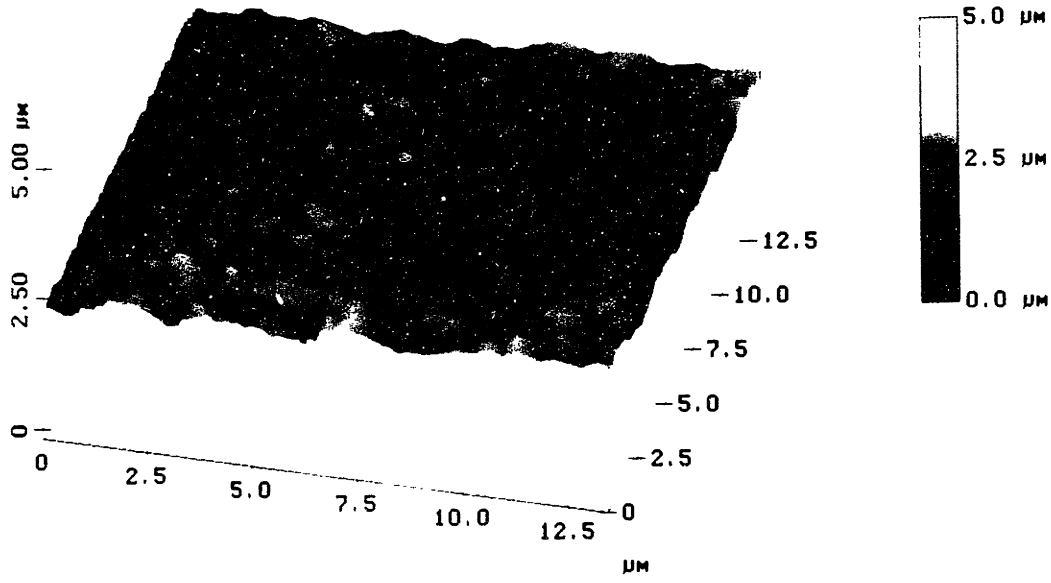


(a)

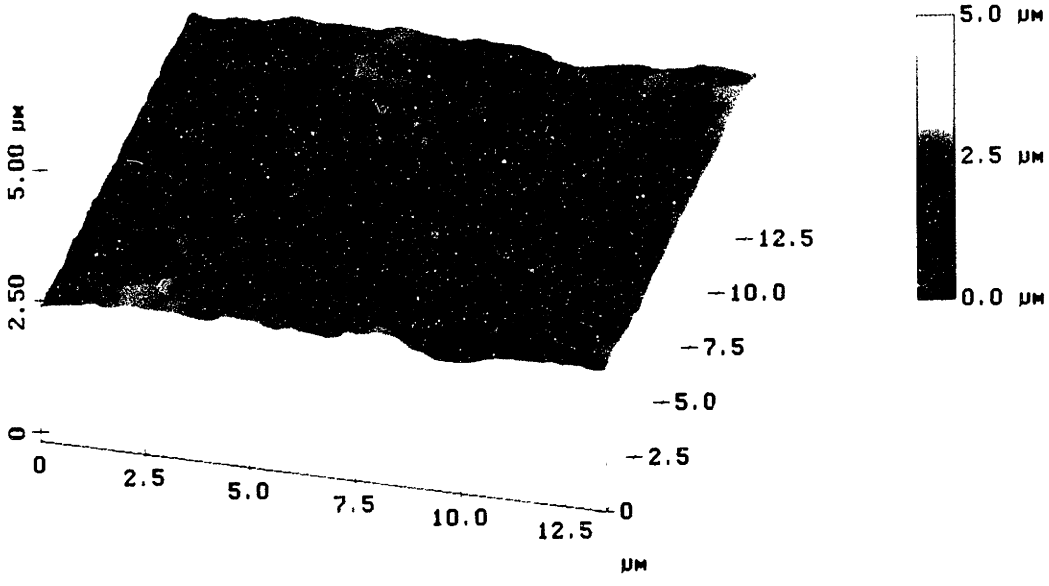


(b)

**Figure 5.4 AFM images of (a) top surface and (b) bottom surface of a green tape**

application for evaluating delamination during binder removal, however, is highly limited. It has been known[18] that peel force is a function of temperature. Peel force was shown[18] to increase with temperature in a butadiene-styrene random copolymer until the failure mode changed from adhesive failure to cohesive failure. The peel force of this cohesive failure, then, decreased with temperature. Cohesive delamination along the electrode occurs during the binder removal process, as will be shown in 5.3.4.

### 5.3.2 Gas pressure within an electrode layer during the binder removal process

**I. Gas generation rate:**

The gas generation rate is mainly determined by heating rate, atmosphere, and the chemical reaction between the binder and the surface of filler particles for a given binder

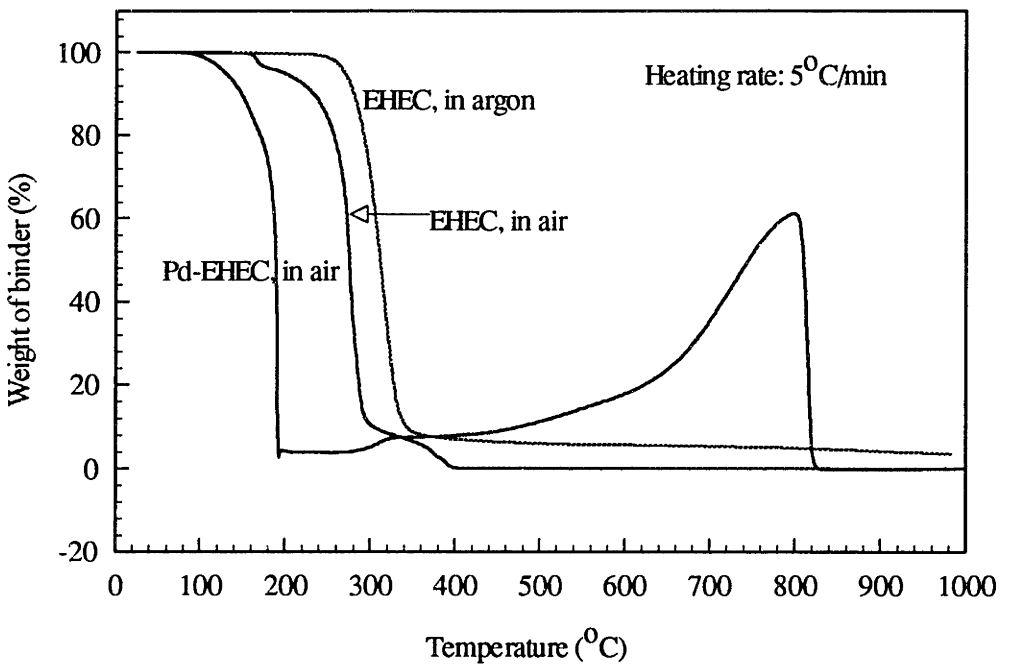


**Figure 5.5. TGA of EHEC and dried electrode paste**

system. Figure 5.5 shows the weight loss of EHEC binder in air and argon. EHEC degrades rapidly between 200 and 300°C in air, producing 10% of material that decomposes slowly between 300 and 400°C. The degradation temperature of EHEC in argon shifted to about 50°C higher than in air. There is still 4 per cent of carbon residue left even after the sample was heated to 980°C. Figure 5.5 also shows the thermal decomposition behavior of the dried electrode paste. The catalyzing effect of Pd powder toward EHEC binder oxidation is dramatic; Pd decreased the complete removal temperature of the EHEC binder in air from 400 to 200°C. The DTA results showed that this catalytic reaction was strongly exothermic.

Figure 5.6 shows the results of isothermal TGA of the dried electrode paste in air at different temperatures. The gas generation rate at different temperatures is shown in

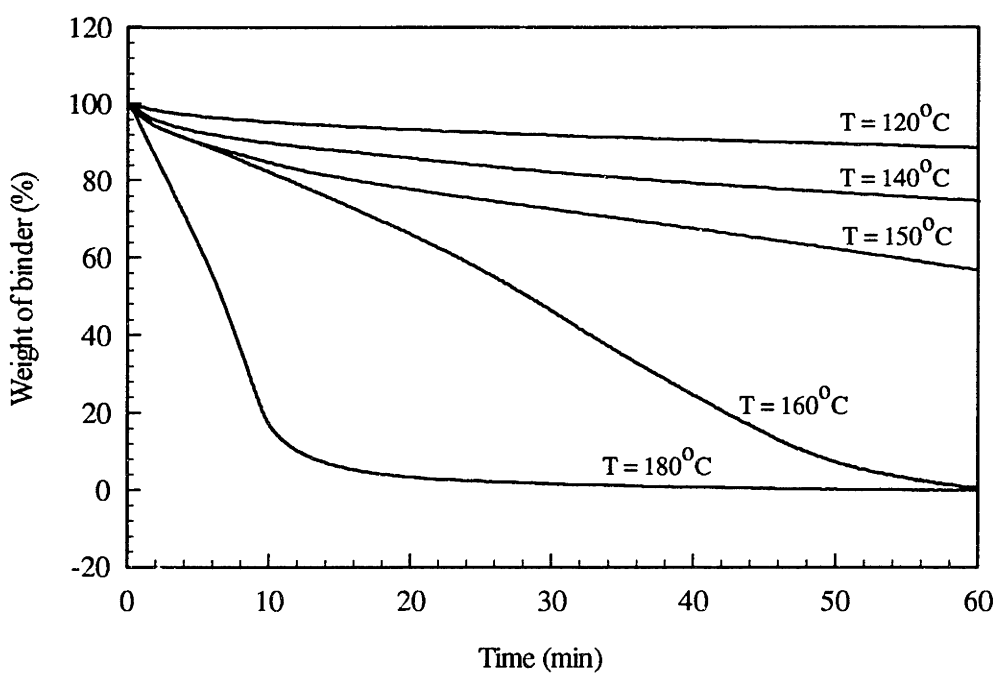


**Figure 5.6 Isothermal TGA of dried electrode paste in air**

Figure 5.7. The oxidation of EHEC in the presence of Pd powder is zero order, and the activation energy is $1.058 \times 10^5$ J/mol. Hot-stage FTIR results showed that the reaction products in air were $CO_2$ and $H_2O$.

When the binder removal of an MLC is conducted in air, the local atmosphere within the electrode layer is somewhere between air and argon. The oxidation reaction of EHEC: $(C_{12}H_{22}O_6)_n + 14.5nO_2 = 12nCO_2 + 11nH_2O$ consumes oxygen, which can cause oxygen deficiency inside the sample.

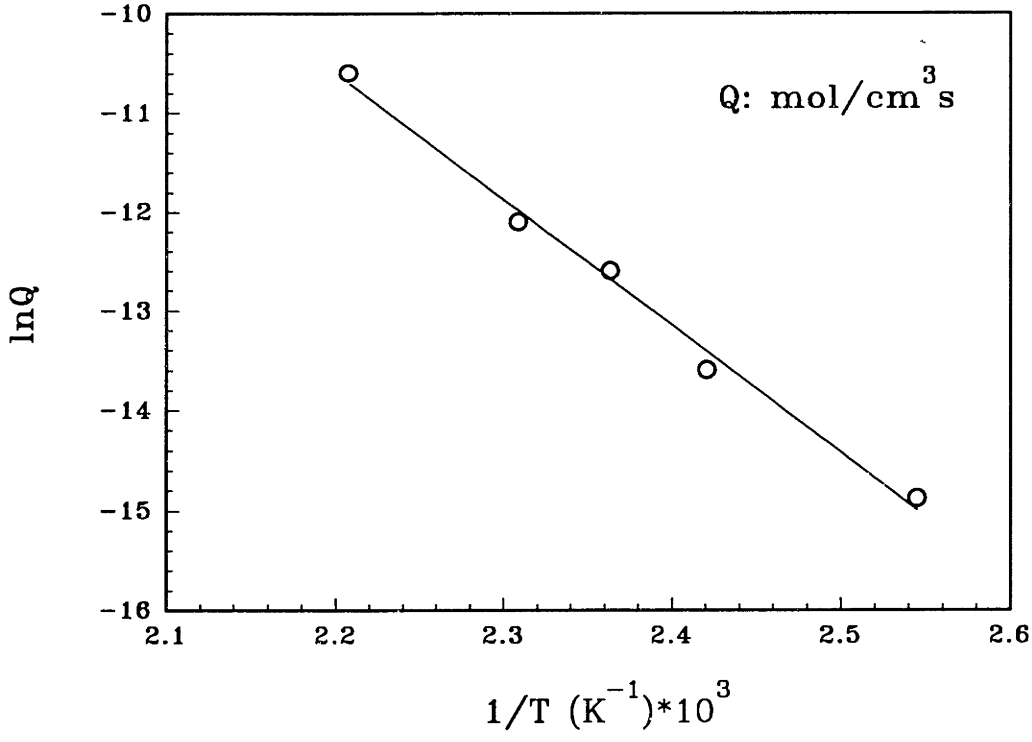


**Figure 5.7 Gas generation rate of the electrode paste as a function of temperature**

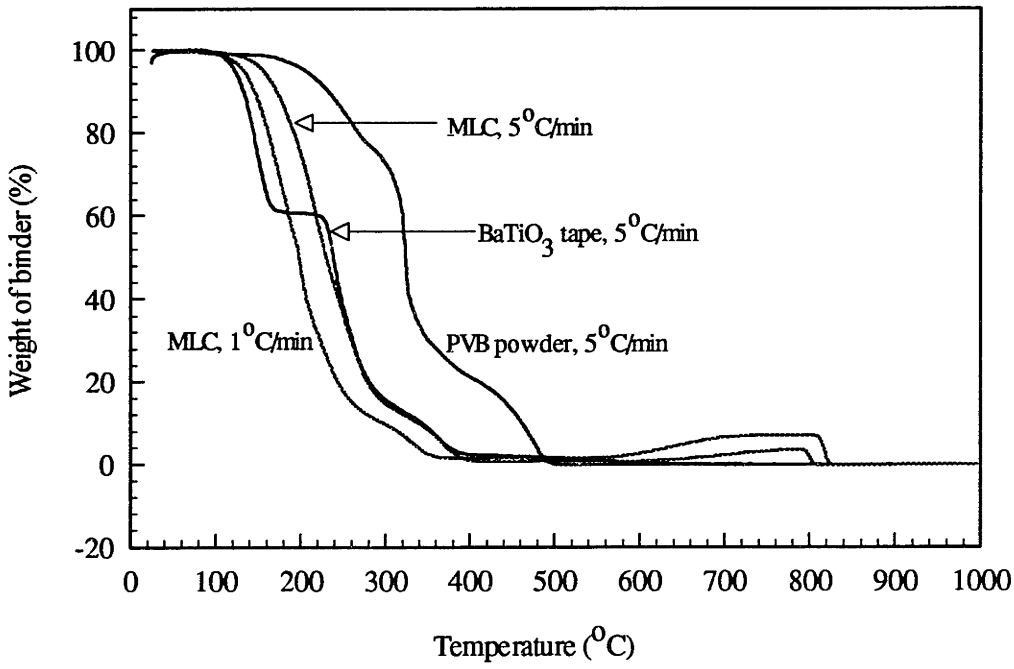


**Figure 5.8 TGA of PVB, single layer dielectric tape, and an MLC greenware**

The weight loss of PVB polymer, the dielectric tape, and an MLC is shown in Figure 5.8. In a single dielectric tape, two distinctive stages, corresponding to the evaporation of BBP plasticizer and the degradation of PVB polymer, are observed. BBP evaporated between 120°C and 160°C, while the degradation of PVB occurred between 200°C and 400°C. In the case of MLC structures, a rather continuous weight loss is observed between 120°C and 400°C, due to the lowered surface area for evaporation and/or the longer diffusion path[15]. $BaTiO_3$ powder lowered the complete removal temperature of PVB by about 100°C.

## II. Calculation of gas pressure within an electrode layer

A quantitative understanding of gas pressure distribution within an electrode layer is necessary for designing suitable processing conditions. The effect of processing

parameters such as temperature, porosity, sample size, and oxygen partial pressure on delamination should be examined. The dependence of delamination on the size of defects in electrode layers should be established.

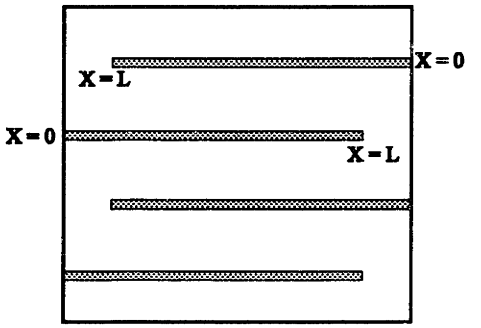


**Figure 5.9 Schematic of the cross-section of an MLC greenware**

The cross-section of an MLC greenware is shown schematically in Figure 5.9. The following assumptions are made in calculating the gas pressure distribution inside the electrode layer:

1. The gas generation rate is uniform, and it equals the gas generation rate measured from pure electrode film in air.
2. Permeability of the electrode is constant and is independent of pressure and time.
3. The top, bottom, and the close end of the electrode are impermeable.
4. The only flowing phase is a gas of constant composition.
5. The gas is an ideal gas.
6. The flow obeys Darcy's law, i.e. is in the viscous range.
7. Gravitational forces are negligible.

The above assumptions are necessary in order to simplify the calculation procedure. However, assumption 1 may cause an overestimation of gas pressure. The oxidation of electrode binder: $(C_{12}H_{22}O_6)_n + 14.5nO_2 = 12nCO_2 + 11nH_2O$ may cause an oxygen

deficiency within the electrode layer, especially during early stages of binder removal when porosity of the sample is low. Assumption 2 is only applicable in a short time period, during which the porosity of the electrode can be treated as constant. Assumption 3 is valid in the early stages of binder removal when porosity in the dielectric layers is low. The removal of electrode binder and the BBP plasticizer of the dielectric layer occurs in the same temperature range. Therefore, porosity increases in both the electrode and dielectric layers as binder removal proceeds. The role of gas exchange between the dielectric and the electrode layers is unknown at this time. Assumption 4 is roughly valid, since the viscosity of $CO_2$ ($15\times10^{-6}$ kg/m·s at 20°C) is similar to that of $H_2O$ ($10\times10^{-6}$ kg/m·s at 20°C)[19]. It is anticipated that no large composition gradient of $CO_2$ and $H_2O$ will be created across the sample.

Darcy's law is expressed as:

$$F = -\frac{KP}{\mu RT}\cdot\frac{\partial P}{\partial X} \tag{5.2}$$

where $F$ is the flux of gas (mole/cm$^2$·s), $K$ is the permeability of the sample, $P$ is gas pressure, and $\mu$ is the viscosity of gas.

Based on mass conservation, we have:

$$\varepsilon\cdot\frac{\partial(\frac{P}{RT})}{\partial\tau} = -\frac{\partial F}{\partial X} + Q \tag{5.3}$$

where $Q$ is the gas generation rate (mole/cm$^3$·s), $\tau$ is time, and $\varepsilon$ is porosity of the sample.

Combining Eq.5.2 and Eq. 5.3 gives the following expression:

$$\frac{\partial P}{\partial\tau} = \frac{K}{\varepsilon\mu}\cdot\frac{\partial}{\partial X}(P\frac{\partial P}{\partial X}) + \frac{QRT}{\varepsilon} = \frac{K}{2\varepsilon\mu}\cdot\frac{\partial^2 P^2}{\partial X^2} + \frac{QRT}{\varepsilon} \tag{5.4}$$

Let $x = \frac{X}{L}$.

L is the length of the electrode layer.

Dividing each side of Eq. (5.4) by $\frac{KP_0^2}{2\varepsilon\mu L^2}$ gives:

$$\frac{\partial(\frac{P}{P_0})}{\partial(\frac{\tau K P_0}{2\varepsilon\mu L^2})} = \frac{\partial^2(\frac{P}{P_0})^2}{\partial x^2} + QRT \cdot \frac{2\mu L^2}{KP_0^2}. \tag{5.5}$$

Let $U = \frac{P}{P_0}$. (5.6)

$$t = \frac{KP_0\tau}{2\varepsilon\mu L^2} \tag{5.7}$$

$$A = QRT \cdot \frac{2\mu L^2}{KP_0^2} \tag{5.8}$$

Eq. (5.5) becomes:

$$\frac{\partial U}{\partial t} = \frac{\partial^2 U^2}{\partial x^2} + A \tag{5.9}$$

Constant $A$ depends on gas generation rate, temperature, permeability, and length of the electrode.

The permeability ($K$) can be expressed as[20]:

$$K = \frac{C\varepsilon^3}{\alpha S^2} \tag{5.10}$$

where $C$ is the Kozeny constant (typically near 0.6), $S$ is pore surface area, and $\alpha$ is tortuosity. The permeability of a random packing of spherical particles is[19]:

$$K = \frac{\varepsilon^4 d_P^2}{90(1-\varepsilon)^2} \tag{5.11}$$

where $d_P^2$ is the particle diameter. Eq. 5.11 is used in this calculation to estimate the permeability of the electrode layers, since the $S$ and $\alpha$ in Eq. 5.10 are unavailable. However, the error caused by Eq. 5.11 can be high since the morphology of pores in the electrode layers during early stages of binder removal is not the same as that of a particle bed.

The gas viscosity ($\mu$) is[21]:

$$\mu = \frac{2}{3\pi^{3/2}} \cdot \frac{\sqrt{mkT}}{d^2} \tag{5.12}$$

where $m$ and $d$ are the mass and diameter of a gas molecule, and $k$ is the Boltzmann constant. Assuming $d$ does not change with temperature, the gas viscosity at temperature $T$ is then:

$$\mu_T = \mu_0 \sqrt{\frac{T}{T_0}} \tag{5.13}$$

where $T_0$ is a reference temperature (usually $T_0 = 20°C$) at which the gas viscosity is known, and $\mu_0$ is gas viscosity at $T_0$.

The time constant $\tau$ in Eq. 5.7 is calculated to be 63 seconds when $t$ is set to be one, assuming $L$, $T$, and $\varepsilon$ are 2 mm, 160°C, and 0.2, respectively. This indicates that the system will take about 63 seconds to reach steady state.

For steady state: $\frac{\partial U}{\partial \tau} = 0$. Eq. (5.9) becomes:

$$\frac{\partial^2 U^2}{\partial x^2} + A = 0 \tag{5.14}$$

The following boundary conditions apply:

$$P(0) = P_0 \,, \Rightarrow U(0) = 1$$
$$\frac{\partial P}{\partial X}\Big|_{X=L} = 0 \,, \Rightarrow \frac{\partial U}{\partial x}\Big|_{x=1} = 0$$

Integrating Eq.(5.14) and applying the boundary conditions gives the following solution:

$$U = [1 + Ax(1 - \frac{x}{2})]^{\frac{1}{2}} \tag{5.15}$$

$$U_{\max} = U|_{x=1} = (1 + \frac{A}{2})^{\frac{1}{2}} \tag{5.16}$$

The constant $A$ is:

$$A = \frac{2\mu L^2 QRT}{KP_0^2} = \frac{3.884 e^{-\frac{1.058\times10^5}{RT}} T^{\frac{3}{2}} L^2 (1-\varepsilon)^2}{\varepsilon^4 d^2} \tag{5.17}$$

Figure 5.10 shows the pressure distribution in electrode layers of 2 mm length. The pressure first rises rapidly from the edge of the layer, and then increases slowly with the increasing of distance from the edge. Increasing the porosity from 0.1 to 0.4 causes a decrease of the maximum pressure from 6.52 atm to 1.04 atm. The pressure reaches maximum at the end of the electrode where x = 1.

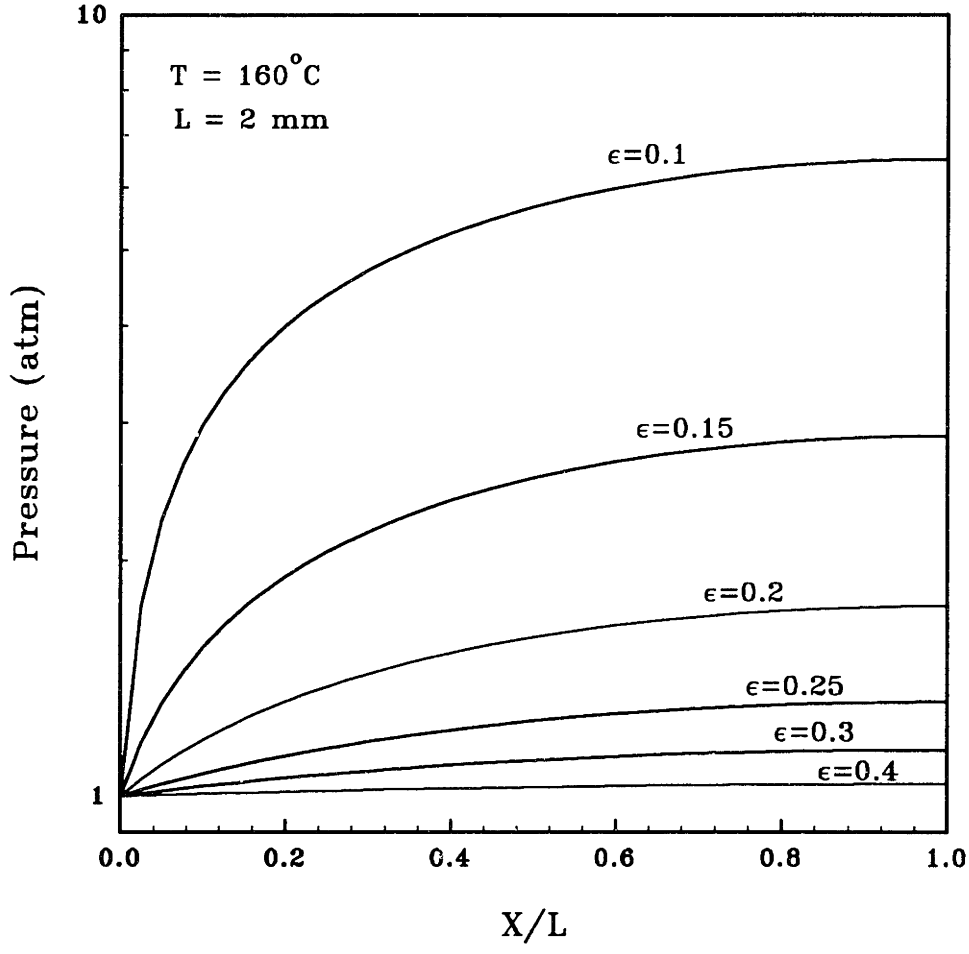


**Figure 5.10 Pressure distribution within a 2 mm electrode layer**

Figure 5.11 shows the maximum pressure versus porosity at different temperatures. The gas pressure increases rapidly with the decrease in porosity. It also increases with temperature since both gas generation rate and gas viscosity increase with temperature.

Delamination nucleates at defects in the electrode layers. These defects are assumed to be cylinders with radius r and height h. The critical force ($F_c$) for this defect to grow is:

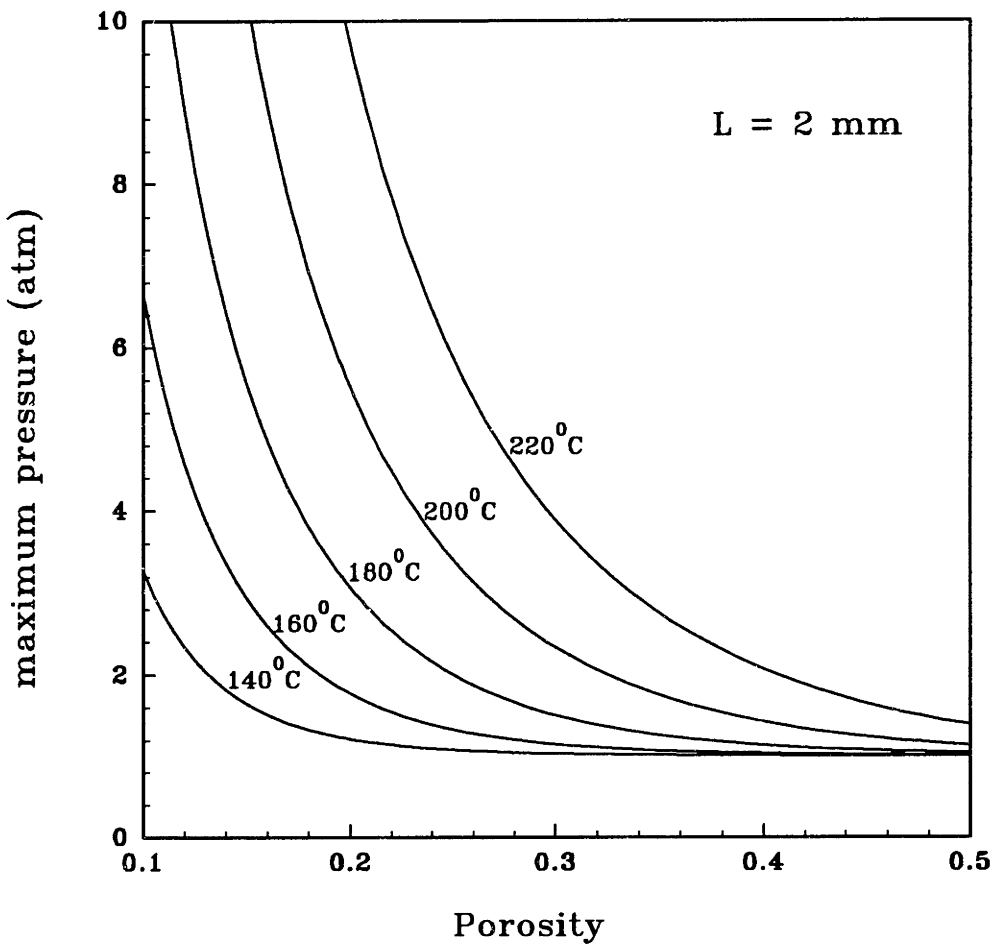


**Figure 5.11 Maximum pressure in a 2 mm electrode at different temperatures**

$$F_c = 2\pi rf \tag{5.18}$$

where f is the peel force of the electrode layer. The critical gas pressure ($P_c$) for the defect to propagate is:

$$P_c = \frac{F}{A} = \frac{2\pi rf}{2\pi rh + 2\pi r^2} = \frac{f}{h+r} \tag{5.19}$$

where A is the surface area of the defect. Assuming $h = r$, Eq. 5.19 becomes:

$$P_c = \frac{f}{2r} = \frac{f}{d_c} \tag{5.20}$$

where $d_c$ is the diameter of the defect.

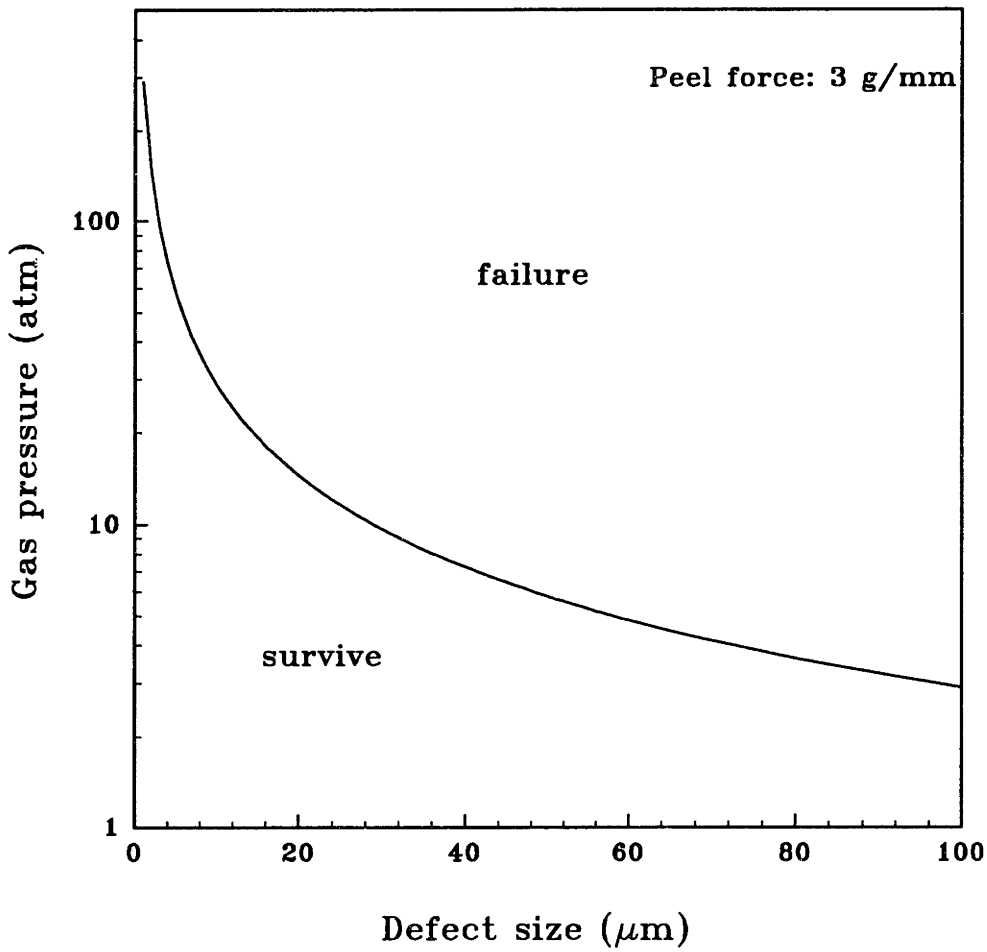


**Figure 5.12 The gas pressure to cause a delamination**

The peel force $f$ can be measured experimentally. Eq. 5.20 indicates that the pressure to cause a delamination to grow from a defect is inversely proportional to defect size. The critical pressure ($P_c$) for delamination versus defect size is shown in Figure 5.12. $f$ is taken as the peel force at room temperature in Fig. 5.12, which is 3 g/mm (Fig. 5.3). This approximation will produce some error in the calculated critical pressure since peel force is a function of temperature.[18,20] Increasing temperature also causes the failure mode to change from interfacial to cohesive. The transition region from adhesive failure to cohesive failure of our system lies somewhere between room temperature and 155°C, since peeling at room temperature is adhesive while delamination between 155°C and 200°C is cohesive.

The critical gas generation rate of 2 mm electrode layers with different porosities is shown in Figure 5.13 (solid lines). The measured gas generation rates at 180°C is also shown in Figure 5.13(dashed line). Any defect smaller than 18 μm is safe at 180°C in a 2 mm electrode layer of 0.1 porosity, while defects larger than 18 μm can grow and cause delamination. This critical defect size increases to 44 μm and 90 μm when the porosity is increased to 0.15 and 0.2, respectively.

The critical porosity of electrode layers of 1 mm to 6 mm length at 180°C is shown in Figure 5.13. The critical porosity in an electrode layer increases with the length of the electrode layer and with defect size. For example, a 2 mm electrode layer with porosity higher than 0.11 is safe for any defect smaller than 20 μm. This critical porosity increases from 0.11 to 0.18 when the electrode length is increased from 2 mm to 6 mm. An increase of defect size from 20 μm to 40 μm in a 2 mm electrode layer causes the critical porosity to increase from 0.11 to 0.15.

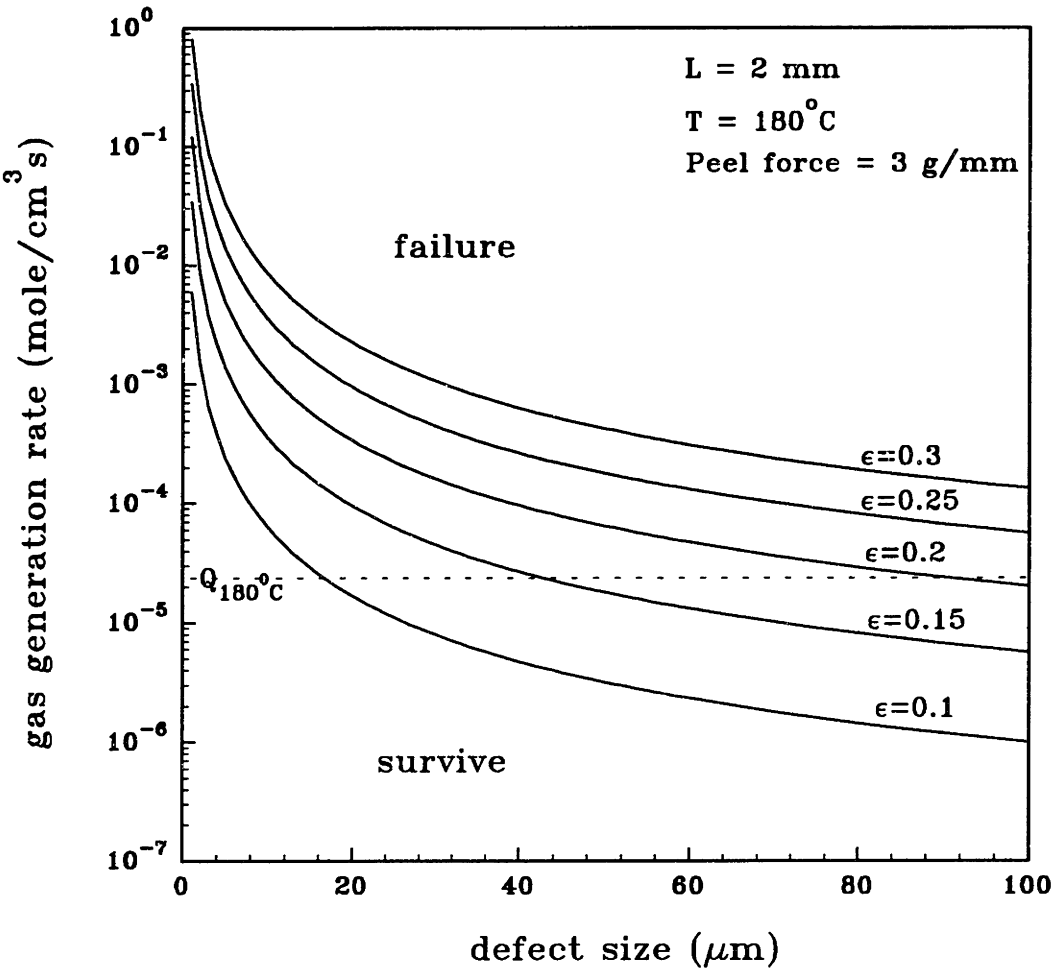


**Figure 5.13 Critical gas generation rate of an electrode**

The gas pressure in an electrode layer increases with temperature and length of the electrode layer, and it decreases with the porosity. The effect of porosity is dramatic. The porosity of the samples is low during the early stages of binder removal. This can easily cause delamination even though the gas generation rate is also low due to the lower temperature at this early stage. The porosity increases as binder removal proceeds, which reduces the gas pressure within the electrode layer and results in healing of the delamination, as observed in our experiments.

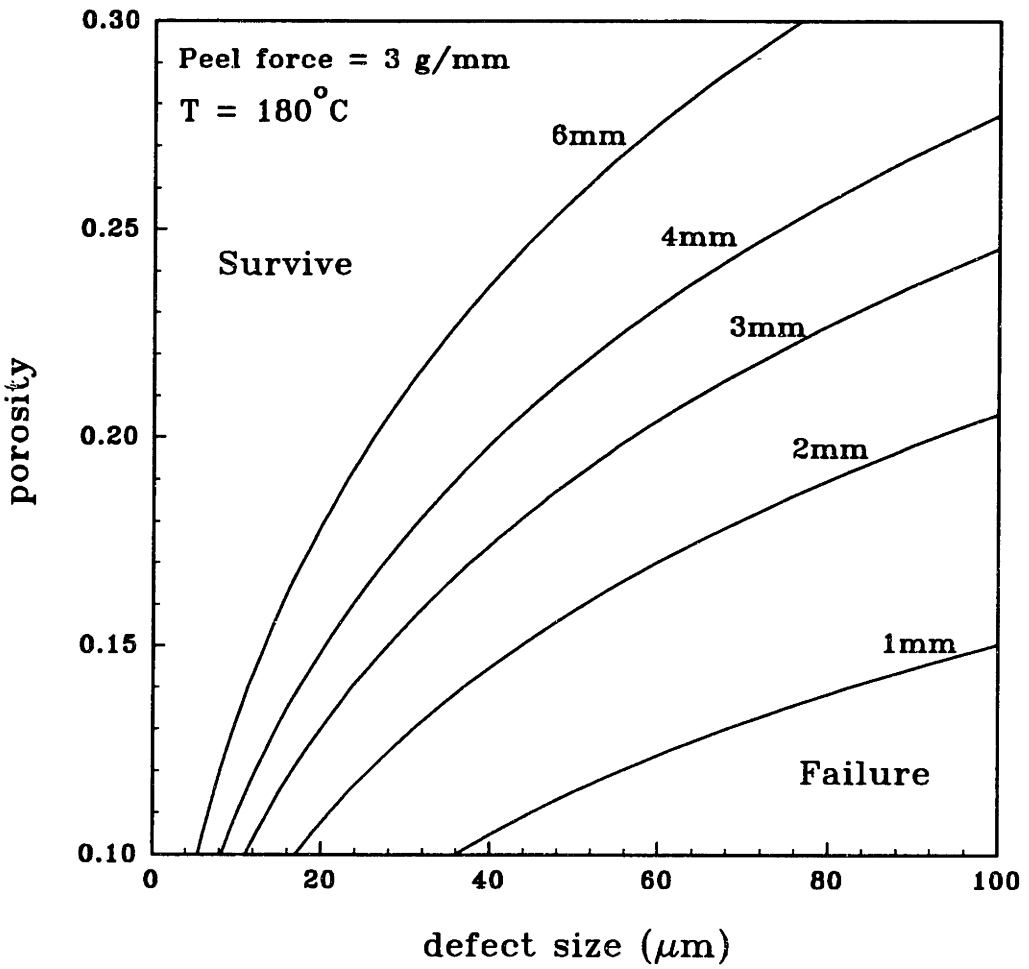


**Figure 5.14 Critical porosity of electrode layers versus defect size**

The critical gas pressure in an electrode layer is inversely proportional to the size of defects within the electrode. Large defects are more detrimental since they grow with lower gas pressure than that required for small defects. However, the critical defect size, from the above calculation, is large in the temperature range of 155°C to 200°C, during which delamination was shown to occur.[23] For example, the critical defect sizes for a 2 mm electrode with a porosity of 0.1 are 18 μm and 9 μm at 180°C and 200°C respectively. Such large defects are rare in electrode layers with a thickness of 3 μm. The

size of a typical defect in the electrode layers is in the same order of magnitude as the diameter of a palladium particle, which is 1.5 μm. Therefore, delamination will only occur in the electrode layers which contain defect larger than the critical defect size, instead of occurring in every electrode layer.

### 5.3.3 Shrinkage Mismatch Between the Dielectric and Electrode Layers During the Binder Removal Process

The dimensional change of both the dielectric tape and the cast electrode film during binder removal is shown in Figure 5.15. The net shrinkage of the electrode film and the dielectric tape are 5.1% and 2.5%, respectively. Therefore, in an electrode-dielectric

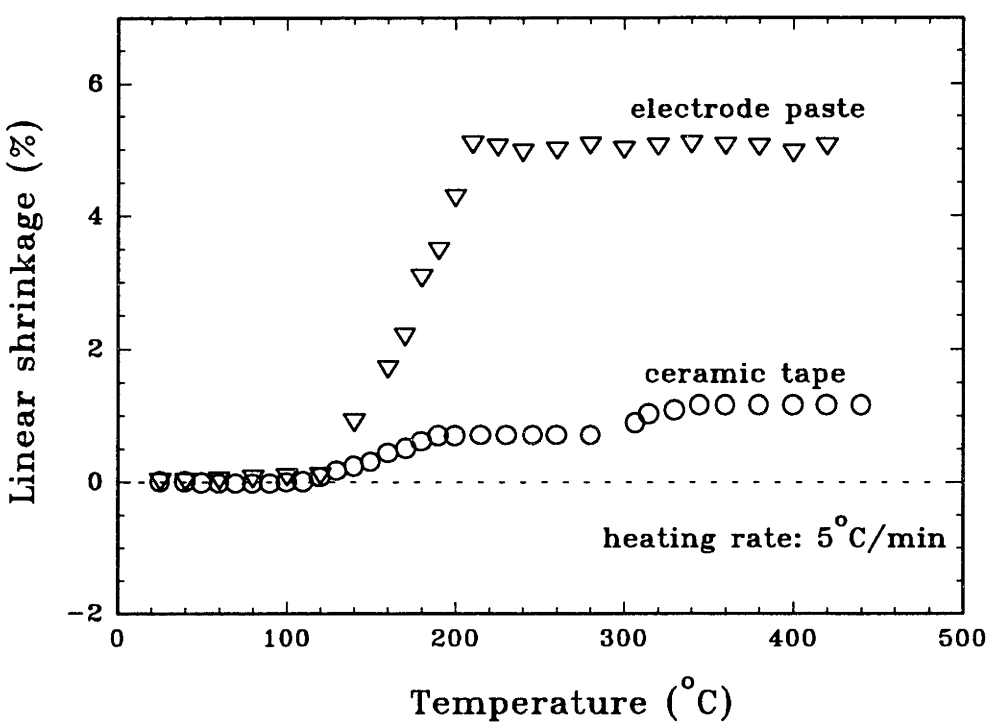


**Figure 5.15. Dimensional change of the dielectric tape and electrode layer during binder removal**

composite, the dielectric layer is under compressional stress, while the electrode layer is under tensile stress, during the binder removal process. The shrinkage of the electrode print in an MLC greenware during binder removal, however, may not be exactly 5.1% since the thin electrode print in an MLC may have high residual orientation in the x-y plane from the silk screening and from the subsequent drying, as discussed in Chapter 4. This residual orientation will result in higher shrinkage than the cast 50 μm electrode film used in the shrinkage measurement.

The curvature of dielectric layers and dielectric-electrode strips during binder removal is shown in Figure 5.16 and Figure 5.17, respectively. A pure dielectric layer bent toward the bottom surface when it was heated in air. After 80°C, it began to reverse its direction such that, by 120°C, it had returned to its original state. It then continued to

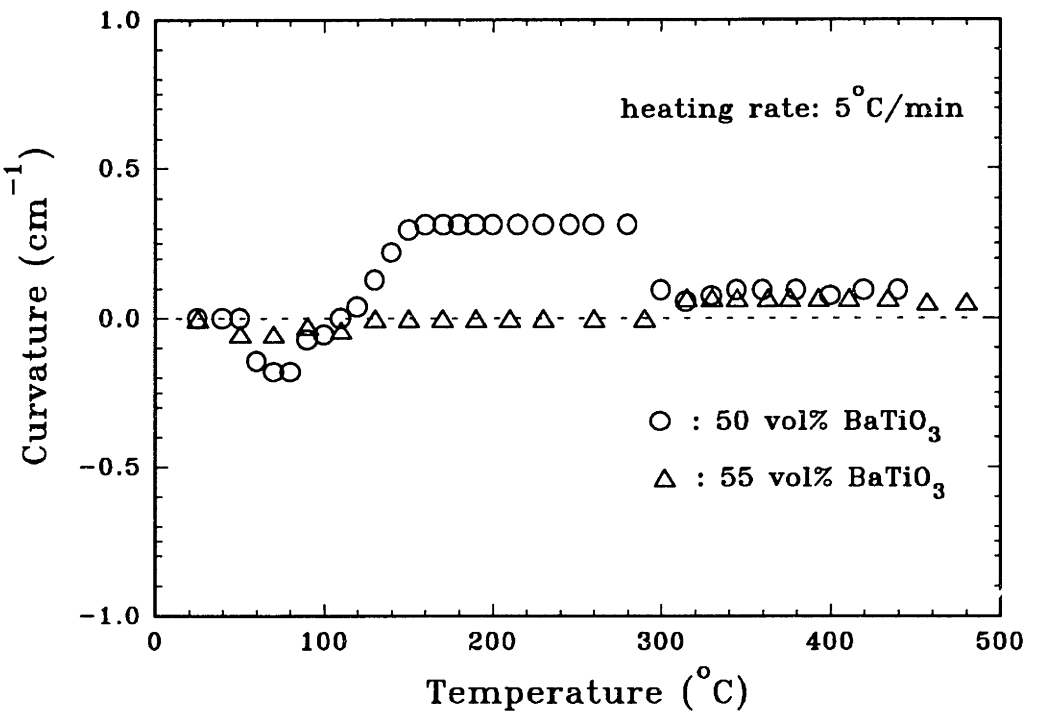


**Figure 5.16. Curvature of the dielectric tapes during binder removal**

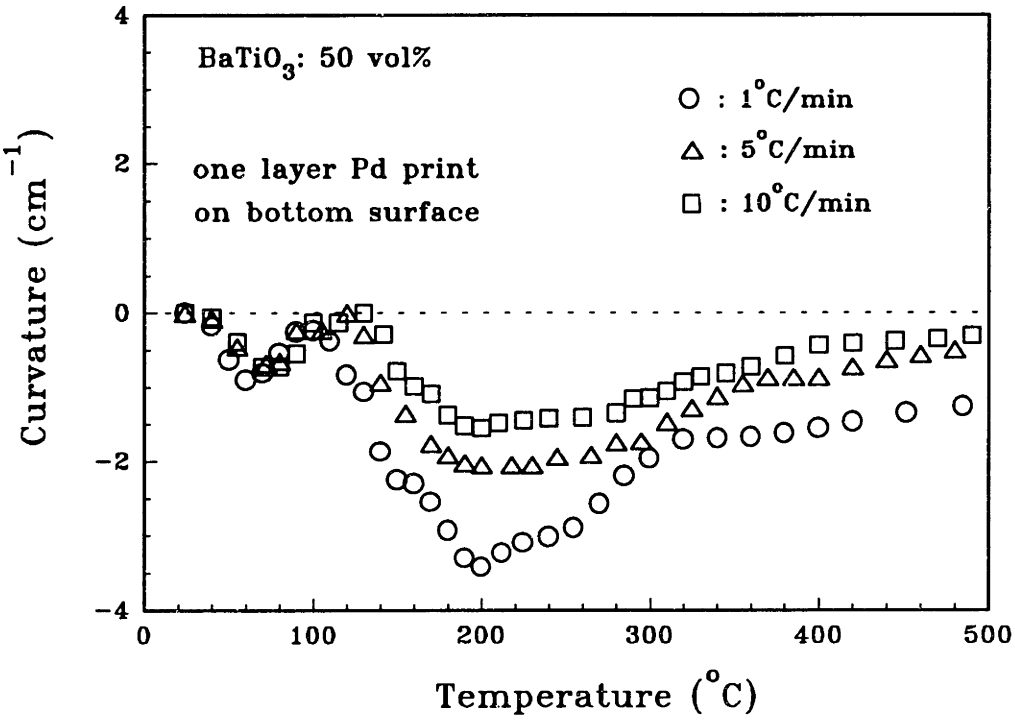


**Figure 5.17. Curvature of a dielectric tape with one layer Pd paste printed on its bottom surface**

bend toward the top surface (casting surface) until the temperature reached 160°C. The movement then slowed down and finally stopped. The deformation of a dielectric-electrode strip behaved similarly to the pure dielectric layer below 120°C. The sample bent toward the bottom surface which printed with the electrode between 120°C and 200°C. The tape then slowly recovered toward its original state above 200°C. Increasing heating rate decreased the camber of the tape.

The curvature of the dielectric layer decreased substantially when the ceramic loading increased from 50 to 55 vol%, as shown in Figure 5.16. The curvatures of this tape with one layer electrode (~ 3 μm) printed on either the top or the bottom surface is shown in Figure 5.18. The dielectric-electrode strips remained straight at temperatures lower than 120°C. The samples then bent toward the surface with the electrode print

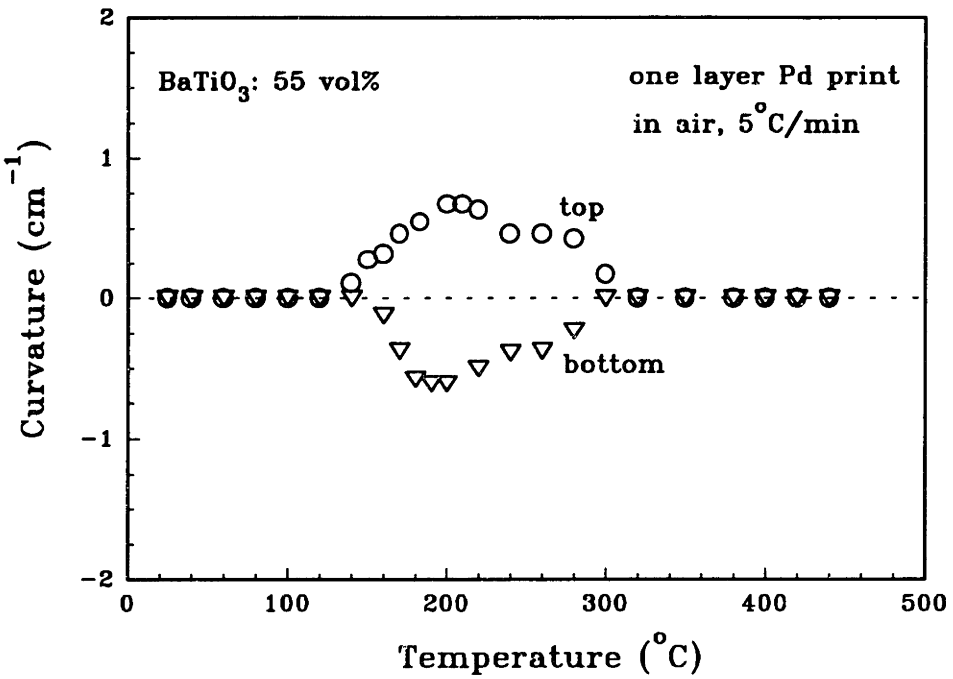


**Figure 5.18. Curvature of a dielectric tape with one layer Pd paste printed on its top or bottom surface**

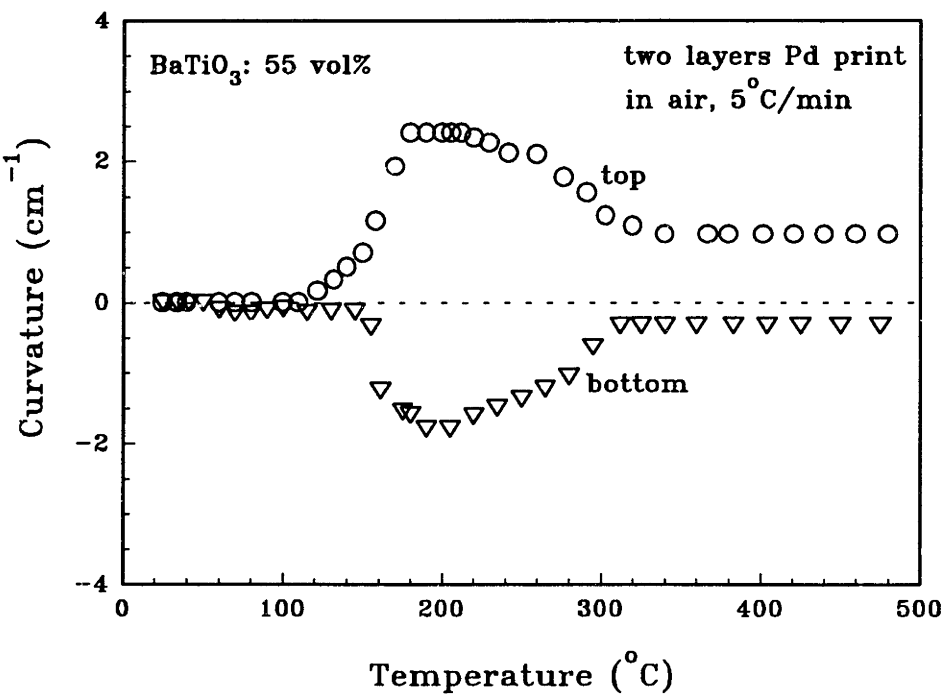


**Figure 5.19. Curvature of a dielectric tape with two layers Pd paste printed on its top or bottom surface**

between 120°C and 200°C. Further increase in temperature caused the tapes to recover to their original states. A complete recovery was observed after temperature exceeded 320°C, regardless of which surface of the tape the electrode was printed on.

Figure 5.19 shows the curvature of the dielectric tapes with 55 vol% ceramic powders printed with two layers of electrode paste (~6μm) on either the top or the bottom surface. The maximum curvature of these samples was approximately three times that of the composite with single layer of electrode print. Residual deformation of the strips remained after the binder removal process was completed. The dielectric and electrode layers stayed intact throughout the binder removal process in all of the above samples.

The bending of a dielectric-electric composite strip is determined by the shrinkage mismatch, the mechanical properties of the dielectric and electrode layers, and the geometry of the sample. An elastic approach gives the following relationship[24]:

$$\frac{1}{r} = \frac{(\varepsilon_1 - \varepsilon_2)}{h} \frac{6(1+a)^2}{3(1+a)^2 + (1+ab)(a^2 + \frac{1}{ab})} \qquad (5.21)$$

where $a = \frac{h_1}{h_2}$ and $b = \frac{E_1}{E_2}$

$E_1$, $E_2$, $h_1$, $h_2$, and $\varepsilon_1$, $\varepsilon_2$ are modulus, thickness, and the shrinkage of the electrode and dielectric layers, respectively, while $h$ is the total thickness of the composite. Eq. 5.21 shows that the curvature of a bi-material strip is proportional to the mismatch of the dimensional change of the two layers, and inversely proportional to the total thickness of the sample. The curvature also increases with the increase of $h_1/h_2$ in the case of $h_1 \leq h_2$.

The electrode layer experienced higher shrinkage than the dielectric layer in the binder removal process, which caused the composite strip to bend toward the electrode

layer direction. The binder removal process in the electrode layer was completed at 200°C and shrinkage in this layer stopped. Therefore, the curvature of the strip reached maximum at 200°C. The tensile stress in the electrode layers and the compressive stress in the dielectric layers also reaches maximum at 200°C. Further increase in temperature results in stress relaxation of the dielectric tape, which causes the curvature of the composite to decrease.

### 5.3.4 Direct Observation of Delamination During Binder Removal

*Delamination observation via Method 1*: Delamination was first observed on the surface of an MLC greenware at 180°C when the sample was heated in air at 10°C/min. This delamination continued to grow until the temperature reached 210°C. The width of a delamination versus temperature, measured from the surface of an MLC, is shown in Figure 5.20. This delamination shrunk back gradually from 210 to 240°C. The second healing period occurred between 280 and 320°C. Residual delamination of approximately two-thirds of the maximum separation remained at 500°C, when all the binder had been removed. The delamination in the middle of the sample is expected to be more severe and would start at a temperature lower than 180°C since delamination always starts from inside the sample (usually from the sample center). The residual delamination in the center of this same sample, measured from an SEM micrograph of a fracture surface through the sample center, was 54 μm. It was more than six times larger than the residual delamination observed on the surface, which was 8.8 μm. The delaminated MLC samples were then sintered at 1340°C. Delamination remained after sintering. The dimension of this delamination increased from 54 μm to 85 μm.

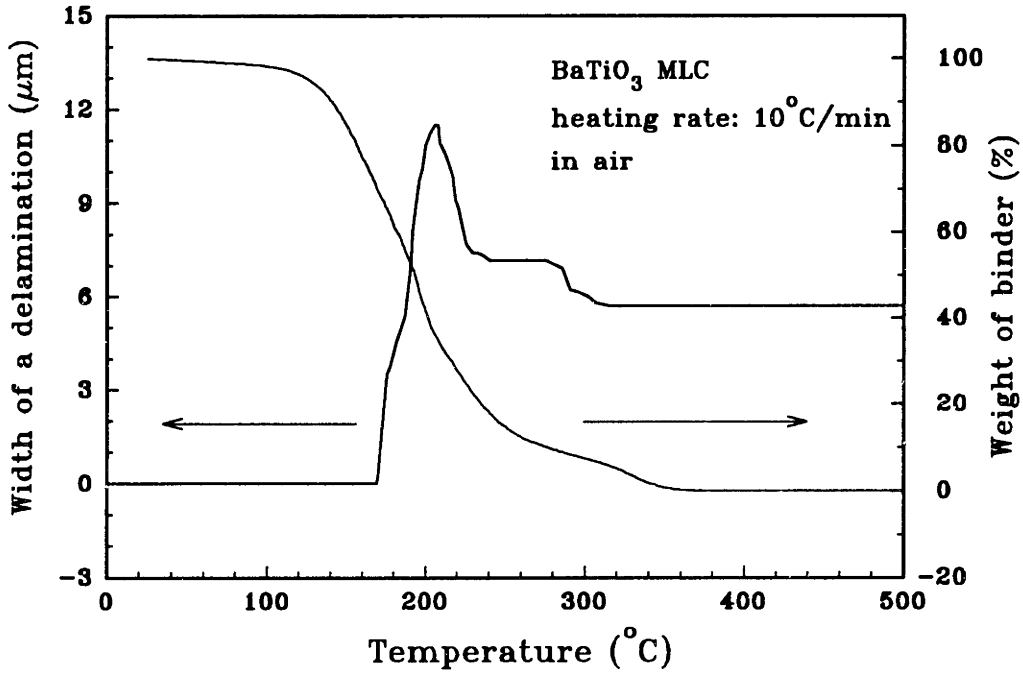


**Figure 5.20. Width of a delamination versus temperature measured from sample surface**

*Delamination observation via Method 2*: No delamination was observed from the surface of the samples heated at 1°C/min to a number of final temperatures. The SEM micrographs of the fracture surfaces of these samples shown in Figure 5.21, however, revealed the same delamination-and healing process observed for 10°C/min with Method 1. Delamination was first observed in the sample heated to 155°C, corresponding to 20% binder removal of the MLC sample. Delamination was severe (~10 μm) in the sample heated to 165°C, which had lost 30% of the binder. Higher temperatures caused the extent of delamination to diminish such that the samples were completely healed at 190°C and 50% binder removal. No further delamination was observed at higher temperatures at a 1°C/min heating rate in an initially defect-free MLC sample.

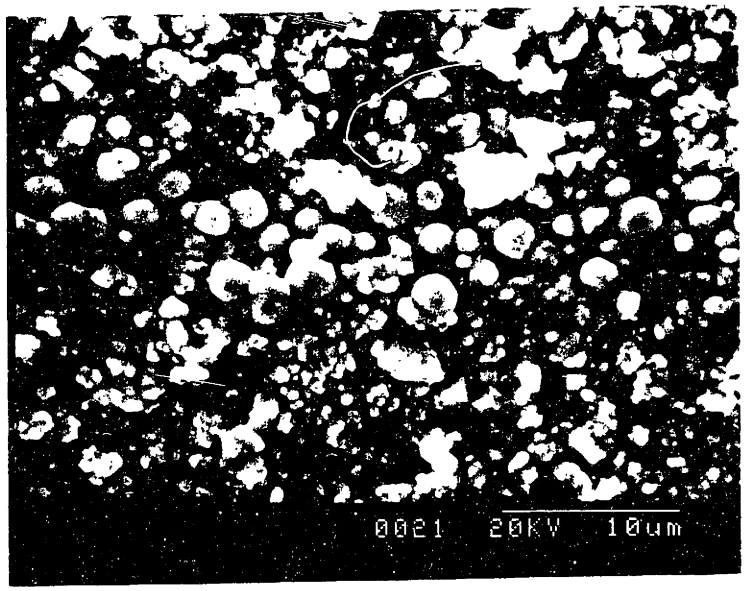


(a)

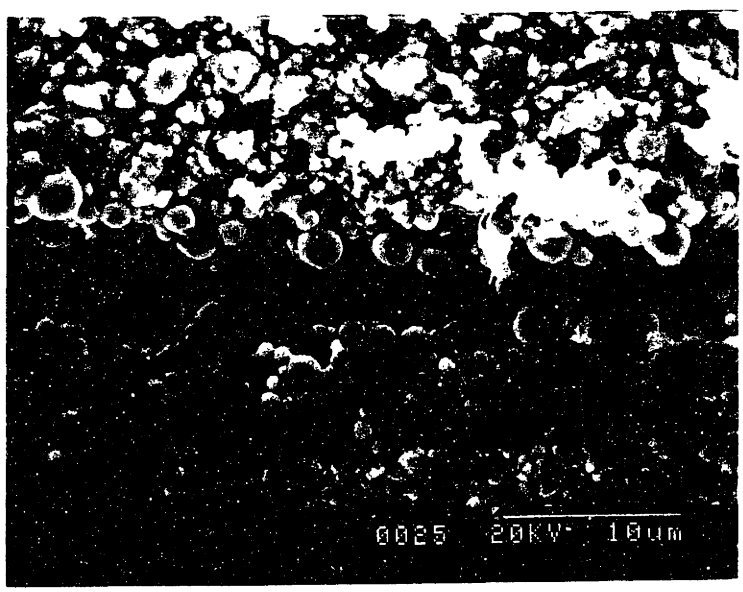


(b)

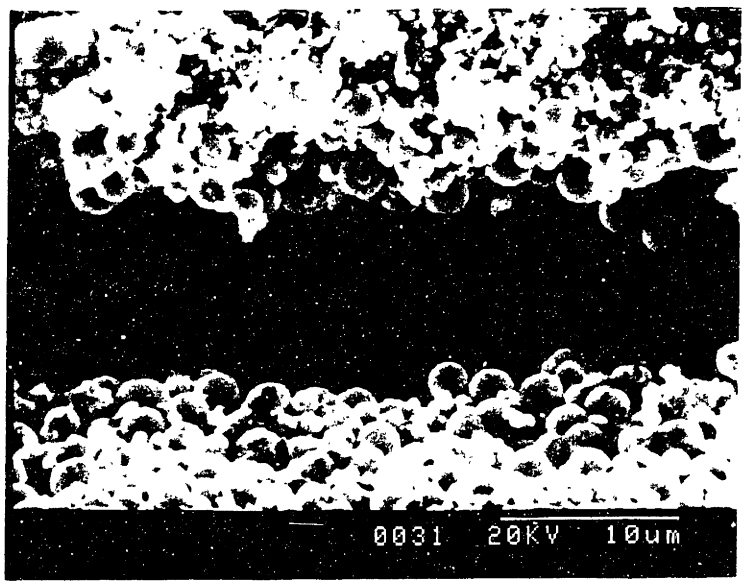


(c)

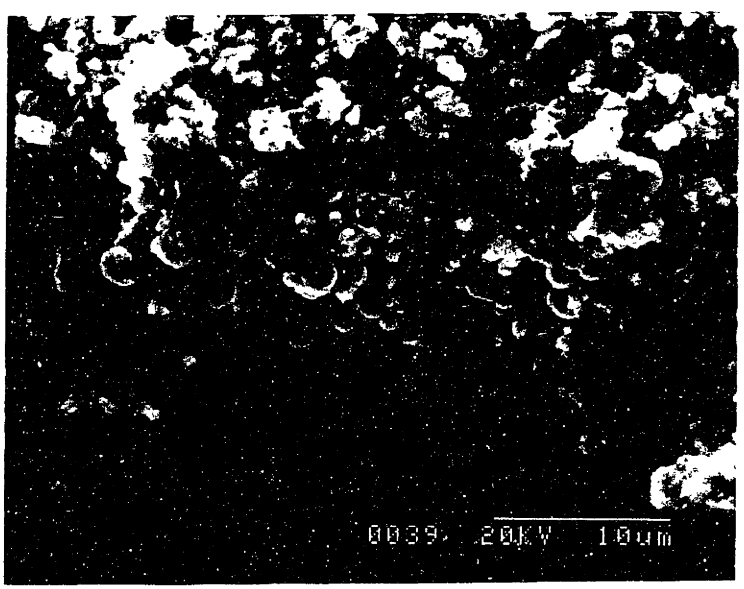


(d)

**Figure 5.21. Fracture surface of MLC samples after different amount of binder has been removed: (a) 10%, (b) 20%, (c) 30%, and (d) 50%**

Figure 5.22 shows the SEM micrograph of fracture surface of an MLC sample which was heated at 1°C/min in air to 90% binder removal and then quenched. Residual delamination of 5 μm was observed in the vicinity of a large electrode agglomerate. The thickness of this agglomerate was about six times the normal electrode thickness of 3 μm.

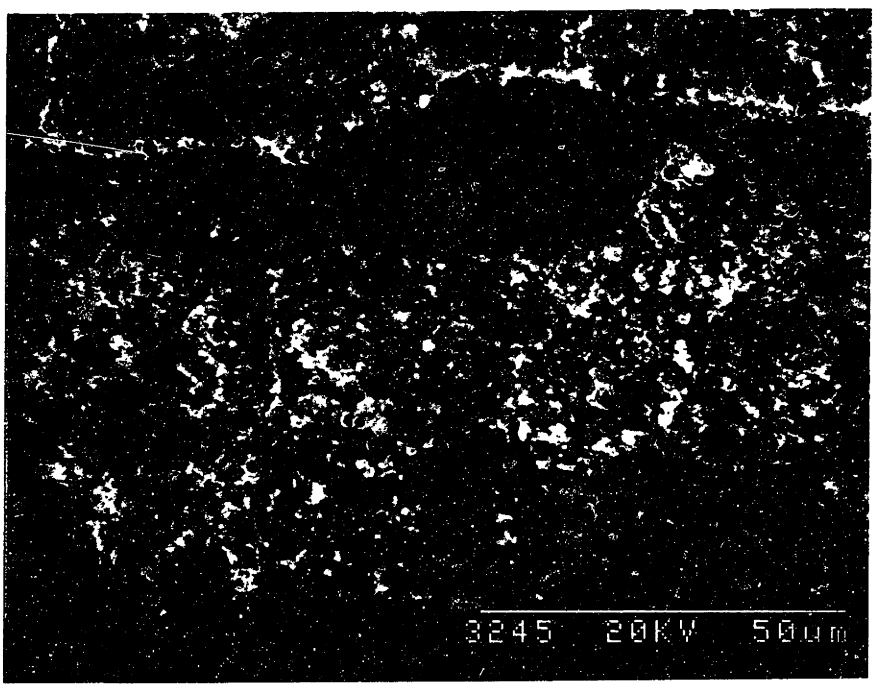


**Figure 5.22. Fracture surface of an MLC sample after 90% binder removal shows the effect of defect in the electrode**

The width of delaminations in $E_1$ and $E_2$ samples at 1°C/min, measured from the SEM micrographs of their fracture surfaces, is shown in Figure 5.23. The $E_1$ samples have one layer of electrode print, while the $E_2$ samples have two layers of electrode print

on their third and eighth layer of dielectric tapes. Delamination in the $E_1$ sample was first observed when the sample lost 20% of its total binder. This delamination became severe in samples which had lost 30% and 40% of the binder. The delamination then healed completely after 50% of the binder was removed. $E_2$ sample, on the other hand, did not delaminate until 30% of the binder was removed. This delamination shrunk back after 50% binder removal. The recovery, however, was incomplete; approximately 4 μm residual delamination remained in the sample.

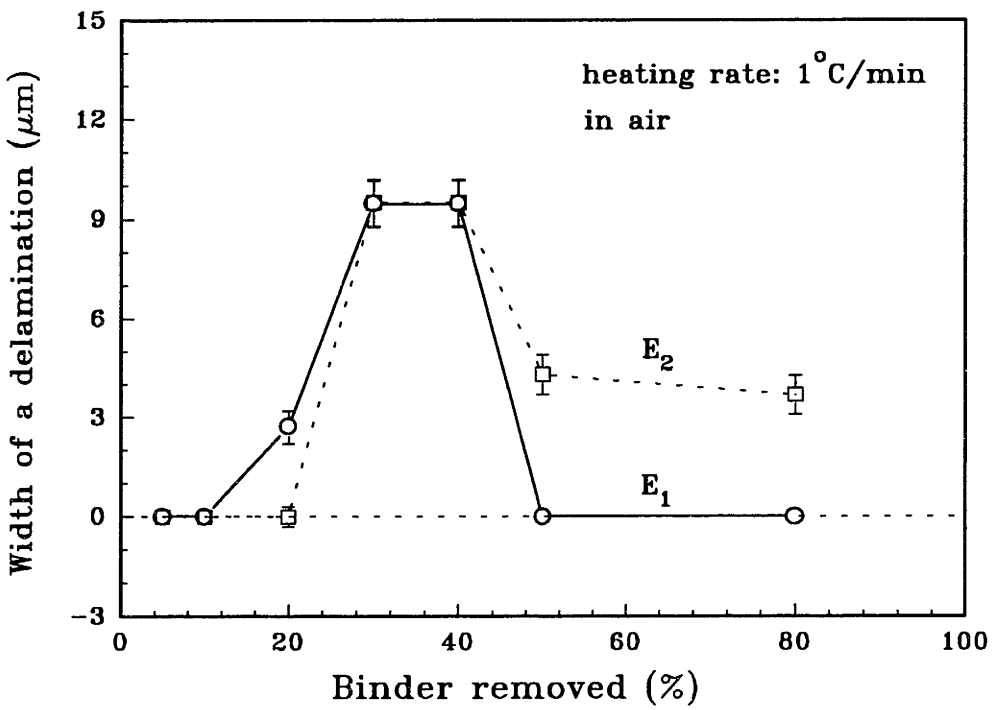


**Figure 5.23. Width of delamination within $E_1$ and $E_2$ samples after different amount of binder has been removed**

Cohesive delamination within the electrode layer was observed in all the MLC samples used in this research. However, no delamination was observed in the laminated ceramic tapes and the cast electrode paste, even at a heating rate of 10°C/min.

## 5.4 Discussion

The combination of the above three types of experiments and the direct observation of delamination provide insight into the origins of delamination. The effects of the following factors on delamination: the gas generation rate, the bond strength between the electrode and dielectric layers, and the shrinkage mismatch between the dielectric and electrode layers, are discussed below.

The importance of the gas generation rate of the sample during binder removal is straightforward when comparing the delamination at different heating rates. A high gas generation rate, resulted from a high heating rate such as 10°C/min, creates high gas pressure within the greenware, especially inside the electrode layer. The resultant delamination is severe, and considerable residual delamination remains in the sample after the completion of the binder removal process. Lowering heating rate lowers the gas generation rate and, therefore, the gas pressure within an MLC sample. The corresponding delamination is small and transient, therefore, it does not affect the integrity of the final products.

Gas pressure alone is unlikely to cause delamination in the current system since neither the laminated ceramic tapes nor the cast electrode greenware delaminated, even at a heating rate of 10°C/min. Apparently, the interaction between the dielectric and electrode layers is also critical to delamination. Mismatch of dimensional changes of the electrode and dielectric layers creates stresses within an MLC sample. Stresses in the electrode layers are composed of an axial tensile stress in regions away from the ends of the strip, and an interfacial shear stress which is concentrated at the ends[25]. Stress distribution in the dielectric layers is similar to that of the electrode layer, except that an axial compressive stress instead of tensile stress exists in regions away from the ends of

the strips. Since delamination appeared to originate from the middle of an MLC sample, we are only going to consider the stresses in this region in the following discussion.

An elastic approximation of the stresses and strains within the samples are[26]:

$$\sigma_1 = \frac{E_1}{(1-\upsilon_1)(1+\frac{h_1}{h_2}\frac{E_1}{1-\upsilon_1}\frac{1-\upsilon_2}{E_2})}(\varepsilon_2 - \varepsilon_1) \qquad (5.22)$$

$$\sigma_2 = -\frac{h_1}{h_2}\sigma_1 \qquad (5.23)$$

$$\varepsilon_1' = \varepsilon_2' = \varepsilon_1 + \frac{\sigma_1}{E_1}(1-\upsilon_1) \qquad (5.24)$$

$$\Delta\varepsilon_1 = \varepsilon_1 - \varepsilon_1' = -\frac{\sigma_1}{E_1}(1-\upsilon_1) \qquad (5.25)$$

$$\Delta\varepsilon_2 = \varepsilon_2 - \varepsilon_2' = -\frac{\sigma_2}{E_2}(1-\upsilon_2) \qquad (5.26)$$

where $\sigma_1$, $\sigma_2$ and $\upsilon_1$, $\upsilon_2$ are stress and Poisson's ratio of the electrode and dielectric layers, $\varepsilon_1$ and $\varepsilon_2$ are free strains of the electrode and dielectric layers (if they are heated up separately), $\varepsilon_1'$ and $\varepsilon_2'$ are strains of the electrode and dielectric layers in the central region (within an MLC). Eq. 5.22 to Eq.5.26 indicate that increasing the thickness of the electrode layers decreases the stress and differential strain ($\Delta\varepsilon_1$) in the electrode layers and increases the stress and differential strain ($\Delta\varepsilon_2$) in the dielectric layers. Thus, we expect the ratio of the thickness of the electrode and dielectric layers play an important role in delamination.

Binder removal of a thin electrode layer is achieved by gas flow and diffusion through this thin electrode layer toward its termination. Thus, changing the thickness of the electrode layer does not change the gas pressure within it, but it changes the stress distribution and the strain in both the electrode and dielectric layers. The difference of delamination and healing behavior between $E_1$ and $E_2$ samples illustrates the effect of this stress and strain. The electrode layers are thin and the stresses are high in the $E_1$ sample.

Thus, delamination can nucleate easily. On the other hand, the stresses in the dielectric layers are low and the strains in the dielectric layers from the thermal expansion mismatch ($\Delta\varepsilon_2$) is low. Shrinkage stops after the binder in the electrode layers is removed, and van de Waals forces keep the Pd particles together. The still viscoelastic dielectric layer, then, is able to recover from its deformation, as has been observed in semicrystaline polymers and particle filled elastomers[27]. The stresses in the electrode layers decrease when the thickness of the electrode layers increases, as in the case of the $E_2$ sample. Therefore, the nucleation of the delamination occurs at a higher temperature. On the other hand, the stresses in the dielectric layers increases with the thickness of the electrode layer, which results in higher deformation ($\Delta\varepsilon_2$) in the dielectric layers than in the case of $E_1$ samples. Thus, only partial recovery of the delamination can be achieved after the shrinkage of the electrode layer stopped and the gas pressure decreased.

Pre-existed defects in the electrode layer such as large agglomerates can also cause large delamination which remains after the of binder removal process is completed. A large agglomerate increases the local gas pressure since the gas generated has to flow through an electrode layer much thinner than the diameter of the agglomerate. The agglomerate also causes high local strain in the dielectric layer during lamination and binder removal. This strain will remain in the final products.

Cohesive failure of the electrode layers is the only kind of delamination observed in this system. Apparently, the adhesive strength between the electrode and dielectric layers is stronger than the cohesive strength of the electrode layers in the temperature range over which delamination occurs, even though it is the opposite at room temperature. Therefore, the adhesive strength between the electrode and dielectric layers does not affect delamination during the binder removal process.

The above discussion indicates the controlling mechanisms of the nucleation, growth, and healing of the delamination during the binder removal process. Delamination nucleates within the electrode layer due to the tensile stress from shrinkage mismatch between the dielectric and electrode layers. The growth of a delamination, on the other hand, is mainly controlled by the gas pressure within the electrode layers. The healing of a delamination is determined by the maximum strain level in the dielectric layers. Large deformation of the dielectric layers caused by high gas pressure or by thick electrode layers results in an incomplete healing.

It is believed[28] that the sintering process not only does not heal a defect in a greenware, but also enhances it. This is confirmed by the experiment since the thickness of a delamination increased from 54 μm to 85 μm after sintering. This indicates that delamination created during the binder removal process will remain in the final products.

## 5.5 Conclusion

We have shown that delamination during binder removal is a cohesive failure along the electrode layer, as opposed to the conventional concept of adhesive failure. The following factors have been shown to control the delamination and healing of a delamination during binder removal from MLC structures: the gas pressure within electrode layers, the shrinkage mismatch between the dielectric and electrode layers, and the ratio of thickness of the two layers.

Gas generation rates of both the electrode and dielectric layers during binder removal were studied. Gas pressure within the electrode layers was calculated based on viscous flow model. The model shows that gas pressure increases with temperature and length of the electrode layers and decreases with porosity in the electrode. The critical gas

pressure for causing a delamination to grow is inversely proportional to the size of defect in the electrode layers. The porosity of the electrode layers has a great impact on the gas pressure during binder removal. The gas pressure increases rapidly when the porosity decreases, indicating that delamination is most likely to occur in the early stages of binder removal when the porosity of the sample is low.

The electrode layer experienced higher shrinkage during binder removal than the dielectric layer. This causes tensile stress in the electrode layers and compressive stress in the dielectric layers. The magnitude of stress in the electrode layers increases as the thickness of the electrode layer decreases.

Delamination during binder removal was observed *in situ*. It was shown that delamination occurred in the early stages of binder removal. The magnitude of a delamination remained the same as the thickness of electrode layer was doubled, but it increased with the heating rate. Delamination healed or partially healed at the late stages of binder removal. While a small delamination healed completely, a large delamination caused by high gas pressure or by thick electrode layers only healed partially.

Delamination was proven to nucleate in an electrode layer due to the stress within this layer from shrinkage mismatch. This delamination propagates along the electrode layer due to a high gas pressure caused by a high gas generation rate. The healing of delamination, after the shrinkage in the electrode layer stopped and the gas pressure in the electrode layer decreased, is controlled by the maximum strain level in the dielectric layers.

**References**


1. A.F. Dyson, "Improvements in Multilayer Ceramic Capacitors," *Electrocomponent Science and Technology*, 11, 53-63 (1983).

2. R.A. Gardner and R.W. Nufer, "Properties of Multilayer Ceramic Green Sheets," *Solid State Technol.*, 17, 38(1974).

3. M. Kahn, "Effects of Partial Oxygen Pressure During Burnout of Multilayer Structures"; pp.185-88 in Advances in Ceramics, Vol.19, *Multilayer Ceramic devices*. Edited by J.B. Blum, and W.R. Cannon. American Ceramic Society, Westerville, OH, 1987.

4. R.R. Tummala, "Ceramics in Microelectronic Packaging"; pp. 3-16 in Advances in Ceramics, Vol. 26, *Ceramic Substrates and Packages for Electronic Applications*. Edited by M.F. Yan, K. Niwa, H.M. O'Bryan, Jr., and W.S. Young, American Ceramic Society, Westerville, OH, 1987.

5. R.A. Vogel, "Fine Line Printing for Consumer Electronics," *Solid State Technol.*, 15, 51-54 (1972).

6. J.G. Pepin, William Borland, Patrik O'Callaghan, and Richard J.S. Young, "Electrode-Based Causes of Delaminations in Multilayer Ceramic Capacitors," *J. Am. Ceram. Soc.*, 72 [12] 2287-91 (1989).

7. J.G. Pepin, "High Fire Multilayer Ceramic Capacitor Electrode Technology"; Present in American Ceramic Society, Cincinnati, OH, 1991.

8. M. Kahn and M. Chase, "Effects of Heat Treatments on Multilayer Piezoelectric Ceramic-Air Composites," *J. Am. Ceram. Soc.*, 75 [3] 649-56 (1992).

9. H. Verweij and W.H.M. Bruggink, "Reaction-Controlled Binder Burnout of Ceramic Multilayer Capacitors," *J. Am. Ceram. Soc.*, 73 [2] 226-31 (1990).

10. P.C. Carman, Flow of Fluids Through Porous Materials. Reinhold Publishing Corporation, New York (1961).

11. G.R. Youngquist, "Diffusion and Flow of Gases in Porous Solids"; pp. 58-69 in Flow Through Porous Media, American Chemical Society, Washington, D.C., 1970.

12. R.M. German, "Gas Flow Physics in Porous Metals," *Inter. J. Powder Met. Powder Tech.*, 15 [1] 23-30 (1979).

13. B.A. Meyer and D.W. Smith, "Flow Through Porous Media: Comparison of Consolidated and Unconsolidated Materials," *Ind. Eng. Chem. Fundam.*, 24 [3] 360-68 (1985).

14. R.M. German, "Porosity and Particle Size Effects on the Gas Flow Characteristics of Porous Metals," *Powder Tech.*, vol. 30, 81-86 (1981).

15. M.J. Cima, J.A. Lewis, and A.D. Devoe, "Binder Distribution in Ceramic Greenware During Thermolysis," *J. Am. Ceram. Soc.*, 72, 1192-99 (1989).

16. M.R. Barone and J.C. Ulicny, "Liquid-Phase Transport During Removal of Organic Binders in Injection-Molded Ceramics," *J. Am. Ceram. Soc.*, 73, 3323-33 (1990).

17. J. Woodthorpe, M.J. Edirisinghe, and J.R.G. Evans, "Properties of Ceramic Injection Molding Formulation III. Polymer Removal," *J. Mater. Soc.*, 24, 1028-49 (1989).

18. D. Satas, "Peel"; pp. 61-96 in Handbook of Pressure Sensitive Adhesive Technology. Edited by D. Satas, Van Nostrand Reinhold, 1989.

19. R.M. German, "Theory of thermal debinding," *Int. J. Powder Metall.*, 23 [4] 237-45 (1987).

20. R.M. German, "Porosity and Particle Size Effects on the Gas Flow Characteristics of Porous Metals," *Powder Technol.*, 30, 81-86 (1981).

21. R.B. Bird, Transport Phenomena. John Wiley & Sons, 1976.

22. A.N. Gent, and R.P. Petrich, "Adhesion of Viscoelastic Materials to Rigid Substrates," *Proc. Roy. Soc.* A. 310, 433-448 (1969).

23. Y. Tang and M.J. Cima, "Deformation During Binder Removal from Multilayer Ceramic Greenware"; pp. 115-124 in Ceramic Transactions, Vol. 26, Forming Science and Technology for Ceramics. Edited by M.J. Cima. The American Ceramic Society. Westerville, OH, 1991.

24. S. Timoshenko, "Analysis of Bi-metal Thermostats," *J. Opt. Soc. Amer. and Rev. Sci. Instr.*, vol.11, p.233, 1925.

25. N.G. McCrum, C.P. Buckley, and C.B. Bucknall, Principles of Polymer Engineering. Oxford University Press, New York, 1988.

26. G.W. Scherer, Relaxation in Glass and Composites. John Wiley & Sons, New York, 1986.

27. R.P. Wool, "Crack Healing in Semicrystalline Polymers, Block Copolymers, and Filled Elastomers"; pp. 341-62 in Polymer Science and Technology, vol. 12A: Adhesion and Adsorption of Polymers. Edited by Lieng-Huang Lee. Plenum press, New York, 1980.

28. W.D. Kingery, "Firing-The Proof Test for Ceramic Processing"; pp. 291-306 in Ceramic Processing Before Firing. Edited by G.Y. Onoda and L.L. Hench, Wiley, New York, 1978.

# CHAPTER 6

# PHYSICAL ASPECTS OF BINDER REMOVAL FROM MULTILAYER CERAMIC GREENWARE

## 6.1 Introduction

Binder removal from multilayer ceramic greenware is a critical step in the production of high quality ceramic components. As the green ceramic components are heated, volatile species evaporate, polymers decompose, and combustion may occur in an oxidizing environment. This binder removal process is often associated with a variety of defects such as cracks, voids and delaminations. An understanding of such physical and chemical processes as binder distribution, mass and heat transport, particle rearrangement and the resulting dimensional change of the sample during binder removal, is necessary in order to optimize processing conditions.

Investigations have previously been focused on studying the thermolysis process and characterizing particle packing as well as sample deformation of both single layer ceramic green sheets[1-3] and injection molded ceramic bodies[4-8]. In the early stage of binder removal, capillary pressure brings binder to the surface where it evaporates. Shrinkage from particles moving toward each other under the capillary pressure occurs during this stage. As binder removal continues, particles touch each other through their adsorption layer and shrinkage stops. Further removal of binder produces porosity within the sample. Gas flow and diffusion dominates the binder removal process in the late stage, even though capillary action still plays a role.

Little is known about the thermolysis of binders from multilayer ceramic greenware such as multilayer ceramic capacitors (MLCs) and multilayer ceramic substrates[9, 10]. Due

to both the presence of metal paste between ceramic tapes and the lamination process, it is expected that the binder distribution and particle rearrangement processes of multilayer ceramic structures will be different from that of single sheet ceramic tapes. Both particle rearrangement and defect formation causes dimensional change of the sample. Thus, monitoring sample deformation during binder removal will provide information about these processes.

## 6.2 Experimental Procedure

The composition of both the ceramic tape and the printed electrodes is shown in Table 1. Tape-cast ceramic sheets consisted of 50 vol% $BaTiO_3$ particles, 47 vol% binder and plasticizer, and 3 vol% trapped gas. These tapes were silk screened with electrode paste and laminated together. The structure of a sample is shown in Figure 6.1. An MLC

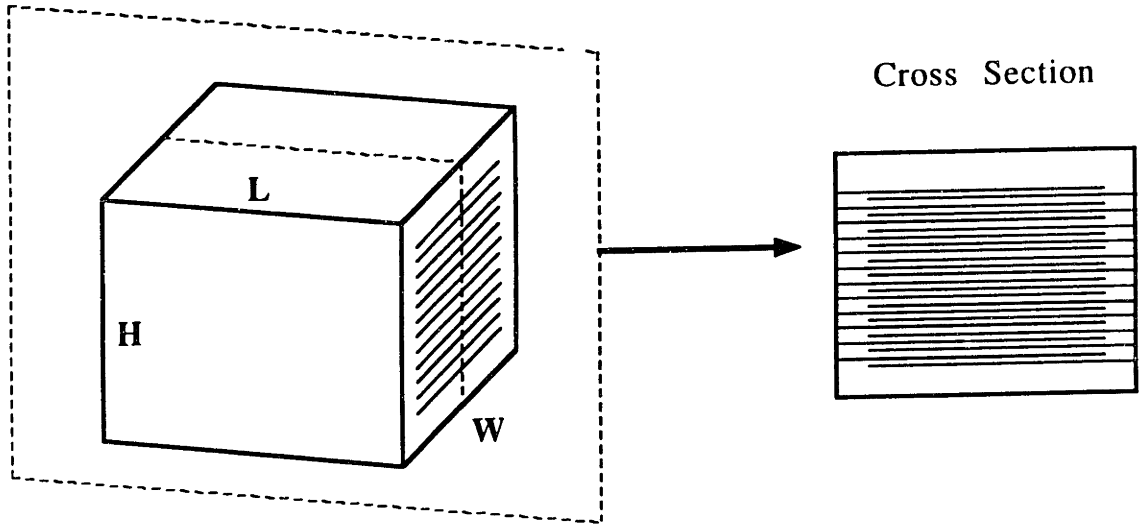


**Figure 6.1. The structure of a $BaTiO_3$ multilayer ceramic capacitor**

sample was composed of forty layers of ceramic tapes of which the middle thirty layers were printed with palladium electrode paste. The individual ceramic sheets were 34 μm thick and were separated by 3 μm thick electrode layers. The dimensions of an MLC sample were $L \times W \times H = 1.62 \times 1.32 \times 1.34$ mm$^3$. A sample solely composed of forty layers of laminated ceramic tapes was also made which had the dimensions of: $L \times W \times H = 1.62 \times 1.32 \times 1.30$ mm$^3$. This sample is designated as sample B. The third kind of sample (sample C) was similar to sample B except for the fact that the loading of ceramic powder increased from 50 to 55 vol%. The width of the above samples was along the casting direction of the ceramic tape, and the length was along the transverse direction of the tape.

**Table 6.1. Composition of ceramic tape and electrode paste**

| | Name | Wt% | Vol% | Description |
|---|---|---|---|---|
| Ceramic tape | barium titanate | 85 | 50 | ceramics |
| | polyvinyl butyral (PVB) | 9 | 28 | polymer |
| | benzyl butyl phthalate (BBP) | 6 | 19 | plasticizer |
| | trapped gas | | 3 | |
| Electrode paste | palladium | 88 | | electrode |
| | ethyl hydroxyethyl cellulose | 12 | | binder |
| | (EHEC) | | | |

Sample D was designed to study the binder distribution at different stages of binder burnout, such as whether the binder is removed from the surface of the MLC sample or form the dielectric-electrode interface. It consisted of 46 layers of ceramic tapes, in which the middle four layers had electrode paste on top of them. The dimensions of this sample are $L \times W \times H = 5.13 \times 3.76 \times 1.52$ mm$^3$. Sample D was placed on a flat alumina substrate, and heated in a quartz tube furnace at 0.5°C/min in flowing air to 160, 180, and 210°C, respectively. It was then glued to a flat steel plate using Duco Cement. The steel plate was fixed on a milling machine. The sample was milled, layer by layer. The milled

crumb from each layer was collected. The thickness of each milled layer was 76 μm. TGA was performed on each layer to determine the binder content. Each milled layer was heated at 5°C/min to 160°C, and was held at this temperature for thirty minutes to remove all the plasticizer. It was then heated at 10°C/min to 600°C to remove the PVB polymer.

Three methods were chosen to measure the deformation of an MLC greenware during the binder removal process. In the first method, the microscope was focused on a recognizable feature on the top of a sample placed in a hot-stage. When the temperature was increased, the sample either expanded or contracted. The microscope focus was adjusted continually to keep the feature in focus as the sample deformed. Thus, the linear expansion or contraction during binder removal could be monitored by a simple calibration of the microscope. The approximate error in calibration was ±1 μm, which is about ±0.08% of linear deformation. The advantage of this method is that no mechanical stress is applied to the sample while its dimensions are measured. Unfortunately, only one point, or at most several points, on the surface can be monitored during the heating process, and the sample cannot be turned around in order to observe changes in other dimensions. In the second method, TGA was used to monitor the weight loss of the sample, which was then quenched when the desired amount of binder was removed. Different samples were burned out to different stages, followed by quenching. The size of the sample could then be measured using an optical microscope before and after the binder was removed. In the third method, TGA was used again to heat one sample until 5% of the binder was removed, followed by quenching. The dimensions of the sample were measured. The same sample was then reheated at the same heating rate to a higher temperature to remove more binder, then quenched, and the dimensions were again recorded. This process was repeated until all the binder was removed.

## 6.3 Results and Discussion

### 6.3.1 Binder Distribution In an MLC During Binder Removal

Figure 6.2 shows the TGA curves of a single layer $BaTiO_3$ tape, Pd paste, and an MLC greenware. No overlap of the removal temperature ranges of BBP and PVB occurred in a single tape. They were 100-150°C and 200-450°C, respectively, at a heating rate of 5°C/min. The TGA curve of the MLC was continuous, indicating that the decomposition of PVB had started before the complete removal of BBP occurred. The EHEC binder for the electrode paste decomposed and evaporated rapidly in the presence of Pd powders between 150 and 180°C.

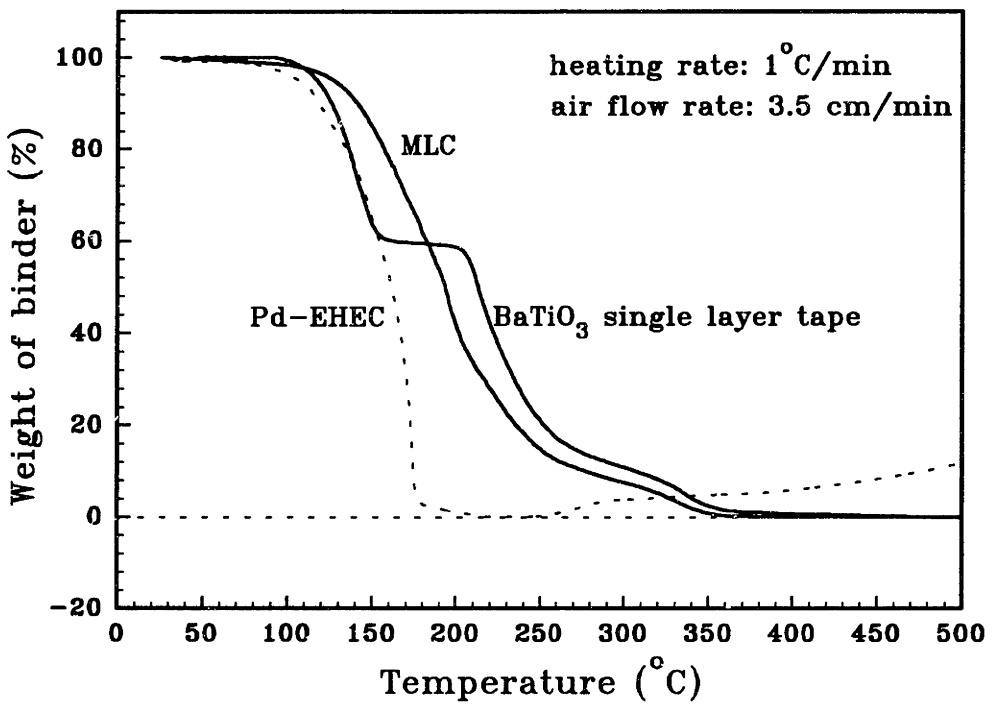


**Figure 6.2. Thermal gravimetric analysis of a single layer $BaTiO_3$ green tape, Pd paste, and an MLC greenware**

The distribution of binder in sample D, after being heated to three different temperatures, is shown in Figure 6.3. Region M was where the electrode layers located. At 160 and 180°C, 6 and 12% of the binder was removed from the sample, respectively. This is equivalent to the removal of 15 and 30% of the plasticizer. No decomposition of the PVB occurred at these temperatures. The binder distributions were nearly uniform throughout the sample. Nonuniform binder distribution was observed after the sample was heated to 210°C. Less binder was left in regions near the electrode layer and in regions near the bottom surface. The region with the lowest binder concentration, however, was not on the top surface. It was located in the region about 200 μm below the top surface of the greenware. This region was designated as A. From region A to the top surface, the concentration of binder increased. Figure 6.4 shows the distribution of BBP, PVB, and the total amount of binder in the sample heated to 210°C. The

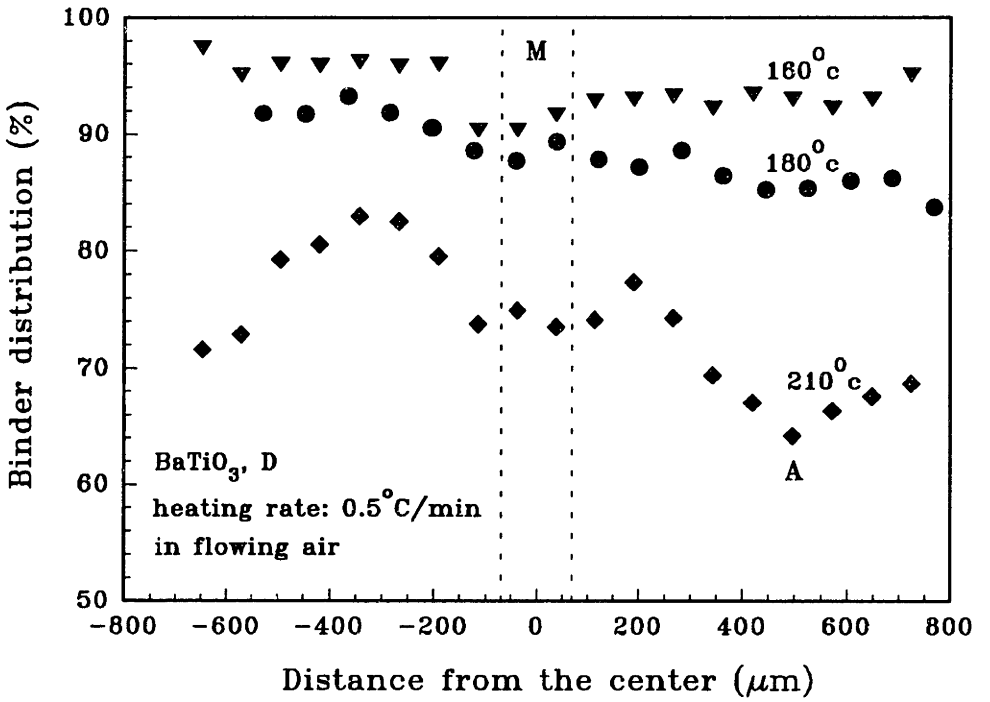


**Figure 6.3. Distribution of binder in a multilayer greenware during early stages of binder removal**

distribution of BBP was still uniform throughout the sample. PVB, on the other hand, distributed nonuniformly in the sample, resulting in the nonuniformity of the total amount of binder in the greenware.

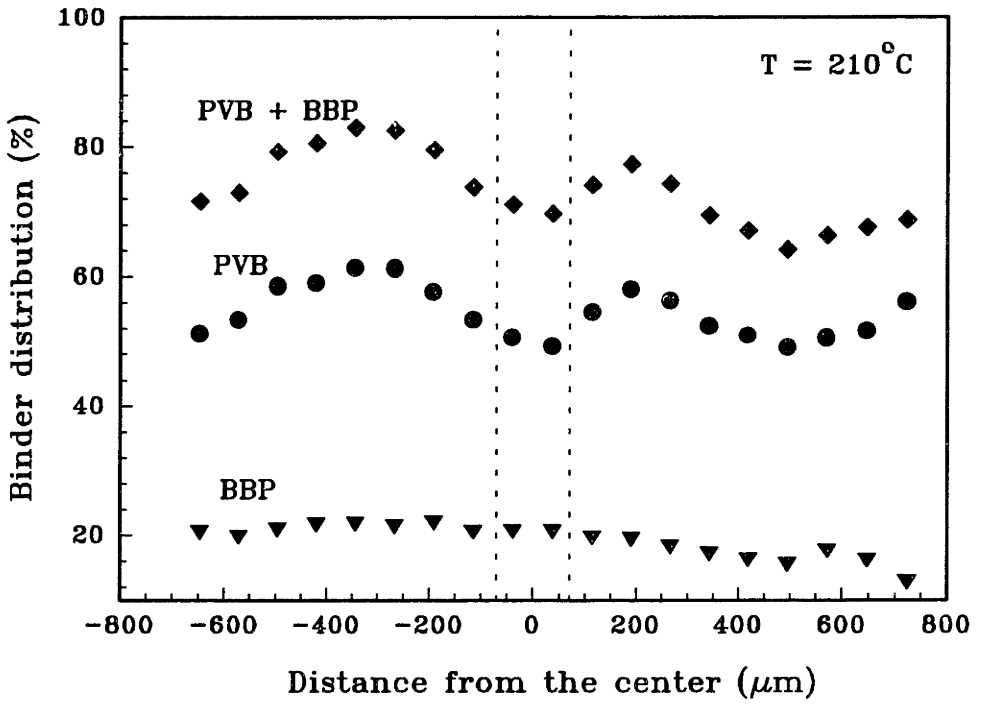


**Figure 6.4 Distribution of PVB, BBP, and PVB+BBP in sample D at 28% binder removal**

The distribution of binder at an early stage is controlled by capillary forces. Binder becomes viscous liquid as the temperature increases to above its glass transition region. The plasticizer starts to evaporate from the sample surface. Capillary forces draw liquid binder to the surface where the plasticizer evaporates freely. PVB, however, is rejected at the surface and it has to diffuse back to the interior of the sample. The evaporation rate is low at the early stages of binder removal since the temperatures are low. The viscosity of the binder is relatively low due to the presence of large amounts of plasticizer. Therefore, the liquid transport is the fast step and the rate of binder removal is limited by the

evaporation rate. This assumption is verified by the constant isothermal binder removal rate at low temperatures [1]. A uniform binder distribution, therefore, can be achieved. This uniform binder distribution throughout the binder removal process was also observed by Barone and Hengst [11] with injection molded samples when a low molecular weight wax was used as binder.

The evaporation rate of BBP on the sample surface increases with temperature. A higher amount of PVB is then rejected on the surface until a point is reached where the counter diffusion of PVB to the interior of the sample can no longer keep up with the PVB generation rate on the surface. A higher PVB concentration on the surface is expected. On the other hand, the low molecular PVB molecules start to decompose above 200°C. The removal of polymer at low temperatures is nonuniform and the polymer removes preferentially from the surface layer[11]. The binder distribution, therefore, is determined by the overall effect of these two aspects. The PVB-rich top surface indicates the effect of slow PVB counter diffusion. The preferential removal of PVB from the surface results in a lower PVB concentration on the bottom surface. The binder in the electrode (EHEC) is removed at relatively low temperatures, producing porous thin electrode layers. The low PVB concentration in region M and in regions near the electrode layers is apparently caused by the transport of decomposed PVB products along the electrode layers.

### 6.3.2 Dimensional Change of MLC Greenware During Binder Removal

#### I. Observation

*Sample deformation measurement via Method 1*: Figure 6.5 shows the deformation in the direction ($L$) perpendicular to the dielectric-electrode interface. Samples heated at

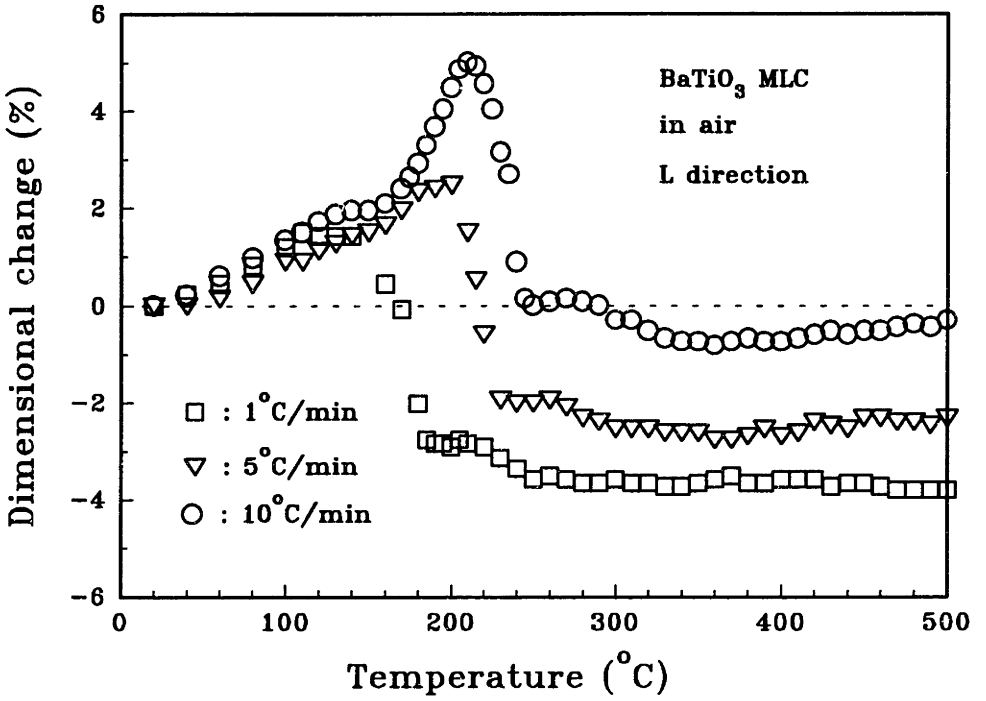


**Figure 6.5. Dimensional change of an MLC sample in L direction vs. temperature at different heating rates**

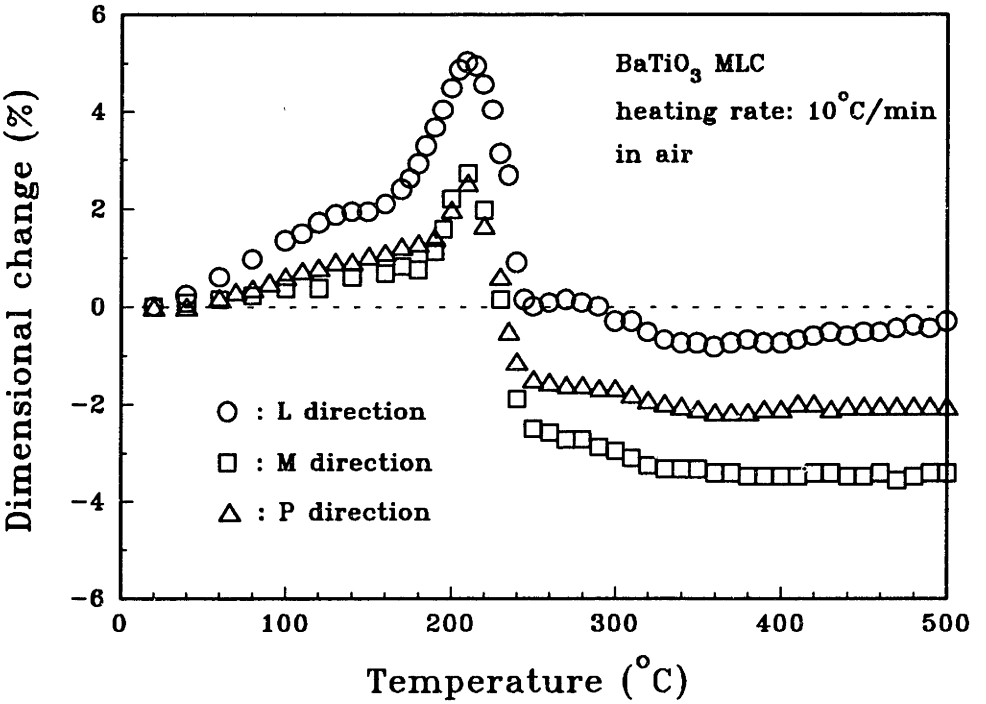


**Figure 6.6. Dimensional change of an MLC sample in different directions vs. temperature at 10°C/min heating rate**

all rates experienced expansion below 160°C, and the sample heated at 10°C/min experienced a very large expansion above 160°C followed by a sharp shrinkage. At lower heating rates, the expansion was smaller and the net shrinkage was larger. The dimensions remained the same within the next 50°C following the rapid shrinkage. The sample then started to shrink again, producing a 0.7% linear shrinkage. Figure 6.6 shows the dimensional change in different directions for a sample heated at 10°C/min. After a slow expansion before 160°C, a rapid expansion was observed in all directions followed by a sharp shrinkage which started at 210°C. The expansion in the direction perpendicular to the dielectric-electrode interface (*L*) was greater than in the parallel directions (*M* and *P*). The magnitude of net shrinkage in the three directions, (*l*), was $l_M > l_P > l_L$. The linear expansion versus temperature in the *M* direction (tape casting direction) was also observed for samples heated at 1°C/min. The net shrinkages were the same as their respective values at 10°C/min, as can be observed from Figure 6.7. A sharp shrinkage

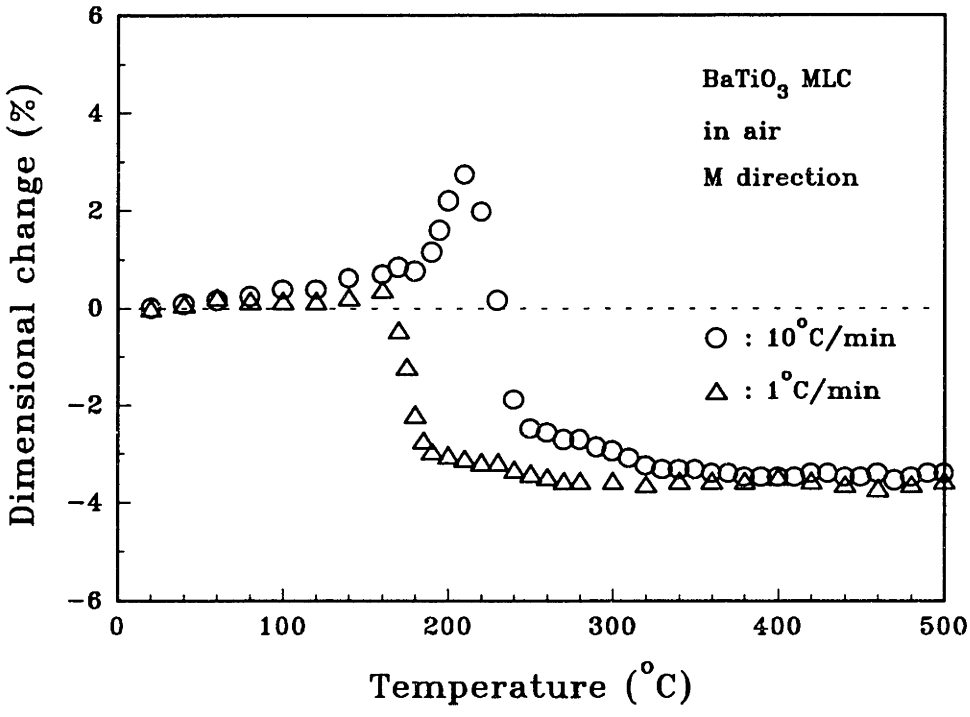


**Figure 6.7. Dimensional change of an MLC sample in *M* direction vs. temperature at 1 and 10°C/min heating rate**

occurred at all heating rates and along all directions. At a heating rate of 1°C/min, the linear net shrinkages in the *L*, *M*, and *P* directions were 3.7%, 3.5%, and 2.4%, respectively. This corresponds to a 9% volume shrinkage.

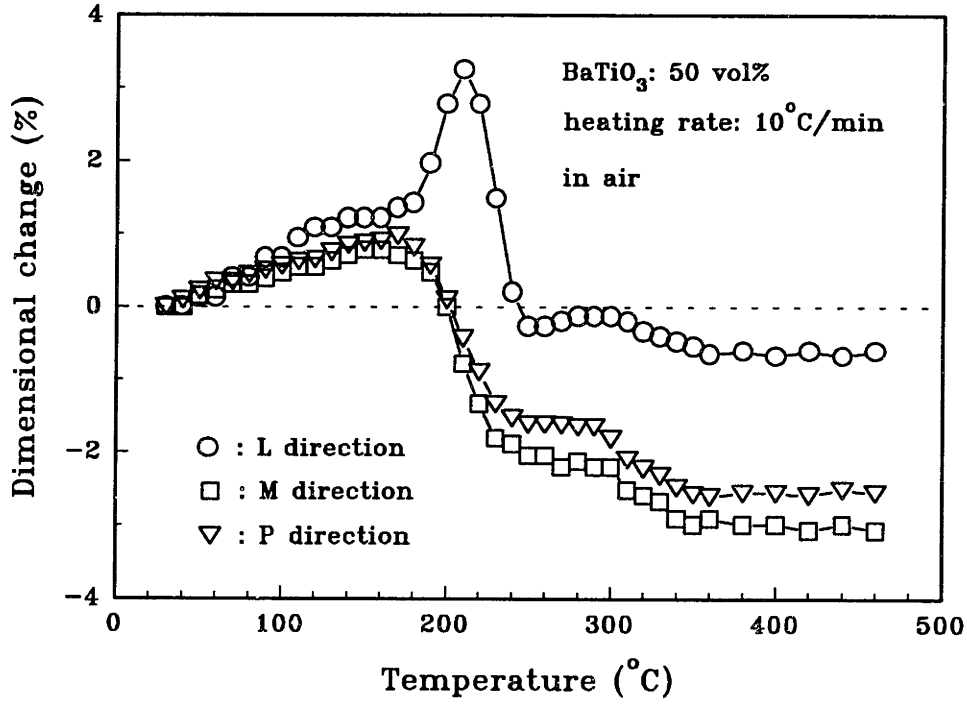


**Figure 6.8. Dimensional change of laminated ceramic tapes (sample B) during binder removal at 10°C/min**

The dimensional change of sample B during binder removal is shown in Figure 6.8. An expansion in all three directions was observed below 170°C. A further increasing of temperature caused shrinkage in the *M* and *P* directions. In the *L* direction, however, a rapid expansion occurred, which was followed by shrinkage from 210 to 240°C. The second stage of shrinkage occurred between 290 and 330°C, similar to the MLC sample. The shrinkage produced in this stage is 0.7% in all directions. Only 0.7% shrinkage in the L direction was observed after the binder removal, while the shrinkage in the *M* and *P* directions were 3.0 and 2.6%, respectively. Deformation of sample B at a lower heating rate, 1°C/min, is shown in Figure 6.9. Two major differences existed between Figure 6.9

and Figure 6.8. First, the corresponding dimensional change shifted to lower temperatures at a lower heating rate. Second, the maximum expansion in the *L* direction decreased from 3.2% to 2% and the total shrinkage after binder removal increased from 0.7% to 2.7%, when the heating rate was lowered from 10°C/min to 1°C/min.

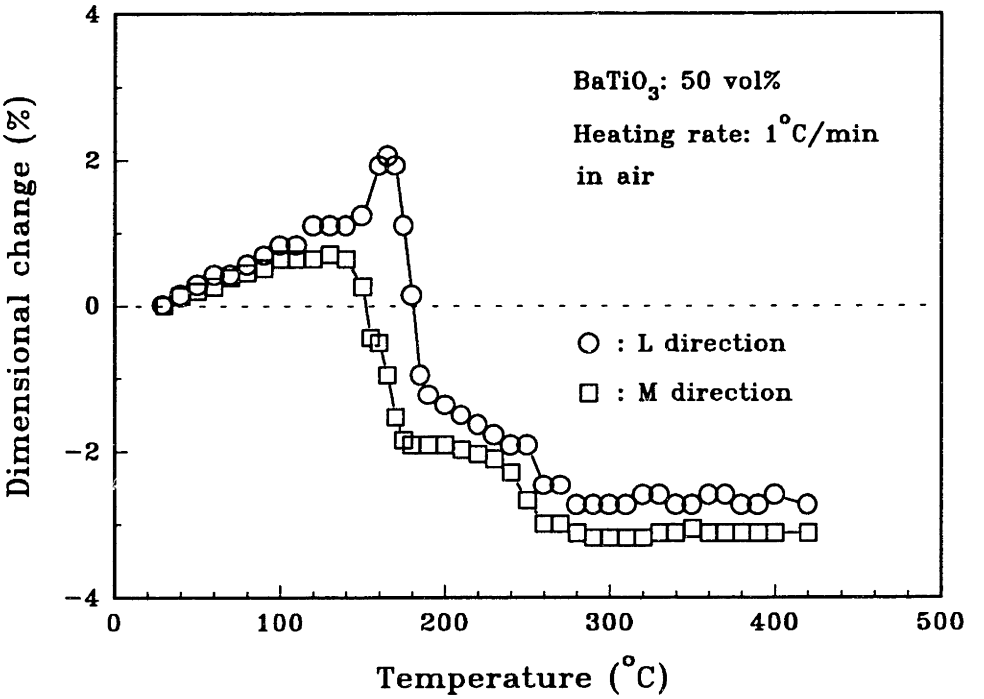


**Figure 6.9 Dimensional change of laminated ceramic tapes (sample B) during binder removal at 1°C/min**

Deformation of sample C during binder removal is shown in Figure 6.10. The maximum expansion in the L direction decreased from 3.2% to 2.4% when the loading of ceramic powder in the green tape increased from 50 to 55 vol%. A 1.6% shrinkage was observed in all three directions after the binder removal process was completed.

*Sample deformation measurement via Methods 2 and 3*: Figure 6.11 shows the volume shrinkage of samples quenched at different stages of binder removal. The solid line represents a series of samples which were burned out to different stages, and followed

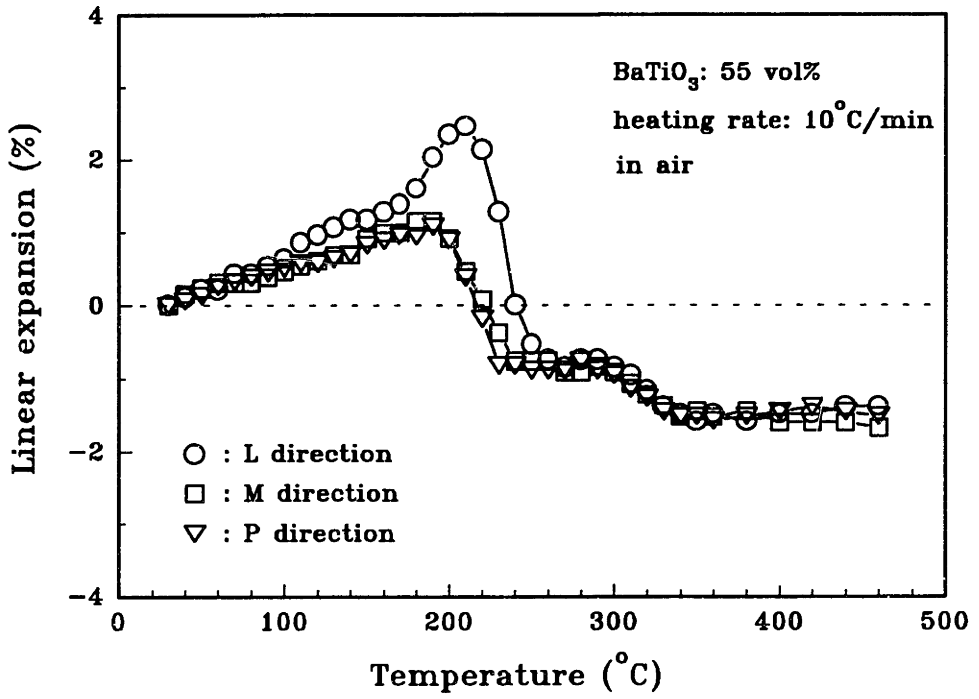


**Figure 6.10. Dimensional change of laminated tapes with 55 vol% ceramic loading (sample C) during binder removal at 10°c/min**

by quenching. The dashed line represents one sample which was heated in cycles until all the binder was removed. Table 2.2 lists the quenching temperatures of the samples used in the above two experiments.

In the early stages of binder removal, the decrease in sample volume was very close to the volume of binder lost by evaporation. When 20% of the binder was removed, this shrinkage stopped. A slight expansion, followed by a slow healing process, occurred in samples where more binder was removed.

**Table 6.2 Quenching temperature at different amounts of binder removal**

| Amount of binder removal (wt%) | 5% | 10% | 20% | 30% | 40% | 50% | 60% |
|---|---|---|---|---|---|---|---|
| T(°C): a series of samples | 123 | 138 | 155 | 165 | 179 | 189 | 198 |
| T(°C): one sample | 123 | 133 | 140 | 151 | 171 | 184 | 195 |

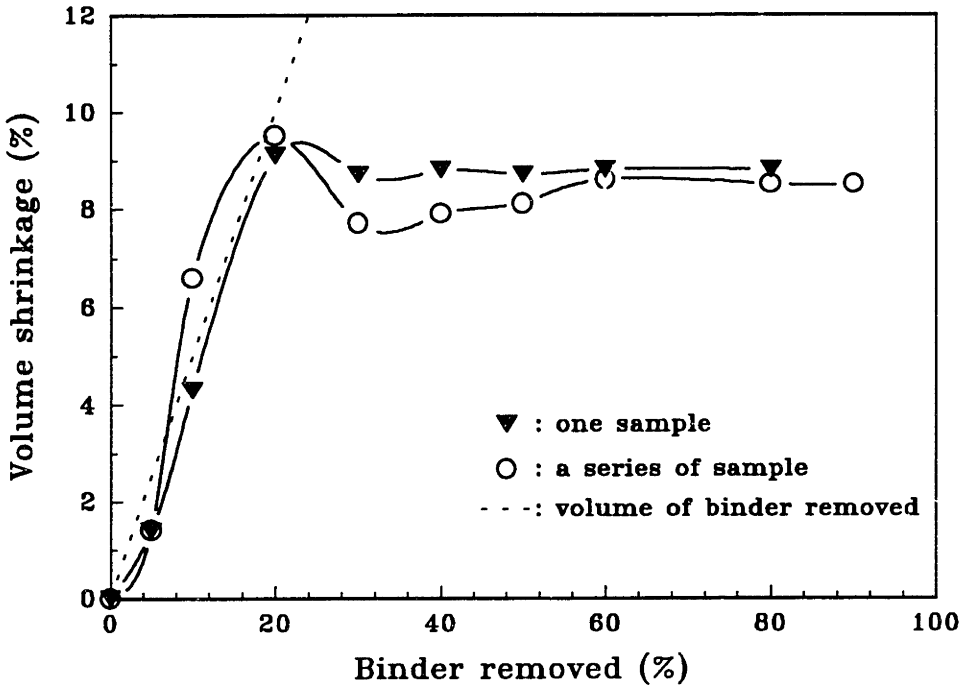


**Figure 6.11. Volume shrinkage of MLC samples vs. amount of binder removed**

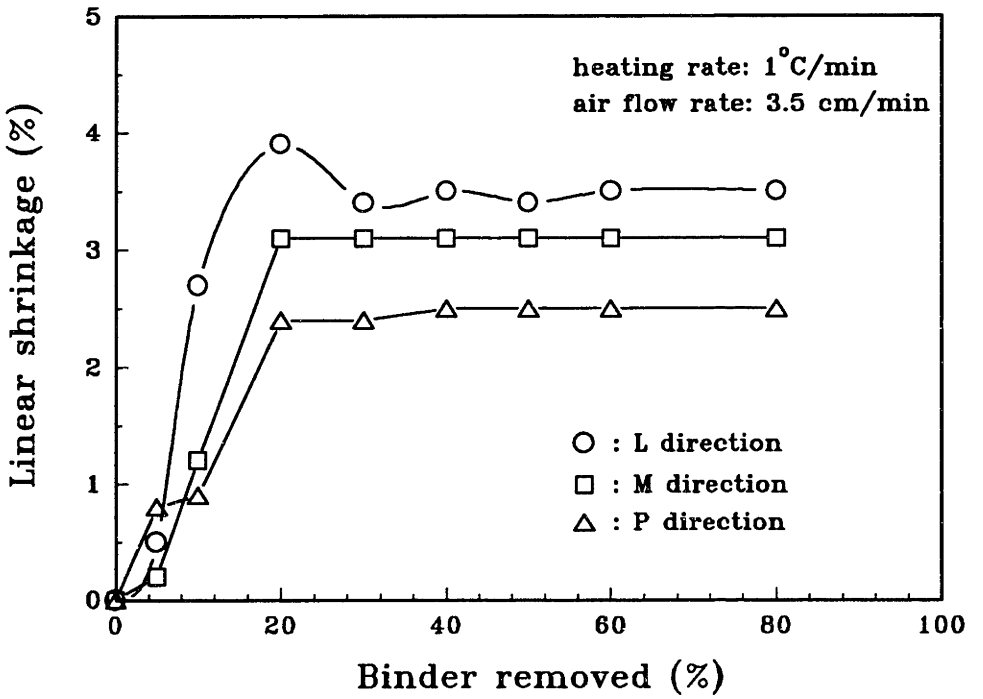


**Figure 6.12. Average linear shrinkage of an MLC sample vs. amount of binder removed**

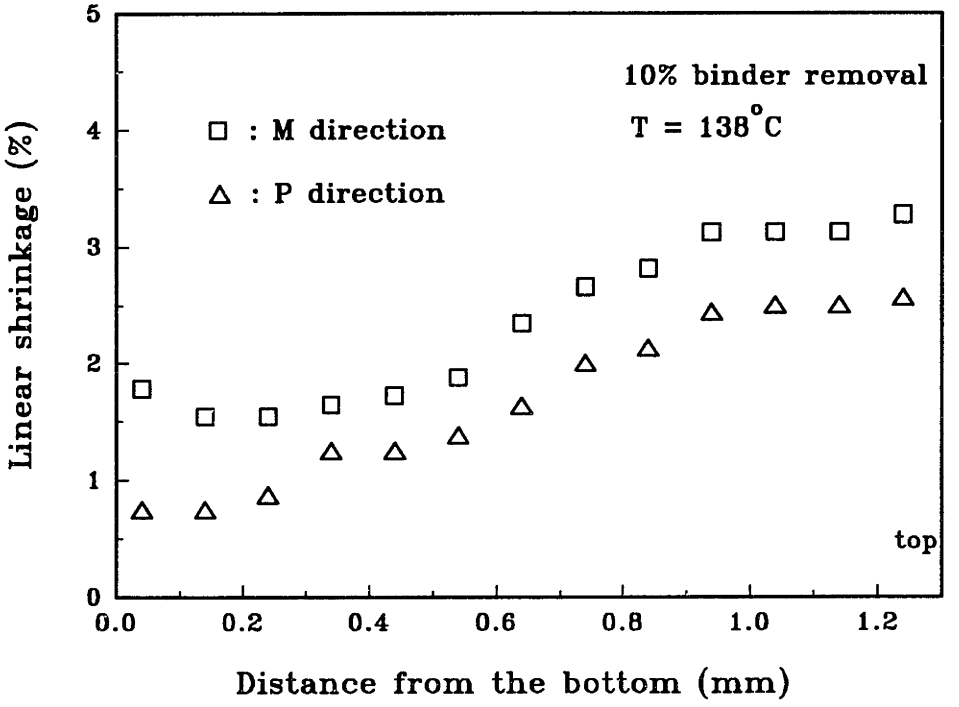
10% binder removal
T = 138°C
□ : M direction
△ : P direction
top
Linear shrinkage (%)
Distance from the bottom (mm)
0
1
2
3
4
5
0.0
0.2
0.4
0.6
0.8
1.0
1.2

(a)

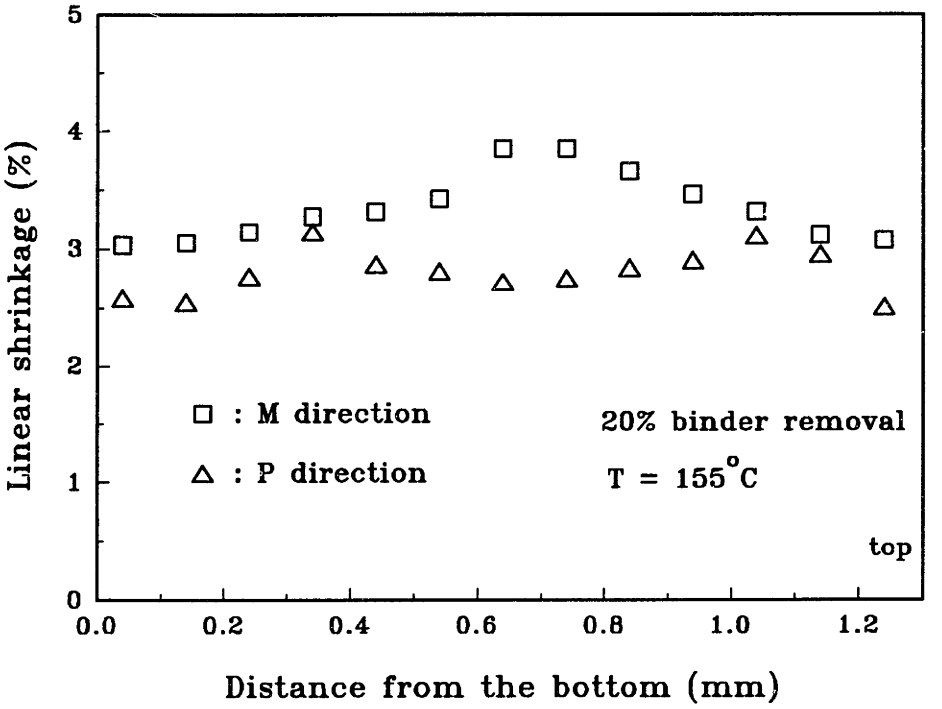
□ : M direction
△ : P direction
20% binder removal
T = 155°C
top
Linear shrinkage (%)
Distance from the bottom (mm)
0
1
2
3
4
5
0.0
0.2
0.4
0.6
0.8
1.0
1.2

(b)

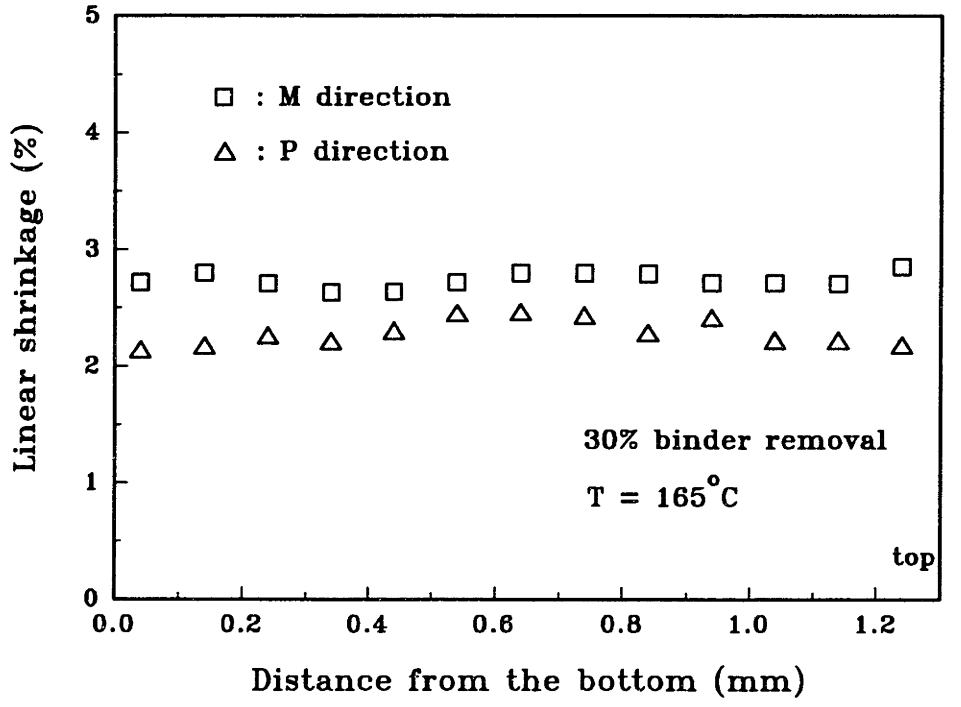


(c)

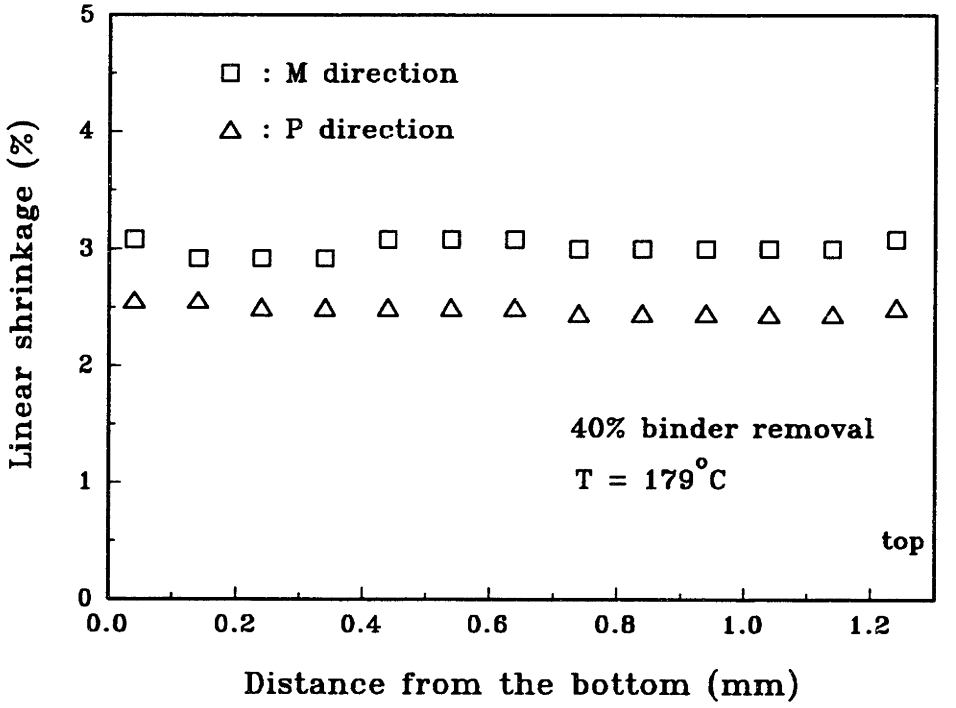


(d)

**Figure 6.13. Linear shrinkage in the M and P directions vs. distance from the bottom of the sample: a) 10% binder removed, b) 20% binder removed, c) 30% binder removed, and d) 40% binder removed**

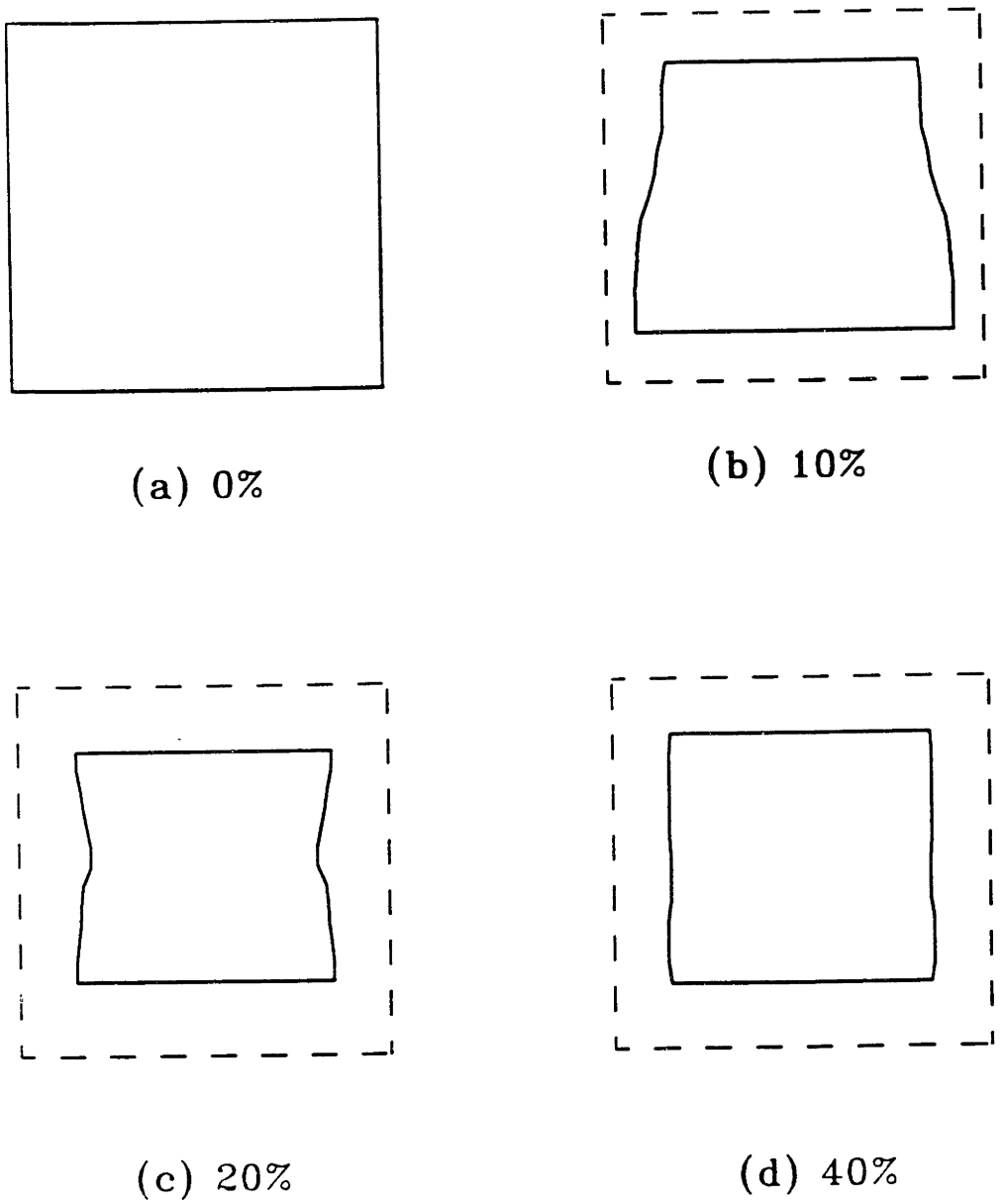


**Figure 6.14. Cross section of perpendicular to P direction of an MLC sample at different stages of binder removal ( in (b), (c) and (d), the shrinkage was magnified 10 times)**

The linear shrinkage of the cyclically heated sample at different stages of burnout is shown in Figure 6.12. The linear shrinkage along the L direction reached a maximum at 20% binder removal. The total linear shrinkage in the *L*, *M*, and *P* directions was 3.5%, 3.1%. and 2.5%, respectively.

Figure 6.13 shows the linear shrinkage in the M and P directions versus the distance from the sample bottom for a series of samples which were heated to different stages. At 138°C, or 10% binder removal, the sample showed much greater shrinkage in the top surface region than in the bottom surface region. When the temperature reached 155°C, corresponding to 20% binder removal, greater shrinkage occurred in the middle of the sample than in the surface areas. At a higher temperature, the sample smoothed out

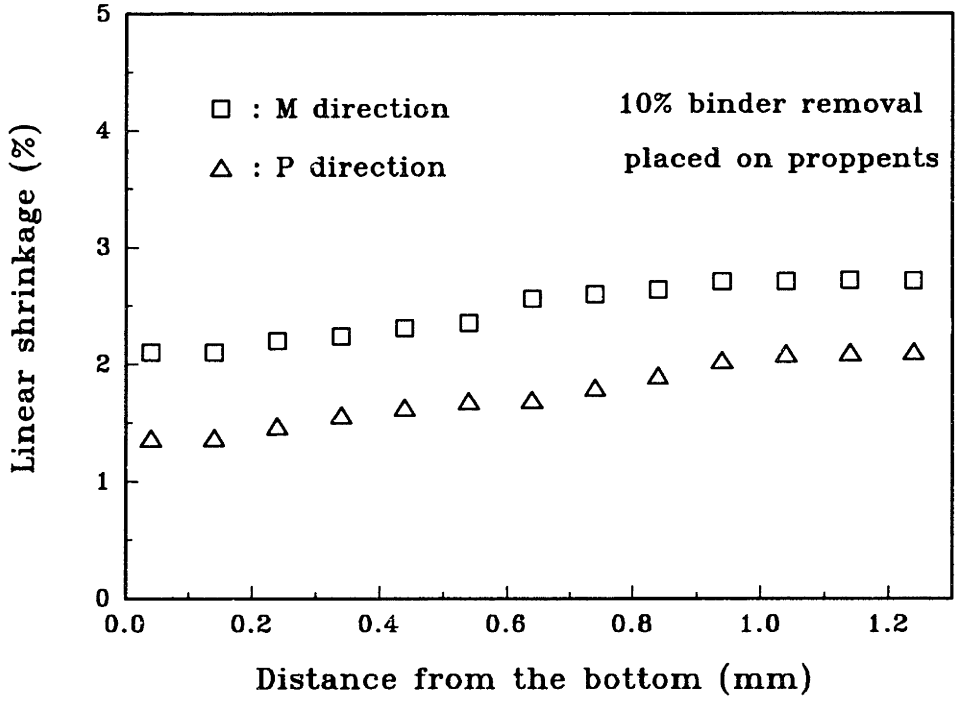


**Figure 6.15. Linear shrinkage in the M and P directions vs. distance from the bottom of the sample at 10% binder removal (the sample was placed on proppens)**

such that at 165°C and 179°C, the shrinkage became very uniform throughout the thickness of the sample. A cross section in the M direction of an MLC sample at different stages of binder removal is shown in Figure 6.14. In Fig. 6.14b, c, and d, the shrinkage was magnified ten times in order to observe the deformation more clearly.

An MLC sample which had lost 10% of its binder was cut into three sections corresponding to the top, middle and bottom. TGA was performed on each section to determine the remaining binder concentration, which was found to be the same in all three sections. When an MLC was placed on spherical particles (proppents, ~ 800 μm) instead of on a platinum TGA pan, the shrinkage at 10% binder removal became more uniform, as can be observed from Figure 6.15.

## II. Discussion

A ceramic greenware first experiences thermal expansion and stress relaxation when it is heated up. Taking the ratio of the respective thermal expansion coefficients for typical binder materials and ceramic powders as $10^3$[12], it appears that in comparison to the binder, the expansion of ceramic powders is negligible. The thermal expansion of the composite, therefore, is proportional to the binder concentration. A typical thermal expansion coefficient of PVB based polymer materials is $2\times10^{-4}/°C$[13]. Thus, a 1% linear expansion is expected between room temperature and 120°C for an MLC sample which consists of 50 vol% binder. This is consistent with the expansion shown in Figure 6.5 to Figure 6.10.

The relaxation of stresses in a ceramic tape causes the single layer tapes to bend, as indicated in Chapter 4. In a laminated structure, however, individual layers can not bend freely. The stress relaxation is achieved by particle rearrangement. The stress relaxation

of a tape causes shrinkage in the casting and transverse directions and expansion in the thickness direction, similar to the dimensional change of tape cast polymer films during annealing. The shrinkage in the casting direction (*M* direction) is higher than the transverse direction (*P* direction). For an MLC greenware, delamination occurs in the electrode layer at a high heating rate. The expansion from stress relaxation and from delamination results in a higher overall expansion in the *L* direction. Delamination also expands the MLC in the *M* and *P* directions.

Shrinkage of the sample occurs as plasticizer starts to leave the samples. The decrease in volume of the sample is equal to the volume of binder lost by evaporation in the early stages of binder removal. Substantial particle rearrangement is consistent with the capillary flow known to occur as PVB-based binders are removed[14]. Capillary forces created by the retreating vapor interface of the molten binder within the pores rearranges the particles to higher packing density. Apparently, the particle rearrangement was constrained at low temperatures by the substrate near the bottom of the sample (Fig. 6.13b) when the viscosity of the sample was high. Replacing the platinum substrate with spherical particles lowered the friction between sample and substrate. It resulted in more uniform shrinkage across the sample thickness (Fig. 6.15). Increasing the temperature decreased viscosity, and thus, diminished the constraints exerted by the substrate. The compressional stresses imposed by the electrode layer on the tape caused greater shrinkage in the middle of the sample than in the top and bottom regions. These nonuniform shrinkages resulted in a stress gradient within the MLC sample. This stress gradient may serve as an origin for the nucleation of delamination.

Shrinkage stops after the particles come in contact with each other through their adsorption layer. Further removal of binder only creates porosity within the greenbody. No dimensional change of the sample can occur until the adsorbed PVB layer starts to

decompose. The removal of this adsorption layer brings particles to contact with each other and causes shrinkage of the sample. The magnitude of this shrinkage is determined by the thickness of the adsorption layer, particle size distribution, shape, and packing arrangement of the particles. An approximation of the linear shrinkage is[4]:

$$\Delta\varepsilon = \frac{\delta}{\delta + r} \cong \frac{\delta}{r} \qquad (\delta << r) \qquad (6.1)$$

where $\delta$ is the thickness of adsorption layer, and $r$ is the radius of the particles. Eq. 1 produces a one percent linear shrinkage of the greenware, taking $\delta$ and r as 5.1 nm and 0.52 μm, respectively. This value agrees with the experimental result, which is 0.7%.

## 6.4 Conclusion

Binder distribution in a multilayer ceramic greenware was studied. A uniform distribution of the binder across the sample was observed when 6 and 12% of the binder was removed. At 28% binder removal, the distribution of PVB became nonuniform, even though BBP was still uniformly distributed in the sample. There was less PVB near the electrode layers and in the bottom surface regions. Liquid transport by capillary pressure is believed to be the cause of uniform BBP distribution. Preferential removal of PVB from the surface or the porous electrode layer resulted in the lower binder concentration in these regions. A PVB-rich surface region was observed, which was attributed to the slow counter diffusion of PVB to the interior of the sample.

Sample deformation was observed in order to monitor changes in particle packing and formation of defects during the binder removal process. A laminated sample and an MLC greenware first experienced thermal expansion and stress relaxation. Stress relaxation caused the laminated sample to shrink in the casting and transverse direction and to expand in the thickness direction. The shrinkage in the casting direction, however,

was higher than in the transverse direction. MLC greenware then experienced delamination, which expanded the sample in all directions. Particle packing density increased at higher temperatures as the binder was removed due to the capillary action of the molten binder. The decrease in the volume was equal to the volume of plasticizer lost by evaporation. This movement stopped when the particles came into contact with each other through their adsorption layer. Further increase in temperature did not cause dimensional change; it only created porosity within the sample. The second stage of shrinkage occurred when the decomposition of the PVB adsorption layer started. The elimination of this adsorption layer produced 0.7% linear shrinkage in all three directions.

The shrinkage of the sample during an early stage of binder removal could be constrained by the substrate, resulting in nonuniform deformation in the thickness of the MLC greenware. The higher shrinkage of the electrode layer put the ceramic tape under compressive stresses, and caused higher shrinkage in the middle of the sample. These nonuniform shrinkages may serve as origins for the nucleation of delamination.

## References


1. M.J. Cima, J.A. Lewis, and A.D. Devoe, "Binder Distribution in Ceramic Greenware During Thermolysis," *J. Am. Ceram. Soc.*, 72, 1192-99 (1989).

2. D.W. Sproson and G.L. Messing, "Organic Removal Processes in Closed Pore Powder-Binder System"; pp. 528-37 in Ceramic Transactions: Ceramic Powder Processing Science. Edited by G.L. Messing, E.R. Fuller, Jr., and H. Hausner. American Ceramic Society, Westerville, OH, 1988.

3. Y.-N. Sun, M.D. Sacks, and J.W. Williams, "Pyrolysis Behavior of Acrylic Polymers and Acrylic Polymer/Ceramic Mixtures"; pp. 538-48 in Ceramic Transactions: Ceramic Powder Processing Science. Edited by G.L.Messing, E.R.Fuller, Jr., and H.Hausner. American Ceramic Society, Westerville, OH, 1988.

4. J.K. Wright, M.J. Edirisinghe, J.G. Zhang, and J.R.G. Evans, "Particle Packing in Ceramic Injection Molding," *J. Am. Ceram Soc.*, 73, 2653-68 (1990).

5. C.A. Sundback, M.A. Costantini, and W.H. Robbins, "Part Distortion During Binder Removal"; pp. 191-200 in Ceramic Materials and Components for Engines. Edited by V.J. Tennery. American Ceramic Society, Westerville, OH, 1989.

6. J.K. Wright, J.R.G. Evans, and M.J. Edirisinghe, "Degradation of Polyolefin Blends Used for Ceramic Injection Molding," *J. Am. Ceram. Soc.*, 72, 1822-28 (1989).

7. J. Woodthorpe, M.J. Edirisinghe, and J.R.G. Evans, "Properties of Ceramic Injection Molding Formulation III. Polymer Removal," *J. Mater. Sci.*, 24, 1028-49 (1989).

8. B.C. Mutsuddy, "Oxidative Removal of Organic Binders from Injection-molded Ceramics"; pp. 397-408 in Proceeding of the International Conference on Non-oxide Technological and Engineering Ceramics, N. I. H. E. Limerick, 1985.

9. R.A. Gardner and R.W. Nufer, "Properties of Multilayer Ceramic Green Sheets," *Solid State Technol.*, 17 5 38-43 (1974).

10. J.G. Pepin, "Electrode-Based Courses of Delaminations in Multilayer Ceramic Capacitors," *J. Am. Ceram. Soc.*, 72, 2287-91 (1989).

11. M.R. Barone, J.C. Ulicny, R.R. Hengst, and J.R. Pollinger, "Removal of Organic Binders in Ceramic Powder Compacts"; pp. 575-83 in Ceramic Transactions: Ceramic Powder Processing Science. Edited by G.L. Messing, E.R. Fuller, Jr., and H. Hausner. American Ceramic Society, Westerville, OH, 1988.

12. M.R. Barone and J.C. Ulicny, "Liquid-Phase Transport During Removal of Organic Binders in Injection-Molded Ceramics," *J. Am. Ceram. Soc.*, 73, 3323-33 (1990).

13. Information provided by Monsanto Corp., Amherst, MA.

14. M.J. Cima, M, Dudziak, and J.A. Lewis, "Observation of Poly(Vinyl Butyral) - Dibutyl Phthalate Binder Capillary Migration," *J. Am. Ceram. Soc.*, 72, 1087-90 (1989).

# CHAPTER 7

# CONCLUSIONS AND FUTURE WORK

This study investigated the physical issues during binder removal from multilayer ceramic greenware. A multilayer ceramic capacitor was chosen as an example for study, but the knowledge gained from this system can be generalized and applied to other multilayer systems and injection molded samples. The major conclusions of this research are summarized below, and the suggestions for future research in this field are also stated.

1. PVB chains were shown to adsorb on the surface of $BaTiO_3$ powder through hydrogen bonding, forming a 4.5 nm adsorption layer. This adsorption layer has low mobility, and behaves as part of the $BaTiO_3$ particles. The volume of the adsorption layer was equivalent to 8.6% of the volume of $BaTiO_3$ powder. The maximum packing density of the particles plus their adsorption layers was calculated to be 0.646. This corresponds to a critical particle volume concentration (CPVC) of 0.598 for the green tape.

2. The dynamic mechanical analysis (DMA) of the green tapes was conducted over a wide temperature range (-80°C to 150°C). 50 vol% of ceramic particles in green tape was found to broaden the glass transition region of the binder matrix from the -70 to 20°C range to the -70 to 70°C range. The broad glass transition region is believed to be caused by low mobility polymer layers near ceramic particle surfaces. Broadening of the glass transition region as well as shifting toward high temperatures occurred when the ceramic loading in the green tapes exceeded the CPVC of this system, due to the lack of free binder layer between ceramic particles. DMA indicated that the ceramic loading in a green tape should be below the CPVC in order for the tape to have enough flexibility to be processed.

3. The curvature and the shrinkage of the green tapes were measured *in situ* during annealing and binder removal. The tapes bent toward the top surface due to a differential shrinkage across the tape thickness. The tape casting direction had higher curvature and shrinkage than the transverse direction. The tape annealed at 70°C for 24 hours showed the same magnitude of curvature and the same amount of differential shrinkage in the casting and transverse directions. Residual stresses in the polymer matrix from shearing and drying processes are believed to be the causes of bending, as oppose to the conventional concept of differential particle packing density. Three kinds of residual stresses are speculated; preferred orientations of polymer chains in the plane parallel to the substrate, a density gradient across the tape thickness, and a residual orientation of polymer chains from shearing along the tape casting direction. The first two kinds of stresses are believed to also exist in solvent cast pure polymer films.

4. A theoretical model was developed to calculate the gas pressure distribution in the electrode layers and to estimate the critical gas generation rate and the critical defect size above which delamination will propagate. The gas pressure was shown to increase with temperature and length of the electrode layer and decrease with the porosity. The critical gas pressure needed to cause a delamination was shown to be inversely proportional to defect size in the electrode layers. The gas pressure increases rapidly when the porosity of the electrode layer decreases, indicating that delamination is most likely to occur in the early stages of binder removal when the porosity of the sample is low. This was confirmed by experimental observation.

5. Delamination during binder removal was shown to be a cohesive failure along the electrode layers. It nucleated within the electrode layer due to the stress from shrinkage mismatch between the electrode and dielectric layers. Propagation of delamination along the electrode layer occurred due to high gas pressure caused by a high gas generation rate.

Delamination healed or partially healed after the binder in the electrode layer was removed, and this healing was controlled by the maximum strain level in the dielectric layers from delamination. A minor delamination can heal completely, while a major delamination caused either by high gas pressure or by a thick electrode layer can only partially heal.

6. The removal of plasticizer from an MLC was uniform throughout the sample, which is believed to have been caused by the redistribution of liquid binder by capillary forces. The removal of PVB, on the other hand, was nonuniform at early stages. Preferential removal of PVB from the surfaces or from the dielectric-electrode interfaces occurred. A PVB-rich top surface layer was observed in an early stage, when 28% of the binder was removed. This is believed to be caused by a slow counter diffusion of the PVB (which is brought to the top surface by capillary forces) to the interior of the sample.

7. Four types of deformation were observed in ceramic tapes during the binder removal process: thermal expansion; stress relaxation which causes shrinkage in the tape casting and the transverse directions and expansion in the tape thickness; shrinkage from the evaporation of the plasticizer; and shrinkage from the elimination of the adsorbed PVB layer. In an MLC greenware, delamination, as well as the above four types of deformation, occurred.

Further research in a few areas is needed in order to gain a more complete understanding of the structural inhomogeneity and anisotropy of the green tape. The study of pure polymer film as a model system can certainly shed light on stress distribution in polymer films cast from a solution and on the design of processing conditions so that both the stress and the stress gradient in the film will be lowered. Further study is needed, for example, on the effect of polydispersity of polymer binder on the stress distribution in

the film. Polydispersity is defined as the ratio of the weight average molecular weight to the number average molecular weight. The PVB that has been used in this current research has a polydispersity of 3. It is unclear what role the wide molecular weight distribution of this polymer plays in the stress gradient of the dried film. A model system such as polymethyl methacrylate (PMMA) should be used for this purpose since no narrow molecular distribution PVB is available. Films cast from a solution of PMMA that has a low or a high polydispersity can be characterized and compared. The effect of polydispersity on drying kinetics and on stress distribution can be understood from this experiment.

The effect of drying parameters on the stress distribution in a film is another area that requires further research. The dependence of the stress on drying rate, drying temperature, and concentration of binder solution is not understood. The effects of the surface energy of the substrate, as well as the effects of interfacial energy between the substrate and the binder solution, on the stress are other interesting areas to explore.

The redistribution of both a binder solution and a ceramic slurry during drying may affect the stress distribution in dried films. Our previous experiments indicate that thick or thin edges can form on the film during drying, even from a slip of uniform thickness coated with the doctor blade. This variation appears to be affected by the drying rate, the surface energy of the substrate, and by the concentration of the solution. It would be interesting to quantify the profile of the thickness across the width of the tape. The factors affecting this profile need to be identified and quantified. The causes of redistribution of the solution toward or from the edges need to be studied. The relation between this profile and the stress distribution need to be established.

One approach toward achieving lower residual stress in dried ceramic tapes is to reduce the drying rate to allow the polymer chains enough time to relax. The relaxation time of polymer chains near a solid surface needs to be modeled. The settling time of powders with adsorbed polymer layers also needs to be calculated. Comparing the above two time constants may provide guidance on drying rate control.

Our research indicates that $CO_2$ and water adsorbed on the surface of $BaTiO_3$ powder. The effects of these impurities on the rheology of slurry and on the strength of the green tapes are not clear. These effects can be studied by heating the powder to 800°C to remove the adsorbed water and to decompose $BaCO_3$ and then to mix the powder with a binder solution to make a slurry. The viscosity of this slurry can be measured and compared with a slurry made from as-received $BaTiO_3$ powder. Green tape cast from this slurry can be characterized and compared with conventional tape, following the same procedure as described in chapters 3 and 4.